MOLECULAR RECOGNITION IN BMP LIGAND-RECEPTOR INTERACTIONS

DISSERTATION ZUR ERLANGUNG DES
NATURWISSENSCHAFTLICHEN DOKTORGRADES
DER JULIUS-MAXIMILIANS-UNIVERSITÄT WÜRZBURG

VORGELEGT VON

STEFAN HARTH

AUS BAD NEUSTADT AN DER SAALE

WÜRZBURG, SEPTEMBER 2010

Eingereicht am: .....

Mitglieder der Promotionskommission:

Vorsitzender: .....

1. Gutachter: Prof. Dr. Walter Sebald

2. Gutachter: Prof. Dr. Thomas Müller

Tag des Promotionskolloquiums: .....

Doktorurkunde ausgehändigt am: .....

MEINEN ELTERN

1. Summary

Bone Morphogenetic Proteins (BMPs) are secreted multifunctional signaling proteins that play an important role during development, maintenance and regeneration of tissues and organs in almost all vertebrates and invertebrates. BMPs transmit their signals by binding to two types of serine-/threonine-kinase receptors. BMPs bind first to their high affinity receptor, thereby recruiting their low affinity receptor into the complex. This receptor assembly starts a Smad (Small mothers against decapentaplegic) protein signaling cascade which regulates the transcription of responsive genes.

Up to date, only seven type I and five type II receptors are known for more than 30 ligands. Therefore, many BMP ligands can recruit more than one receptor subtype. Vice versa, receptors can bind to several ligands, indicating a highly promiscuous ligand-receptor interaction. This raises the following questions: (i) How are BMPs able to induce ligand-specific signals, despite forming complexes with identical receptor composition and (ii) how are they able to recognize and bind various binding partners in a highly specific manner.

From the ligand's point of view, heterodimeric BMPs are valuable tools for studying the interplay between different sets of receptors, thereby providing new insights into how the various BMP signals can be generated.

This study describes the expression and purification of the heterodimers BMP-2/6 and -2/7 from *E.coli* cells. BIAcore interaction studies and various *in vitro* cell activity assays revealed that the generated heterodimers are biologically active. Furthermore, BMP-2/6 and -2/7 exhibit a higher biological activity in most of the cell assays compared to their homodimeric counterparts. In addition, the BMP type I receptor BMPR-IA is involved in heterodimeric BMP signaling. However, the usage of other type I receptor subtypes (e.g. ActR-I) building a heteromeric ligand-receptor type I complex as indicated in previous works could not be determined conclusively. Furthermore, BMP heterodimers seem to require only one type I receptor for signaling.

From the receptors' point of view, the BMP type I receptor BMPR-IA is a prime example for its promiscuous binding to different BMP ligands. The extracellular binding interface of BMPR-IA is mainly unfolded in its unbound form, requiring a large induced fit to adopt the conformation when bound to its ligand BMP-2. In order to unravel whether the binding promiscuity of BMPR-IA is linked to structural plasticity of its binding interface, the

interaction of BMPR-IA bound to an antibody Fab fragment was investigated. The Fab fragment was selected because of its ability to recognize the BMP-2 binding epitope on BMPR-IA, thus neutralizing the BMP-2 mediated receptor activation.

This study describes the crystal structure of the complex of the extracellular domain of BMPR-IA bound to the antibody Fab fragment AbyD1556. The crystal structure revealed that the contact surface of BMPR-IA overlaps extensively with the contact surface of BMPR-IA for BMP-2 interaction. Although the contact epitopes of BMPR-IA to both binding partners coincide, the three-dimensional structures of BMPR-IA in both complexes differ significantly. In contrast to the structural differences, alanine-scanning mutagenesis of BMPR-IA showed that the functional determinants for binding to both the antibody and BMP-2 are almost identical.

Comparing the structures of BMPR-IA bound to BMP-2 or to the Fab AbyD1556 with the structure of unbound BMPR-IA revealed that binding of BMPR-IA to its interaction partners follows a selection fit mechanism, possibly indicating that the ligand promiscuity of BMPR-IA is inherently encoded by structural adaptability.

Zusammenfassung

„Bone Morphogenetic Proteins" (BMPs) sind sezernierte multifunktionelle Signalproteine, die eine wichtige Rolle während der Entwicklung, Aufrechterhaltung und Regeneration von Geweben und Organen in fast allen Vertebraten und wirbellosen Tieren spielen. Die BMP-Signalgebung wird durch die Bindung an zwei Typen von Serin/Threonin Rezeptorkinasen eingeleitet. Hierbei binden BMPs zuerst an ihren hochaffinen Rezeptor, bevor der niederaffine Rezeptor in den Komplex eingefügt wird. Durch das Zusammenfügen beider Rezeptortypen wird eine von Smad (Small mothers against decapentaplegic)-Proteinen gesteuerte Signalkaskade gestartet, die letztendlich die Transkription responsiver Gene reguliert.
Aktuell sind nur sieben Typ I und fünf Typ II Rezeptoren für mehr als 30 Liganden bekannt. Viele BMP-Liganden können demzufolge mehr als einen Rezeptorsubtyp rekrutieren. Umgekehrt jedoch können auch Rezeptoren an unterschiedliche Liganden binden, was auf eine im hohen Maße promiske Ligand-Rezeptor-Interaktion hinweist. Dabei stellen sich folgende Fragen: (i) Wie können BMPs ligandspezifische Signale erzeugen, obwohl sie dafür die gleichen Rezeptoren benutzen? (ii) Und wie können BMPs unterschiedliche Bindungspartner erkennen und trotzdem hochspezifisch an diese binden?

Von Blickwinkel der Liganden aus betrachtet stellen heterodimere BMPs wertvolle Hilfsmittel dar, um das Zusammenspiel zwischen den verschiedenen Rezeptortypen zu studieren. Darüber hinaus können sie neue Einblicke in die Entstehung von unterschiedlichen BMP-Signalen gewähren.
In dieser Doktorarbeit wird die Expression und Aufreinigung von heterodimeren BMP-2/6 und -2/7 aus *E.coli* Zellen beschrieben. Mittels BIAcore Interaktionsstudien und *in vitro* Aktivitätsassays in Säugerzellen konnte gezeigt werden, dass die hergestellten Heterodimere biologisch aktiv sind. Darüber hinaus zeigen BMP-2/6 and -2/7 in den meisten Zellassays eine höhere biologische Aktivität als ihre homodimeren Gegenstücke. Außerdem konnte nachgewiesen werden, dass der BMP Typ I Rezeptor BMPR-IA an der Signalgebung von heterodimeren BMPs involviert ist. Eine Beteiligung weiterer Typ I Rezeptoren (wie z.B. die von ActR-I), die einen heteromeren Ligand-Rezeptor Typ I Signalkomplex bilden, wie es bereits in früheren Studien gezeigt wurde, konnte jedoch experimentell nicht eindeutig belegt werden. Des Weiteren lassen die Ergebnisse darauf schließen, dass heterodimere BMPs für

eine erfolgreiche Signalweiterleitung nur die Präsenz eines einzelnen Typ I Rezeptors benötigen.

Von Blickwinkel der Rezeptoren aus betrachtet, ist der BMP Typ I Rezeptor BMPR-IA ein Paradebeispiel für promiskes Bindeverhalten an verschiedene BMP-Liganden. Das extrazelluläre Kontaktepitop von BMPR-IA ist im Wesentlichen ungefaltet, wenn BMPR-IA in freier ungebundener Form vorliegt. Infolge dessen durchläuft die Binderegion in BMPR-IA weit reichende strukturelle Veränderungen, um die erforderliche Konformation auszubilden, die für die Bindung an BMP-2 essentiell ist. Um herauszufinden, ob das promiske Bindeverhalten von BMPR-IA mit einer strukturellen Plastizität seiner Binderegion einhergeht, wurde die Interaktion zwischen BMPR-IA und einem Antikörper Fab Fragment experimentell untersucht. Das Fab Fragment wurde aufgrund folgender Eigenschaft ausgewählt, nämlich an das BMP-2 Bindeepitop des Rezeptors anzudocken, um so eine BMP-2 vermittelte Rezeptoraktivierung zu verhindern.
In dieser Doktorarbeit wird die Kristallstruktur des Komplexes, bestehend aus der extrazellulären Domäne von BMPR-IA und dem Antikörper Fab Fragment AbyD1556 beschrieben. Die Kristallstruktur zeigt, dass die Kontaktoberfläche von BMPR-IA zu einem sehr großen Teil mit der Kontaktoberfläche bei der Interaktion mit BMP-2 übereinstimmt. Obwohl das Kontaktepitop von BMPR-IA zu beiden Bindungspartnern weitestgehend deckungsgleich ist, unterscheiden sich die dreidimensionalen Strukturen von BMPR-IA in beiden Komplexen sehr stark voneinander. Im Gegensatz zu den strukturellen Differenzen zeigt jedoch eine Mutationsanalyse, bei der wichtige Aminosäuren mit Alanin ausgetauscht wurden, dass die funktionellen Determinanten, die die Bindung an den Antikörper und an BMP-2 bestimmen, beinahe die gleichen sind.
Wenn man die Strukturen von BMPR-IA, das an BMP-2 bzw. an das Fab Fragment AbyD1556 gebunden ist, mit der Struktur von ungebundenem BMPR-IA vergleicht, so fällt auf, dass die Bindung von BMPR-IA an seine Bindungspartner einem sog. „Selektions-Anpassungsmechanismus“ folgt, was möglicherweise zeigt, dass das promiske Ligand-Bindeverhalten von BMPR-IA von Natur aus durch seine strukturelle Anpassungsfähigkeit festgelegt wird.

2. Introduction

From the days of Hippocrates in ancient Greece bone has been known to have considerable potential for regeneration and repair (Adams 1891). But in former times the mechanisms of bone regeneration and repair were not fully understood. First insights were elucidated 23 centuries later, when Nicholas Senn described the utility of antiseptic decalcified bone implants in the treatment of osteomyelitis and certain bone deformities (Senn 1889). Later on, Pierre Lacroix proposed that there might be a hypothetical substance in bone – osteogenin – that is able to initiate bone growth (Lacroix 1945). Finally, in 1965, Marshal R. Urist made the key discovery that demineralized, lyophilized segments of bone, induced new bone formation, when implanted in muscle pouches in rabbits (Urist 1965).

Six years later, Urist and colleagues attributed the osteoinductive properties to "osteogenetic chemical components of the matrix of bone, dentin, and other hard tissues that are deinsulated by demineralization and associated intimately with collagen fibrils" and termed them "bone morphogenetic proteins" (Urist and Strates 1971; Urist and Strates 2009).

But it still took another 16 years until the first bone morphogenetic proteins (BMPs) could be isolated (Sampath et al. 1987; Katz and Reddi 1988) and their gene sequence determined (Wozney et al. 1988). According to gene homology, BMPs were classified as members of the transforming growth factor β (TGF-β) superfamily (Wozney et al. 1988).

2.1. BMPs and other ligands of the TGF-β superfamily

The TGF-β superfamily comprises – besides the BMPs – the growth and differentiation factors (GDFs), TGF-βs, activins, inhibins, nodal, the Müllerian inhibiting substance (MIS), and the glial cell derived neurotrophic factor (GDNF) (Massague 1998). On the basis of their amino acid sequence these members can be divided into different subfamilies (see fig. 2.1 A). Up to date, more than 30 members are known in mammals (Miyazawa et al. 2002). Proteins similar to TGF-β were also found in *Caenorhabditis elegans*, *Drosophila melanogaster* and *Xenopus laevis*, demonstrating that members of the TGF-β superfamily are highly conserved during evolution (Hill 2001; Parker et al. 2004; Savage-Dunn 2005).

BMPs not only play a pivotal role in bone morphogenesis, maintenance and regeneration but also exhibit a variety of other abilities. BMP expression studies and the analysis of BMP

mouse models have demonstrated a broad range of biological activities on various cell types, including monocytes, epithelial cells, mesenchymal cells, and neuronal cells (Balemans and Van Hul 2002). BMPs regulate cell proliferation and differentiation, chemotaxis and apoptosis. BMPs govern fundamental embryonic developmental processes such as mesoderm formation, establishment of left-right asymmetry, neural patterning, vasculogenesis and angiogenesis. In addition, BMPs participate in the development of various organs such as kidney, heart, eye, gut, lung, tooth, skin, hair, limb, and reproductive organs (Hogan 1996a; Hogan 1996b; Chang et al. 2002). Furthermore, BMPs are involved in many diseases including cancer (Chang et al. 2002; Blanco Calvo et al. 2009). As a consequence, BMPs were also named "body morphogenetic proteins", due to their extensive roles in various tissues and organs beyond the bone (Reddi 2005; Wagner et al. 2010). Recently, recombinant BMPs were used on a large scale in clinical applications such as spinal fusion, fracture healing and dental tissue engineering, indicating the economical potential of BMPs (Bessa et al. 2008a; Bessa et al. 2008b).

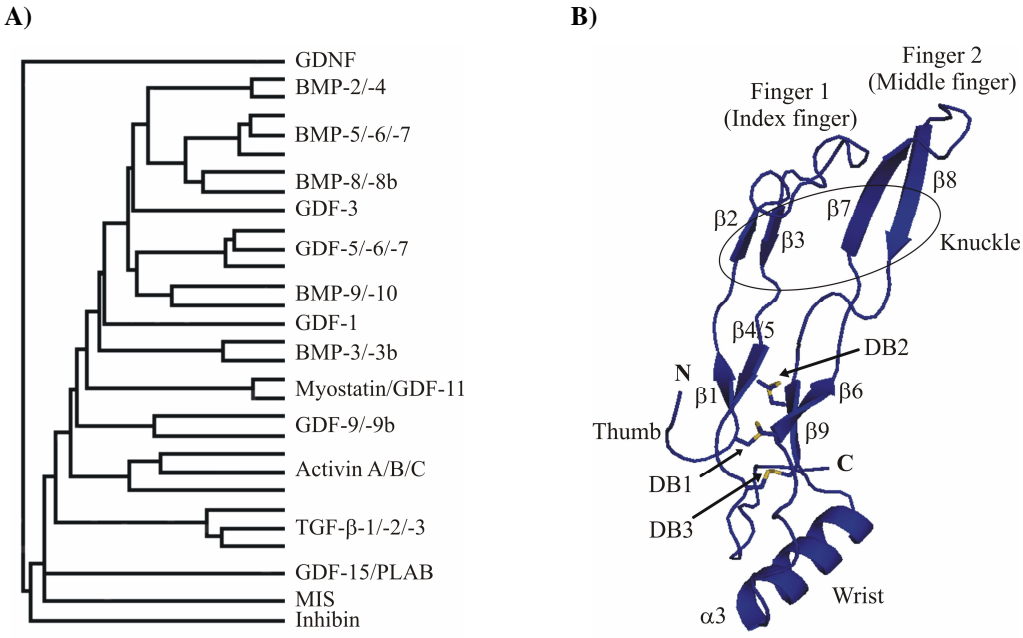

Figure 2.1 – The TGF-β superfamily. Classification and structural characteristics.

A) Members of the TGF-β superfamily can be divided into different subfamilies according to sequence similarities of their mature ligands. The figure shows only human proteins with the exception of murine BMP-8b and GDF-3. Scheme is modified according to Sebald and colleagues (Sebald et al. 2004).

B) Ribbon presentation of monomeric BMP-2. Overall fold of the BMP-2 monomer resembles an "open left hand". The N-terminal end represents the thumb, two β-sheets form the index and the middle finger and a central α-helix acts as the wrist. The cystine knot motif is indicated (DB1-3) and colored in yellow. Scheme is adapted according to Scheufler et al. (PDB entry 3BMP; Scheufler et al. 1999). DB: disulfide bond.

BMPs are secreted as large inactive precursor proteins containing a N-terminal signal sequence, a propeptide and a C-terminal domain consisting of the mature protein.
The propeptide varies in length and seems to be involved in processing, secretion and regulation of the activity of mature ligands (Sebald et al. 2004). After the preprotein has dimerized, the propeptide is cleaved proteolytically from the active C-terminal part following a multibasic motif (–RXXR–). Cleavage is carried out by members of the subtilisin-like proprotein convertase (SPC) family, as for instance by furin (Constam and Robertson 1999). However, the propeptide of all BMPs – with the exception of BMP-2 and a shortened form of BMP-4 – can also remain associated as LAP (latency-associated protein) with the mature ligand to produce an inactive complex (Sengle et al. 2008). Glycoproteins in the extracellular matrix, such as fibrillin, can bind these LAPs directly via disulfide bridges, thus immobilizing the BMPs in the extracellular matrix. Therefore, this immobilizing process can act as a buffering system until the active ligand is needed and subsequently released by proteolytic cleavage. This buffering mechanism was previously observed in TGF-β proteins which bind first to latent TGF-β binding proteins (LTBP) before they were immobilized in the extracellular matrix (Koli et al. 2001).
The C-terminal mature domain comprises 110 - 140 amino acids and is characterized by forming a cystine knot motif (McDonald and Hendrickson 1993), which is highly conserved in the TGF-β superfamily. The cystine knot comprises two consensus sequences constituting a ring of eight amino acids by forming two disulfide bonds. A third disulfide bond passes through the ring and thus establishing the knot. The cystine knot motif is not restricted to the TGF-β superfamily, but is also found in other proteins such as the platelet derived growth factor (PDGF), the nerve growth factor (NGF) and the vascular endothelial growth factor (VEGF). However, these proteins differ in their modes of dimerization and signaling from the TGF-β superfamily (Wiesmann and de Vos 2000).

Within the TGF-β superfamily, the crystal structure of the following proteins have been characterized: TGF-β 2 (Daopin et al. 1992), TGF-β 3 (Mittl et al. 1996), BMP-7 (Griffith et al. 1996), GDNF (Eigenbrot and Gerber 1997), BMP-2 (Scheufler et al. 1999), GDF-5 (Nickel et al. 2005; Schreuder et al. 2005), BMP-9 (Brown et al. 2005), Activin A (Harrington et al. 2006), BMP-3 (Allendorph et al. 2007), BMP-6 (Saremba et al. 2008) and the NMR structure of TGF-β 1 (Hinck et al. 1996).
Deduced from these results, the overall structure of the BMP monomer can be described as an “open left hand” (Scheufler et al. 1999) as depicted in fig. 2.1 B using the example of BMP-2.

The N-terminal end represents the thumb, two β-sheets (each two-stranded and antiparallel) form the index and the middle finger and a central α-helix acts as the wrist. Accordingly, a "knuckle" area is formed at the convex side of the two fingers. Two monomers are connected by an additional intermolecular disulfide bond thus stabilizing the active dimeric ligand (exceptions for GDF-3, GDF-9 and GDF-9B). In the dimer, the wrist of one monomer fits into the concave side of the fingers of the other monomer (see fig. 2.2). Most BMPs exist as homodimers, but heterodimers consisting of two different BMP monomers with different abilities were also detected *in vivo* (Shimmi et al. 2005; Little and Mullins 2009). Besides that, heterodimerization is also observed in other TGF-β superfamily members, for instance in inhibins and activins (Ling et al. 1986).

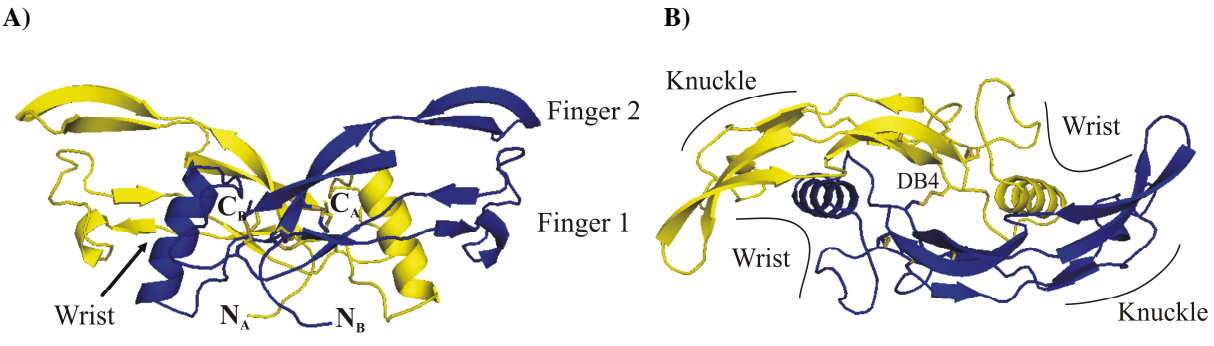

Figure 2.2 – Crystal structure of dimeric BMP-2.

Ribbon presentation in side view **(A)** and top view **(B)** according to Scheufler et al. (PDB entry 3BMP; Scheufler et al. 1999). Monomers BMP-2 A and BMP-2 B are colored in blue and yellow, respectively. Both monomers are connected via an intermolecular disulfide bond (DB4), thus stabilizing the complex. The type I receptor epitope is located in the concave site formed by the α-helix of one monomer and the concave half of the β-sheet of the other monomer building the wrist epitope. The type II receptor epitope is located on the convex back of the two fingers and thus known as the knuckle epitope.

Mutagenesis studies identified the epitopes for receptor binding in BMPs (Kirsch et al. 2000c) (see fig. 2.2 B). The type I receptor epitope is located in the concave site formed by the α-helix of one monomer and the concave half of the β-sheet of the other monomer building the wrist epitope with reference to the open left hand model. The type II receptor epitope is located on the convex back of the two fingers and thus known as the knuckle epitope. The BMP receptors are characterized in detail in the next chapter.

2.2. Receptors of the TGF-β superfamily

Signal transduction of BMPs and other members of the TGF-β superfamily is accomplished by binding of the ligand to two different types of single transmembrane serine/threonine kinase receptor chains (Massague 1998). According to sequence homology and functional properties, the receptor chains can be subclassified as type I and type II receptors (see fig. 2.3 A). Up to date, only seven type I and five type II receptors are known (de Caestecker 2004).

The type I receptors comprise the "activin like kinase 1" (ALK-1), the activin receptors type I and IB (ActR-I = ALK-2; ActR-IB = ALK-4), the BMP receptors type IA and IB (BMPR-IA = ALK-3; BMPR-IB = ALK-6), the TGF-β type I receptor (TβR-I = ALK-5) and ALK-7.

The group of type II receptors contains the TGF-β type II receptor (TβR-II), the BMP receptor type II (BMPR-II), the activin type II and IIB receptor (ActR-II and ActR-IIB) and the Müllerian inhibiting substance receptor type II (MISR-II).

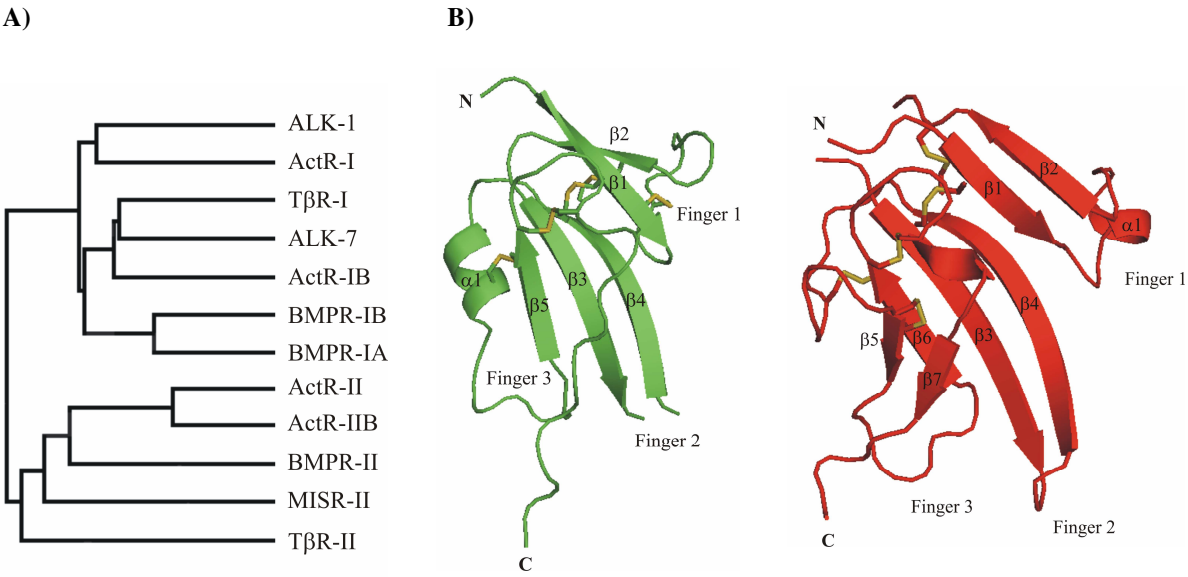

Figure 2.3 - Receptors of the TGF-β superfamily.

A) Sequence similarities of receptor ectodomains in the TGF-β superfamily. Scheme is taken from Sebald and colleagues (Sebald et al. 2004).

B) Ribbon presentation of extracellular domains of representative type I and type II receptors. BMPR-IA (green) is adapted according to Kirsch et al. (PDB entry 1ES7; Kirsch et al. 2000b) and ActR-II (red) according to Greenwald et al. (PDB entry 1BTE; Greenwald et al. 1999). The overall structure of TGF-β receptors resembles the "three finger toxin fold", which is determined by a conserved scaffold of disulfide bonds (in yellow) forming three pairs of antiparallel β-sheets. Despite this conserved core, TGF-β receptors are extremely variable in their peripheral areas.

Both receptor types are glycoproteins with polypeptides of 500 to 570 amino acids, and are organized in three different domains: 1) the extracellular domain, 2) the single span transmembrane region and 3) the intracellular domain.

The extracellular domain is responsible for ligand binding. The domain is N-glycosylated (except for BMPR-IB) and consists of only 100 to 150 residues. Crystal structures of the extracellular domain of ActR-II (Greenwald et al. 1999) and BMPR-IA (Kirsch et al. 2000b) reveal a fold similar to that of a class of toxins known as three-finger toxins (see fig. 2.3 B). The structure of type II receptors is characterized by a conserved scaffold of disulfide bonds, forming three pairs of antiparallel β-sheets. In BMPR-IA, this motif is modified slightly: two pairs of β-sheets build finger 1 and 2, a single β-sheet and a short α-helix form finger 3 (Kirsch et al. 2000b). Despite this conserved core, both receptor types are extremely variable in peripheral segments exhibiting a high flexibility in conformation and amino acid sequence (see fig. 2.3).

The single span transmembrane region contains ~25 amino acids and seems to have no specific structural features. But this has not been analyzed in detail.

The intracellular domain consists of approximately 350 amino acids, except for BMPR-II which has 867 amino acids because of a long C-terminal extension (Liu et al. 1995; Rosenzweig et al. 1995). The largest part of the intracellular domain consists of a serine/threonine protein kinase which is constitutively active in type II receptors (Wrana et al. 1994). So far, the crystal structure of intracellular kinase domains of TβR-I and ActR-IIB are known (Huse et al. 1999; Han et al. 2007). In type I receptors, a highly conserved 30 amino acid region immediately precedes the protein kinase domain. This region is called GS-box, because of a characteristic SGSGSG sequence (Wrana et al. 1994). Upon ligand binding, the phosphorylation of the GS-box is mediated by the type II receptor kinase (Wieser et al. 1995; Attisano et al. 1996), thus activating the kinase domain in type I receptors, which in turn is necessary for downstream signaling.

In addition to the signal-mediating type I and type II receptors, a third group of cell surface proteins are sometimes required for ligand binding and are therefore called type III- or co-receptors. This group contains betaglycan, endoglin, proteins from the EGF-CFC family (e.g. Cripto) and members of the repulsive guidance molecule (RGM) family (e.g. DRAGON) (Bernard et al. 2001; Corradini et al. 2009).

2.3. Signal transduction in the TGF-β superfamily

BMPs and other members of the TGF-β superfamily initiate their signal transduction by binding to two type I and type II receptor chains (ten Dijke et al. 1996; Massague 1998; Shi and Massague 2003) (see fig. 2.4).

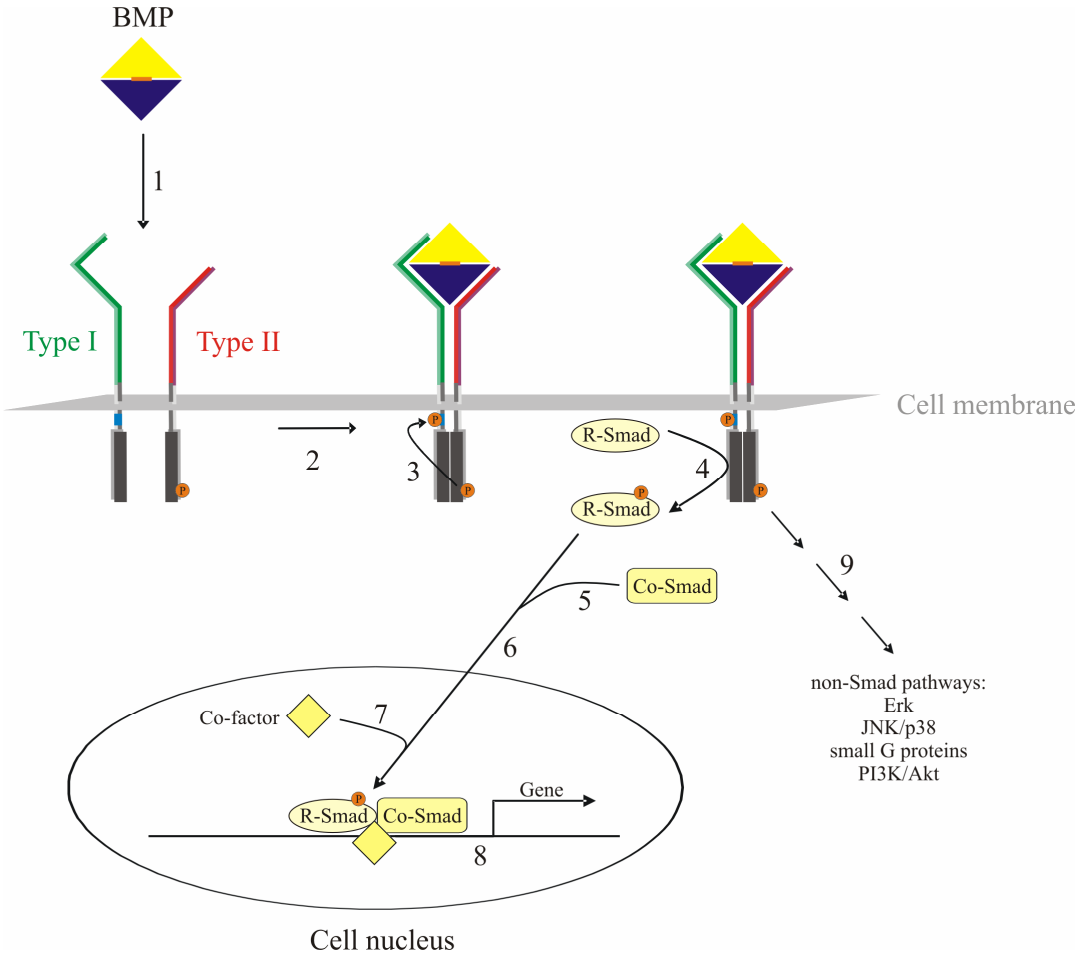

Figure 2.4 – Signal transduction in the TGF-β superfamily.
BMPs and other TGF-β family members bind first to their high affinity receptor (1), thus recruiting the low affinity receptor in the complex (2). Upon receptor oligomerization, the constitutively active type II receptor kinase domain transphosphorylates the type I receptor at its GS-box (3). The active type I receptor kinase subsequently phosphorylates a receptor-regulated Smad protein (R-Smad) (4). The latter forms a complex with a Co-Smad (5) and translocates to the nucleus thereafter (6). In combination with several co-factors (7), the Smad-complex acts as transcription factor regulating the activity of responsive genes (8). Besides this pathway, other non-Smad regulated pathways can be switched on upon activation of type I receptor kinase (9).

The ligand binds in a first step to its high affinity receptor, thus recruiting the low affinity receptor into the complex. Upon receptor hetero-oligomerization, the constitutively active

type II receptor kinase domain transphosphorylates the type I receptor at its GS-box. Thus activated, the type I receptor kinase subsequently transfers the signal to a family of intracellular mediators called Smad (Small mothers against decapentaplegic) proteins (Derynck et al. 1996). Up to date, eight Smads are known, which can be subdivided into three classes: receptor regulated Smads (R-Smads), common mediator Smads (Co-Smads) and inhibitory Smads (I-Smads) (Massague et al. 2005).

R-Smads are directly phosporylated by the activated type I receptor kinase domain and can be classified in two subgroups: Smad-1, -5, and -8 serve principally as substrates for the BMP and Müllerian inhibiting substance type I receptors (ActR-I, BMPR-IA, BMPR-IB, ALK-1), whereas Smad-2 and -3 are specific for TGF-β, activin, and nodal type I receptors (TβR-I, ActR-IB, ALK-7). After phosphorylation, the R-Smads dissociate from the type I receptor, thus forming a complex with Smad-4, also referred to as Co-Smad. This R-Smad/Co-Smad complex translocates to the nucleus and acts – in combination with several co-factors – as transcription factor regulating the activity of responsive genes. Smad-6 and -7 are inhibitory Smads that serve as decoys interfering with Smad/receptor or Smad/Smad interactions (Imamura et al. 1997; Nakao et al. 1997).

Furthermore, TGF-β ligands are also capable of signaling via pathways independent from Smad proteins. The activation of several pathways involving extracellular-signal regulated kinase (ERK), c-Jun N-terminal kinase (JNK), p38, small GTPases and phosphatidylinositol-3-kinase (PI3K)/Akt are summarized in the work of Zhang and colleagues (Zhang 2009).

2.4. Ligand receptor interaction: promiscuity and specificity

One hallmark of the TGF-β superfamily is the numeral discrepancy between the number of ligands (more than 30) and the number of available receptors (seven type I and five type II receptors). This fact indicates that a receptor will usually bind more than one ligand. Moreover, experimental data showed that most BMP ligands can also bind to more than one receptor of either subtype (Nickel et al. 2009). Figure 2.5 summarizes the potential of these ligand-receptor interactions within the TGF-β superfamily.

The interactions exhibits a high binding promiscuity between ligands and type I and type II receptors, a fact apparent especially in the BMP-subfamily and, to a minor degree, also in the activin- and TGF-β-subgroup.

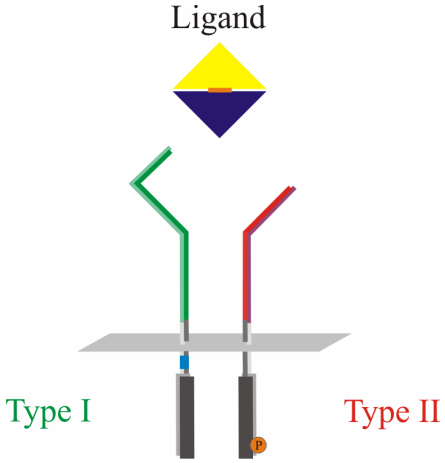

Alk-I TβR-I	low ←	TGF-β 1/2/3	high →	TβR-II
TβR-I ActR-IB	low ←	GDF-8/-11	high →	ActR-II ActR-IIB
ActR-IB	low ←	Activin A Inhibin	high →	ActR-II ActR-IIB
ActR-I	low ←	BMP-6/-7	high →	ActR-II ActR-IIB
BMPR-IA BMPR-IB	high ←	BMP-2/-4 GDF-5	low →	ActR-II ActR-IIB BMPR-II

Figure 2.5 – Promiscuity of ligand-receptor interaction.
Summary of the preferential receptor usage of particular TGF-β ligands. Graded differences in the binding affinities of individual ligand-receptor interactions are indicated. Scheme is constructed according to Nickel and colleagues. (Nickel et al. 2009).

The type I receptors BMPR-IA and BMPR-IB function as physiological relevant receptors for BMP-2/-4 (Koenig et al. 1994) and GDF-5 (Nishitoh et al. 1996), whereas ActR-I is specifically bound by BMP-6 (Ebisawa et al. 1999) and BMP-7 (ten Dijke et al. 1994). ActR-IB binds the activins and GDF-8 (Attisano et al. 1996; Rebbapragada et al. 2003) and TβR-I is specific for the TGF-βs and GDF-8 (Wrana et al. 1992; Rebbapragada et al. 2003). Regarding the type II receptor, ActR-II and ActR-IIB are of particular interest as they exhibit dual signaling specificity (Nagaso et al. 1999). ActR-II and ActR-IIB bind to activin A with high affinity, leading to an activation of the Smad-2/-3 pathway, whereas binding of BMP-2 occurs with lower affinity, resulting in activation of the Smad-1/-5-/-8 pathway (Attisano et al. 1992; Hoodless et al. 1996; Allendorph et al. 2006; Weber et al. 2007). Activin A and BMPs can exhibit opposing activities (Piek et al. 1999), probably due to competition for the ActR-II chain. Therefore, one receptor can be part of different signaling complexes, resulting in distinct cellular responses.

Furthermore, the binding affinity is essential for signal specificity. As an example, GDF-5 preferentially binds to BMPR-IB, but can also interact with BMPR-IA with a ~15-fold lower binding activity (Kotzsch et al. 2009). Clinical and biochemical studies on GDF-5 have shown that this receptor-specificity profile can be crucial for its biological functions (Nickel et al. 2005; Seemann et al. 2005).

On the basis of crosslink studies, the ligand-receptor interactions within the TGF-β superfamily can be classified into two binding modes (Nickel et al. 2009). The first binding mode includes TGF-β induced receptor assembly which is sequential and cooperative, whereas the second binding mode comprises that of BMP which is sequential and not cooperative.

The first group consists of the TGF-βs and activins, which bind in a first step to its high affinity type II receptors. In a sequential step, the low affinity type I receptor is recruited into the ligand-receptor type II complex, thus building a fully active signaling complex. The type I receptors for TGF-βs and activins can recognize the ligands that are bound to the type II receptor, but not ligands that are free in solution (Attisano et al. 1993; Ebner et al. 1993; Franzen et al. 1993; Bassing et al. 1994; Attisano et al. 1996). This sequential and cooperative mode of binding can be structurally explained with receptor-mediated conformational changes and receptor-receptor contacts which increase the binding affinity of the ligand-receptor type I interaction in the presence of the type II receptor, as shown for the TGF-β3/TβR-I/TβR-II complex (Groppe et al. 2008) and the TGF-β1/TβR-I/TβR-II complex (Radaev et al. 2010).

The second binding mode is most prominent in the interaction of BMPs with their receptors. As an example, BMP-2 bind first to the type I receptors BMPR-IA and BMPR-IB with high affinity, then recruiting their low-affinity type II receptor into the signaling complex. In contrast to the TGF-βs and activins, BMP-2 can also bind their type II receptors alone, although their binding affinity is 50- to 100-fold lower than that of the type I receptors (Kirsch et al. 2000c). Moreover, the binding affinity of the BMP-2/type II receptor complex remains unaffected by the presence of the type I receptor BMPR-IA (Allendorph et al. 2006; Weber et al. 2007; Heinecke et al. 2009), therefore ruling out cooperativity in the BMP-binding mode (Nickel et al. 2009).

In addition to the usage of distinct receptors, the specificity of signal transduction can be modulated at several cellular levels (Zeng et al. 2010).

In the extracellular space, a variety of soluble modulator proteins have been identified altering the biological activities of TGF-β ligands (Massague and Chen 2000; Balemans and Van Hul

2002). In principle, these modulator proteins alter the concentration of free ligands available for receptor interaction by binding to the ligand and thereby preventing its interaction with the receptors. Prominent inhibitors for TGF-β ligands are, for example, noggin (Groppe et al. 2002), follistatin (Harrington et al. 2006), members of the chordin family (Zhang et al. 2008) and the CAN family (Avsian-Kretchmer and Hsueh 2004).

At the cell surface, signaling is regulated by various receptor proteins classified as pseudo- and co-receptors (Corradini et al. 2009). BAMBI, as a prototype for pseudo-receptors, resembles the extracellular domain of type I receptors, but lacks the intracellular serine/ threonine kinase domain (Onichtchouk et al. 1999). Therefore, BAMBI interferes with the heterotetrameric receptor complex and the signal transduction to Smad proteins. Co-receptors, such as Betaglycan and members of the RGM family (e.g. DRAGON), act as facilitators and enhancers of signaling by elevating the binding affinities of TGF-β ligands to their receptors (Lopez-Casillas et al. 1993; Samad et al. 2005).

Within the cell, signaling can be controlled at several stages (Moustakas et al. 2001). For example, the inhibitory Smad protein Smad-6 and -7 or transcriptional repressors (Wotton and Massague 2001) can interrupt the activity. Phosphatases (Chen et al. 2006) or ubiquitination-dependent proteolysis (Zhu et al. 1999) terminates receptor signaling. Furthermore, intracellular crosstalks between TGF-β/BMP and other pathways have significant influence on BMP mediated signaling (Guo and Wang 2009).

2.5. Ligand-receptor interplay in the case of heterodimeric BMP-ligands

TGF-β ligands were described in the previous sections as homodimers. However, TGF-β ligands also exist in a heterodimeric form. Heterodimerization was first observed in inhibins and activins (Ling et al. 1986), where activin is composed of the two beta-subunits of inhibin A and B linked by interchain disulfide bonds. In addition, heterodimeric forms of TGF-β 1 and 2 have been identified in porcine platelets (Cheifetz et al. 1987).

Therefore, it was supposed that BMPs could also exist in heterodimeric forms with distinct biological properties since mixtures of the BMPs 2, 3 and 4 were found in highly-purified bovine bone extracts (Wozney et al. 1988). These analyses, however, could not readily distinguish mixtures of homodimeic from heterodimeric forms of the proteins.

Hints for heterodimeric BMPs were demonstrated by the finding that two BMP genes exist which are simultaneously expressed *in vivo* (Lyons et al. 1995). Such co-expression is

required for normal embryonic development (Katagiri et al. 1998; Solloway and Robertson 1999). In addition, *in vitro* studies showed that co-expression of BMP ligands can result in heterodimeric ligand formation (Aono et al. 1995; Hazama et al. 1995; Israel et al. 1996; Butler and Dodd 2003). Moreover, these results demonstrated that heterodimeric ligands can have increased activity compared to their homodimeric counterparts during a variety of biological processes, as for example shown in bone formation (Aono et al. 1995; Hazama et al. 1995; Israel et al. 1996; Butler and Dodd 2003; Zhu et al. 2004; Zhao et al. 2005; Zhu et al. 2006; Valera et al. 2010). Furthermore, heterodimers may play critical roles in embryonic development such as mesoderm induction (Suzuki et al. 1997) and dorsoventral patterning (Little and Mullins 2009).

The presence of BMP heterodimers *in vivo* was first elucidated in Drosophila, where the BMP homolog Decapentaplegic (Dpp) and Screw (Scw) is transported by the BMP binding proteins Sog/Tsg, leading to a robust patterning of the blastoderm embryo (Shimmi et al. 2005). Previously, the existence of a heterodimeric BMP-2/7 could also be verified in vertebrates, patterning the dorsoventral axis in the zebrafish Danio rerio (Little and Mullins 2009).

Deduced from the preferential receptor usage of the individual monomers (see fig. 2.5), heterodimeric ligands can probably extend the options for receptor recruitment and therefore for expanded variation in signaling. While the two type I and two type II receptor-binding interfaces of a homodimeric ligand are symmetrical, a heterodimeric ligand has built-in asymmetry between the pair of type I or II receptor-binding interfaces. Thus, up to four distinct receptors can be theoretically recruited by four structurally distinct receptor-binding interfaces of a heterodimeric ligand (see fig. 2.6).

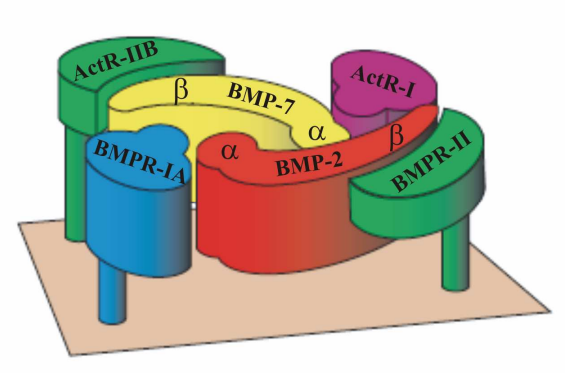

Figure 2.6 – Heterodimeric BMP signaling complex.

Predicted arrangement of a BMP-2/7 heterodimer associated with BMPR-IA and ActR-I as type I receptors and BMPR-II and ActR-IIB as type II receptors. α, β: α-helix and β-strands of ligand monomers, respectively. Scheme is modified according to (Little and Mullins 2009).

With regard to the type I receptor interaction, distinct receptor recruitment for BMP-2/7 has been shown in zebrafish by forming a heteromeric complex with type I receptors ALK-3/-6 and ALK-8, which is the functional orthologue of mammalian ALK-2 in fishes (Little and Mullins 2009). Distinct receptor type I usage has been also demonstrated in human mesenchymal stem cells, where a BMP-2 homodimer can signal via a heterodimeric BMPR-1A/ActR-I complex (Lavery et al. 2008).
However, structural and functional analyses of heterodimeric ligands are not available to date. Therefore, the exact mode of heterodimeric ligand-receptor interaction remains unknown.

2.6. Structural aspects of ligand-receptor interaction using the example of BMPR-IA

In recent years, several crystal structures of TGF-β ligands bound to the extracellular domains of type I and type II receptors have been determined to explain the mechanisms underlying promiscuity and specificity. Up to date, he following crystal structures of TGF-β ligands in combination with their high affinity receptors are described: BMP-2/BMPR-IA (Kirsch et al. 2000b; Keller et al. 2004b), TGF-β3/TβR-II (Hart et al. 2002), BMP-7/ActR-II (Greenwald et al. 2003), Activin A/ActR-IIB (Thompson et al. 2003; Greenwald et al. 2004), BMP-2/BMPR-IB (Kotzsch et al. 2008) and GDF-5/BMPR-IB (Kotzsch et al. 2009).
In addition, the structures of the following ternary complexes are known: BMP-2/ BMPR-IA/ActR-II (Allendorph et al. 2006), BMP-2/BMPR-IA/ActR-IIB (Weber et al. 2007), TGF-β3/TβR-I/TβR-II (Groppe et al. 2008) and TGF-β1/TβR-I/TβR-II (Radaev et al. 2010).
Furthermore, structures of extracellular receptor domains in its free forms are published: ActR-II (Greenwald et al. 1999), TβR-II (Boesen et al. 2002), BMPR-II (Mace et al. 2006) and BMPR-IA (Klages et al. 2008).

For the receptor BMPR-IA, three crystal structures of its extracellular domain (ECD) in complex with BMP-2 are described, showing that binding and structure of BMPR-IA are highly conserved, although crystallization conditions varied in all three cases (Keller et al. 2004b; Allendorph et al. 2006; Weber et al. 2007). Recently, the structure of BMPR-IA_{ecd} in its unbound conformation was determined by NMR (Klages et al. 2008), showing that its core structure is largely superimposable to the structure of the receptor with bound BMP-2 (see fig. 2.7).

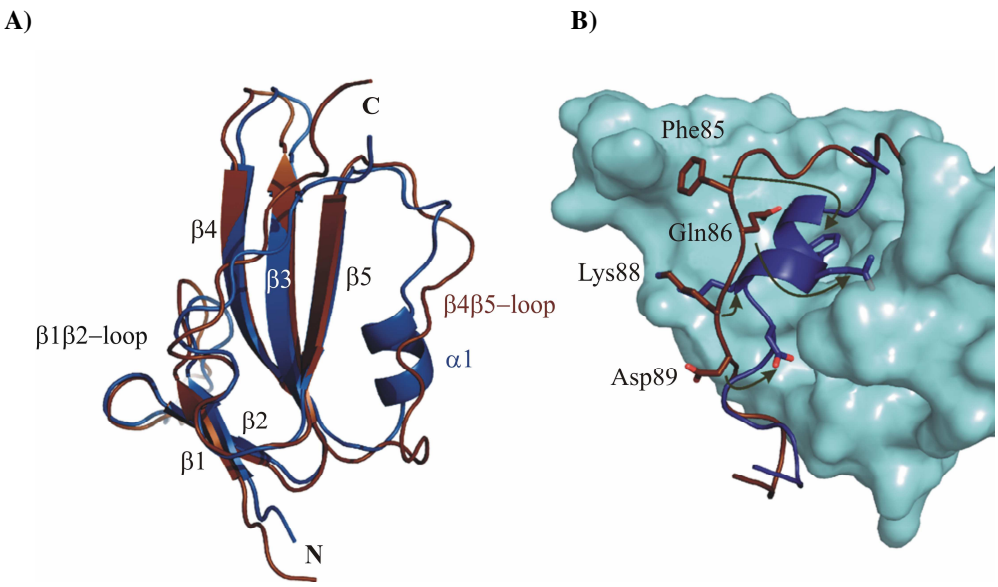

Figure 2.7 – Structure comparison of free and bound BMPR-IA (according to Klages et al. 2008)**.**
A) Cartoon representation of the NMR structure of free BMPR-IA (brown) (PDB entry 2K3G; Klages et al. 2008) and BMPR-IA in the binary complex with BMP-2 (blue) (PDB entry 1REW; Keller et al. 2004b). The core of both receptors represented by the three-stranded β-sheet is highly similar, but clear differences are visible for single loops connecting the β-strands. The β4β5-loop in the bound BMPR-IA harbors a 1.6-turn helix which is missing in its free state.
B) Structural changes in the β4β5-loops of free and bound BMPR-IA. BMPR-IA bound to the ligand BMP-2 (cyan surface) is superimposed with free BMPR-IA. Only the β4β5-loops of free BMPR-IA (brown) and bound BMPR-IA (blue) are shown as backbone trace. Single residues are represented as sticks. The significance of the rearrangement of the β4β5-loop is illustrated by the shifts of Phe85 and Gln86 of BMPR-IA into binding-competent positions. Gln86 represents the main binding determinant in the BMP-2/BMPRIA interaction, demonstrating that a stable complex can be formed only if the β4β5-loop adopts a helical structure.

Nevertheless, the binding epitope of BMPR-IA to BMP-2 remarkably differs by the absence of a short α-helix in the β4β5-loop of the free receptor. Importantly, the α-helical segment of BMPR-IA is in the center of the BMP-2 binding epitope and carries the hot spots of binding, Phe85 and Gln86, for binding to BMP-2. Upon complex formation with BMP-2, disorder-to-order transition occurs in the receptor, indicating an inherent flexibility of a main binding element.
However, the question of whether the binding promiscuity of BMPR-IA is linked to structural plasticity of its binding interface remains open, since additional structural data regarding the ligand/BMPR-IA interaction are not available yet.

2.7. Aim of the study

Members of the TGF-β superfamily are characterized by a highly promiscuous ligand-receptor interaction, as readily apparent from the numeral discrepancy of more than 30 ligands which signal only via seven type I and five type II receptors. Some questions regarding the molecular recognition between ligands and receptors enabling the promiscuous interaction are partially answered by the available structural data. However, many issues on both sides of the ligand-receptor interaction remain unsolved.

From the ligand's point of view, BMP heterodimers combine different properties regarding their monomeric subunits. Therefore, they are valuable tools for studying the interplay between different sets of receptors and provide new insights into how the various BMP signals can be generated.

- Hence, the first goal of this work was the expression and purification of the heterodimers BMP-2/6 and -2/7. Subsequently, their biochemical and biological characteristics were studied using BIAcore analysis and cell-based activity assays to shed light on the heterodimer's mode of signaling (see chapter 4).

From the receptors' point of view, the BMP receptor type IA is a prime example known for its promiscuous binding to different BMP ligands. The extracellular domain of BMPR-IA is subject to a large conformational change on binding to its ligand BMP-2, whereas the extracellular binding interface of BMPR-IA is mainly unfolded in its unbound form, requiring a large induced fit to adopt the conformation when bound to BMP-2.

- Therefore, the second goal of this work was to identify whether the binding promiscuity of BMPR-IA is linked to structural plasticity of its binding interface. An antibody Fab fragment against BMPR-IA was obtained which blocks binding to BMP-2 and thus occupies an epitope on BMPR-IA that overlaps with that of BMP-2. Structural and functional analyses of this antibody-BMPR-IA interplay should therefore provide useful information regarding the mechanisms how ligand-receptor interactions are generated specifically within the BMP system (see chapter 5).

3. Materials and methods

The following chapter covers the materials and methods used in this work. First, a list of all abbreviations in this work is given. Second, all materials are listed in alphabetical order. Lastly, methods are arranged thematically following a timeline order within each section. Solutions and tools used in every method are listed at the end of each section.

3.1. List of abbreviations

ActR-I	Activin receptor type I
ActR-IB	Activin receptor type I B
ActR-II	Activin receptor type II
ActR-IIB	Activin receptor type II B
ALK	Activin like kinase
ALP	Alkaline phosphatase
β-Me	β-Mercaptoethanol
BMP	Bone Morphogenetic Protein
BMPR-IA	Bone morphogenetic protein receptor I A
BMPR-IB	Bone morphogenetic protein receptor I B
BMPR-II	Bone morphogenetic protein receptor II
bp	Base pair
°C	Temperature in degree Celsius
cDNA	complementary DNA
Da	Dalton
dH_2O	distilled water
ddH_2O	double distilled water
DNA	Deoxyribonucleic acid
E.coli	*Escherichia coli*
ecd	extracellular domain
Fab	Fragment antigen binding
fig.	Figure
FPLC	Fast protein liquid chromatography

GDF	Growth and differentiation factor
HPLC	High-performance liquid chromatography
K_D	Dissociation constant
k_{off}	Dissociation rate
k_{on}	Association rate
LB	Luria Broth
M	molar
M_w	molecular weight
OD	optical density
PAGE	Polyacrylamide gel electrophoresis
PCR	Polymerase chain reaction
PDB	Protein data bank
r.m.s.d.	Root mean square deviation
rpm	revolutions per minute
RT	room temperature
RU	resonance unit
SDS	Sodium dodecyl sulphate
sec	second
Smad	Small mothers against decapentaplegic
TB	Terrific Broth
TFA	Trifluoroacetic acid
TGF-β	Transforming growth factor β
TβR-I	Transforming growth factor β receptor I
TβR-II	Transforming growth factor β receptor I
W	Watt

All other abbreviations used in this work are in line with the International System of Units of the Bureau International des Poids et Mesures (BIPM) (BIPM 2006).

The one- and three-letter system of amino acids is in according with the recommendations of the IUPAC-IUB Joint Commission on Biochemical Nomenclature (JCBN) (JCBN 1984). The one-letter system is used for the description of protein variants. The abbreviation rhBMPR-IA F60A defines the recombinant protein of a variant of human BMPR-IA in which the phenylalanine at position 60 is replaced by alanine. Genes are italicized and spelled with a lower case (e.g. *lac*).

3.2. Materials

3.2.1. Antibodies

AbyD1556:	monoclonal	(Antibodies by Design)
AbyD1564:	monoclonal	(Antibodies by Design)

Antibodies AbyD1556 and AbyD1564 are recombinant antibody Fab proteins and were provided by the company Antibodies by Design (Martinsried, Germany). Initially, eight antibodies were selected after phage display to BMPR-IA$_{ecd}$. Antibody activity was determined by western blot, cell assays and interaction analysis during a diploma thesis (Harth 2006). Two of them exhibiting the highest affinities, AbyD1556 and AbyD1564, were produced in mg quantities for further experiments.

Actin (H-300):	(No. sc-10731, Santa Cruz, Heidelberg, Germany)
goat anti-mouse IgG-HRP:	(No. sc-2031, Santa Cruz, Heidelberg, Germany)
pSmad 1,5:	(No. 9516, Cell Signaling, Danvers, MA, USA)
pSmad 2,3:	(No. 3101, Cell Signaling, Danvers, MA, USA)

All antibodies listed above were used for western blotting according to manufacturer's protocols, if not mentioned otherwise.

3.2.2. Bacterial strains

E.coli AD 494 (DE3): (Novagen)
Δ*ara−leu7697* Δ*lacX74* Δ*phoAPvuII phoR* Δ*malF3* F'*[lac+(lacIq) pro] trxB*(Kan^R)(DE3)

E.coli BL21 (DE3): (Novagen)
F– *ompT hsdSB (rB– mB–) gal dcm* (DE3)

E.coli MM294: (ATCC No. 39607)
F- *supE44 hsdR17 endA1 thi-1 lambda*

E.coli Origami B (DE3): (Novagen)
F– *ompT hsdSB (rB– mB–) gal dcm lacY1 ahpC* (DE3) *gor522*::Tn*10* (TcR) *trxB*(Kan ^{R}, Tet ^{R})

E.coli Rossetta (DE3) pLysS: (Novagen)
F– *ompT hsdSB (rB– mB–) gal dcm* (DE3) pLysSRARE (Cam ^{R})

3.2.3. Cell lines

ATDC5:	murine chondrocytic cells	(RIKEN, Ibaraki, Japan, No. RCB0565)
C2C12:	murine myoblasts	(ATTCC, No. CRL-1772)
IH-1:	human myeloma cells	(kind gift from Prof. Dr. Anders Sundan, NTNU, Trondheim, Norway)
INA-6	human myeloma cells	(kind gift from Dr. Martin Gramatzki, Erlangen, Germany)

3.2.4. Chemicals

The following companies supplied basic chemicals of highest purity: Amersham, Bio-Rad, Biolabs, Boehringer Mannheim, Fluka, Gibco-BRL, MBI Fermentas, Merck, Pharmacia, Roth, Serva and Sigma. All solutions were prepared using deionized water in Millipore quality.

3.2.5. Growth factors

Activin A:	Sf-9; recombinant; human	(kind gift from Prof. Dr. Walter Sebald)
BMP-2:	*E.coli*; recombinant; human	(kind gift from Prof. Dr. Walter Sebald)
BMP-2:	CHO; recombinant; human	(R&D Systems, Minneapolis, MN)
BMP-6:	*E.coli*; recombinant; human	(kind gift from Prof. Dr. Walter Sebald)
BMP-6:	NSO; recombinant; human	(R&D Systems, Minneapolis, MN)
BMP-7:	CHO; recombinant; human	(R&D Systems, Minneapolis, MN)
IL-6:	*E.coli*; recombinant; human	(kind gift from Prof. Dr. Walter Sebald)
TGF-β 2:	*E.coli*; recombinant; human	(kind gift from Dr. Joachim Nickel)

3.2.6. Kits

Agarose gel extraction:	Gel Extraction System (Promega)
DNA preparation:	Plasmid Mini Kit (Promega)
	Plasmid Maxi Kit (Qiagen)

3.2.7. Oligonucleotides

Oligonucleotides were manually designed using the primer generator tool (http://www.basic.northwestern.edu/biotools/oligocalc.html). The company Thermo Fischer Scientific (Ulm, Germany) provided the following oligonucleotides:

Oligonucleotides for BMPR-IA$_{ecd}$ mutant genesis:

F60A 5´:	5´-CTA ATG GAC ATT GCG CTG CCA TCA TAG AAG-3´
F60A 3´:	5´-CTT CTA TGA TGG CAG CGC AAT GTC CAT TAG-3´
I62A 5´:	5´-GGA CAT TGC TTT GCC GCC ATA GAA GAA GAT G-3´
I62A 3´:	5´-CAT CTT CTT CTA TGG CGG CAA AGC AAT GTC C-3´
E64A 5´:	5´-GCT TTG CCA TCA TAG CAG AAG ATG ACC AGG G-3´
E64A 3´:	5´-CCC TGG TCA TCT TCT GCT ATG ATG GCA AAG C-3´
D67A 5´:	5´-CAT AGA AGA AGA TGC CCA GGG AGA AAC CAC-3´
D67A 3´:	5´-GTG GTT TCT CCC TGG GCA TGT TGT TGT ATG-3´
M78A 5´:	5´-GCT TCA GGG TGT GCG AAA TAT GAA GGA TCT G-3´
M78A 3´:	5´-CAG ATC CTT CAT ATT TCG CAC ACC CTG AAG C-3´
K79A 5´:	5´-GCT TCA GGG TGT ATG GCA TAT GAA GGA TCT G-3´
K79A 3´:	5´-CAG ATC CTT CAT ATG CCA TAC ACC CTG AAG C-3´
E81A 5´:	5´-GGG TGT ATG AAA TAT GCG GGA TCT GAT TTT CAG-3´
E81A 3´:	5´-CTG AAA ATC AGA TCC CGC ATA TTT CAT ACA CCC-3´
F85A 5´:	5´-GAA GGA TCT GAT GCT CAG TGC AAA GAT TCT CC-3´
F85A 3´:	5´-GGA GAA TCT TTG CAC TGA GCA TCA GAT CCT TC-3´
K92A 5´:	5´-CAA AGA TTC TCC AGC AGC CCA GCT ACG-3´
K92A 3´:	5´-CGT AGC TGG GCT GCT GGA GAA TCT TTG-3´
Q94A 5´:	5´-CTC CAA AAG CCG CAC TAC GCC GGA C-3´

Q94A 3´: 5´-GTC CGG CGT AGT GCG GCT TTT GGA G-3´
R97A 5´: 5´-GCC CAG CTA CGC GCG ACA ATA GAA TGT TG-3´
R97A 3´: 5´-CAA CAT TCT ATT GTC GCG CGT AGC TGG GC-3´
I99A 5´: 5´-CTA CGC CGG ACA GCA GAA TGT TGT CGG -3´
I99A 3´: 5´-CCG ACA ACA TTC TGC TGT CCG GCG TAG -3´

pET32a 5´: 5´-CCG TGG TAT CCC GAC TCT GCT GCT G -3´
pET32a 3´: 5´-GTC ACG CTG CGC GTA ACC ACC ACA C -3´

3.2.8. Plasmids

Maps of all plasmids including the expressed proteins are provided in the result section.

pET28b: (Novagen)
Kan ^{R}, T7*lac*, His-Tag, T7-Tag, protease T, f1 ori

modified pET32a: (Novagen) (LaVallie et al. 1993)
Amp^{R}, T7*lac*, His-Tag, S-Tag, Trx-Tag, protease T and E, f1 ori
Position of thrombin cleavage site is relocated directly in front of the target gene due to deletion of base pair 223 – 297 of the original vector (Kirsch et al. 2000a).

QKA:
Kan ^{R}, Cam ^{R}, T5*lac*, pBR322/Col E1 ori
QKA is an in-house vector consisting of a modified pQE80L/pet24 construct.

3.2.9. Restriction enzymes

Restriction enzymes were obtained from MBI Fermentas (St. Leon-Rot, Germany) and New England Biolabs (Frankfurt am Main, Germany). DNA restriction experiments were performed according to manufacturer's protocols, if not mentioned otherwise.

3.2.10. Sterile working tools

Laboratory glassware were sterilized for 6 h at 180 °C using an hot air oven (Trockenschrank Typ ST5060, Heraeus). Buffer, medium and plastic vessels were autoclaved for 30 min at 120 °C and 1.2 bar (Varioklav Dampfsterilisator, H+P Labortechnik GmbH). Solutions of thermolabile substances were sterile filtered via an aseptic syringe filter with a pore diameter of 0.22 µm. The company Greiner supplied amicrobic plastic material for cell culture. Prior application, flexible dialysis tubes (Zellutrans 3.5 kDa exclusion size, Roth) were first incubated for 1 h at 60 °C in buffer (20 g/l $NaHCO_3$, 0.4 g/l EDTA), then washed thoroughly with dH_2O and finally stored in 20 % ethanol at 4 °C.

3.3. Molecular biological methods

3.3.1. Generation of BMP ligand and BMP receptor expression constructs

The gene representing the mature part of human BMP-2 (residue 283 – 396, SWISS-PROT No. P12643) plus an N-terminal MA extension and the mature part of human BMP-6 (residue 375 – 513, SWISS-PROT No. P22004) with an N-terminal MAPT elongation were cloned into the QKA vector using EcoRI and BamHI restriction sites. Prof. Dr. Walter Sebald provided both expression constructs.
The genetic code of the mature part of human BMP-7 (residue 293 – 431, SWISS-PROT No. P18075) with flanking NcoI and BamHI restriction sites was assembled from synthetic oligonucleotides and cloned into pPCR-Script (GENEART). After enzymatic cleavage and agarose gel purification the BMP-7 gene was ligated with pET28b vector.

The extracellular domain of BMPR-IA (residue 24 – 152, SWISS-PROT No. P36894) was cloned into the modified pET32a vector (Kirsch et al. 2000a) as a thioredoxin fusion protein. After cleavage of the thioredoxin part with thrombin, a N-terminal GSGAMA extension remained in the receptor. Dr. Dionys Weber made the expression construct for BMPR-IA_{ecd} available.

For DNA amplification, the plasmids were transformed into *E.coli* MM 294, cultured in LB medium and transferred to agar plates containing the appropriate antibiotics (see 3.5.4.). Minipreperations of 5 – 10 colonies were performed. Afterwards, Dr. Wolfgang Vaichtinger tested the samples for correct DNA sequence (service of the Department of Human Genetic, Biocenter, University of Würzburg). Positive clones were subjected to DNA maxipreparation, their DNA was transformed into appropriate expression hosts (see result section) and stored as glycerol stocks at -20 °C as described in section 3.5.2.

3.3.2. Mutagenesis of BMPR-IA$_{ecd}$

Mutants of BMPR-IA$_{ecd}$ were generated using the two step PCR method.
In the first step, the mutation of interest within the coding sequence was amplified using two gene-specific forward and reverse primers resulting in a 5´ and 3´ part of BMPR-IA$_{ecd}$-DNA respectively. Both parts overlap in the mutation area and include the mutation and one unique restriction site at the other end (5´ end: NcoI, 3´end: Bpu1102I). The second PCR step concatenated the 5´ and 3´ part and amplified therefore the whole gene of interest using the outer forward and reverse primer. The detailed PCR programs for the two steps are summarized in table 3.1.

Table 3.1 – PCR programs for the generation of BMPR-IA$_{ecd}$ mutants

1. PCR			2. PCR		
Temperature [°C]	Duration [min]		Temperature [°C]	Duration [min]	
95	2		95	2	
95	0.5		95	0.5	
65	0.5	30 cycles	64	0.5	30 cycles
72	2		72	2.5	
72	10		72	10	
4	∞		4	∞	

In this process, primers should be between 25 and 45 bases in length with a melting temperature Tm of ≥ 75 °C (optimum is 78 °C). The mutation should be located in the middle of the primer with flanking sequences of 10 – 15 bases on each side. The minimum GC

content is 40 %. Besides that, the primer should terminate in one or more G or C bases at the 3´end. The melting temperature was calculated using equation 3.1, in which N is the primer length in bases, % GC and % mismatch are whole numbers. The used oligonucleotides are listed in chapter 3.2.7.

Equation 3.1: $Tm\ (in\ °C) = 81.5 + 0.41 \cdot (\%\ GC) - (675 / N) - \%\ mismatch$

After purification via agarose gel electrophoresis (see 3.3.3.), the BMPR-IA_{ecd} insert was cleaved with NcoI and Bpu1102I restriction enzyme, purified again and ligated with an equally processed modified pET32a vector. Subsequent steps for generating expression constructs were performed as depicted in chapter 3.3.1.

3.3.3. Agarose gel electrophoresis

To analyze PCR reactions and to purify DNA preparations, agarose gel electrophoresis was performed. 1 µg/ml ethidium bromide was added to 1 % (w/v) agarose gel buffered with TAE buffer (see below). DNA were mixed with DNA loading buffer (Gel Loading Dye, Blue (6X), NEB) and applied to the gel. According to the grade of DNA separation, the gel was run with a current of 150 mA (PHERO-stab. 500, Biotec-Fischer) for approximately 20 – 40 min in TAE buffer. DNA bands were visualized using an UV illuminator and recorded using the GeneTools analysis software (Syngene).

TAE buffer: 40 mM Tris/HCl pH 8.0
20 mM NaAc
1 mM EDTA

3.4. Protein chemical methods

3.4.1. Polyacrylamide gel electrophoresis (SDS-PAGE)

Polyacrylamide gels were prepared accordingly to a protocol from Laemmli (Laemmli 1970) (see table 3.2). The listed amount is sufficient for two gels. SDS-PAGE was carried out using the Perfect Blue TM Vertical Electrophoresis System (PEQLAB).

Table 3.2 – Components of a SDS polyacrylamide gel

Solution	Stacking gel (5 %)	Separating gel (12 %)
4x lower Tris	-	2.5 ml
4x upper Tris	1.25 ml	-
AA / BAA	0.5 ml	4.0 ml
ddH_2O	3.2 ml	1.5 ml
Glycerin	-	2.0 ml
40 % (w/v) APS	12 µl	14 µl
TEMED	12 µl	14 µl

First, the separating gel was cast between two glass plates which were separated from each other by spacers. To avoid impurities the glass plates were purified before with 70 % ethanol. 2 cm space from the upper edge of the plates remained free for the stacking gel. The separating gel was covered with a layer of dH_2O to guarantee a horizontal planar layer of separating gel. After removing of dH_2O, the stacking gel was poured over the separating gel. A ridge for samples was put into the stacking gel. After gel polymerization the gel was inserted into a gel chamber filled with 1x SDS running buffer.

The protein samples were diluted with SDS sample buffer with a ratio of 1:1 and heated to 95 °C for 5 min. After loading the samples including protein marker (see 3.4.3) as a control, protein separation was carried out at 40 mA per gel for approximately 50 min (PHERO-stab. 500, Biotec-Fischer). Finally, proteins were stained either with coomassie blue (> 1 µg protein) or with silver (< 1 µg Protein) (see 3.4.2).

AA / BAA solution:	30 % acrylamide 1 % N, N' methylenebisacrylamide stored at 4 °C after filtration
40 % (w/v) APS:	400 mg APS 1 ml ddH_2O stored at 4 °C
4x lower Tris:	1.5 M Tris/HCl, pH 8.8 0.4 % (w/v) SDS
4x upper Tris:	0.5 M Tris/HCl, pH 6.8 0.4 % (w/v) SDS
5x SDS running buffer:	125 mM Tris/HCl, pH 8.6 0.95 M glycin 0.75% (w/v) SDS
SDS sample buffer:	62.5 mM Tris/HCl, pH 6.8 2 % (w/v) SDS 20 % glycerin (purchased as 87 % solution) 2% (w/v) bromphenol blue (under reducing conditions: 2 % (v/v) β-Mercaptoethanol was added)

3.4.2. Protein staining

Coomassie blue staining

After finishing gel electrophoresis (see 3.4.1), the stacking gel was removed. The separating gel was incubated for 30 min in staining solution, destained afterwards and treated with 30 % methanol for 1 h. Finally, the gel was packed between two cellophane films, fixed with a frame and dried at room temperature.

Staining solution: 10 g coomassie brilliant blue R250
0.4 l glacial acetic acid
1.6 l methanol
2.0 l dH_2O

Destaining buffer: 0.5 l isopropanol
0.5 l glacial acetic acid
4.0 l dH_2O

Silver staining

Upon completion of electrophoresis (see 3.4.1), the SDS separating gel was put into buffer 1 for 5 min to fix the protein bands in the gel. Then, the gel was cleansed and incubated in dH_2O for 5 min. Subsequently, it was placed in buffer 2 for 5 min, followed by incubation in buffer 3 for 1 min. After washing three times with dH_2O for 5 sec, the gel was transferred to buffer 4 for 8 min. Thereafter, it was washed thoroughly with dH_2O (five times) and treated with buffer 5 until all protein bands appeared. To stop the staining reaction, the gel was rinsed with 1 % glacial acetic acid and washed with dH_2O afterwards. Finally, the gel was treated with 30 % methanol for 1 h, packed in cellophane film, fixed with a frame and dried at room temperature.

Buffer 1: 60 ml 50 % (v/v) acetone in dH_2O
1.5 ml 50 % (w/v) trichloroacetic acid (TCA) in dH_2O
25 µl formaldehyde (purchased as 37 % solution)

Buffer 2: 60 ml 50 % (v/v) acetone in dH_2O

Buffer 3: 100 µl 10 % (w/v) sodium-thiosulphate-pentahydrate ($Na_2S_2O_3 \cdot 5H_2O$) in dH_2O
60 ml dH_2O

Buffer 4: 800 µl 20 % (w/v) silver nitrate ($AgNO_3$) in dH_2O (store in dark)
600 µl formaldehyde (purchased as 37 % solution)
60 ml dH_2O

Buffer 5: 1.2 g sodium carbonate (Na_2CO_3)
25 µl formaldehyde (purchased as 37 % solution)
25 µl 10 % (w/v) sodium thiosulphate pentahydrate ($Na_2S_2O_3 \cdot 5H_2O$) in dH_2O
60 ml dH_2O

3.4.3. Molecular weight standards for SDS-PAGE

A protein marker (LMW Kit, GE Healthcare) was loaded on every SDS gel (see 3.4.1) to determine the size of all protein bands.
The marker consisted of different molecular weight standards listed in table 3.3. According to the staining procedure 1 – 5 µl marker were used.

Table 3.3 – Molecular weight standards for SDS-PAGE

Protein	Molecular weight M_w [kDa]	Concentration [µg / 5 µl]
Phosphorylase b	97	0.67
Albumin	66	0.83
Ovalbumin	45	1.47
Carbonic anhydrase	30	0.83
Trypsin inhibitor	20.1	0.8
α-Lactalbumin	14.4	1.16

3.4.4. Photometric determination of protein concentrations

The protein concentration in solution was calculated with the aid of the Lambert Beer law.

Lambert-Beer law: $E_{280nm} = \varepsilon_{280nm} \cdot c \cdot d = (\varepsilon_{280nm} \cdot c_m \cdot d) \cdot (M_W)_{-1}$

The extinction at 280 nm (E_{280nm}) was determined photometrically via recording the UV absorption spectrum in the range from 250 nm to 320 nm (CARY 50 Bio UV-visible Spectrometer, Varion). The molar extinction coefficients (ε_{280nm} in M^{-1} cm^{-1}) and the molecular weights (M_W in g mol^{-1}) were computed via the ProtParamTool database

(Gasteiger E. 2005) (http://www.expasy.org/tools/protparam.html). The molar extinction coefficients and the molecular weights are summarized both in table 3.4 for all proteins used in this work. The coat thickness (d) is 1 cm, the dimension unit for the molar concentration c is mol l^{-1} and for the mass concentration c_m g l^{-1}.

Table 3.4 – Molecular weight and extinction coefficient ε

Protein	Molecular weight M_w [g mol^{-1}]	Extinction coefficient ε [M^{-1} cm^{-1}]
AbyD1556	49 674	72 810
AbyD1556 - BMPR-IA_{ecd}	64 334	77 885
AbyD1564	50 080	73 270
BMP-2 *E.coli* (monomer)	12 976	18 825
BMP-2 *E.coli*	25 952	37 650
BMP-2 CHO	25 810	37 650
BMP-6 *E.coli* (monomer)	15 944	21 805
BMP-6 *E.coli*	31 888	43 610
BMP-6 NSO	29 748	43 610
BMP-2/6	28 920	40 630
BMP-7 *E.coli* (monomer)	15 738	21 805
BMP-7 CHO	31 361	43 610
BMP-2/7	28 714	40 630
BMPR-IA_{ecd}	14 660	5 075
IL-6	20 813	10 220
TGF-β-2	25 440	54 860
Thioredoxin	14 084	14 060
Thioredoxin - BMPR-IA_{ecd}	28 582	18 962
Thrombin	35 437	65 770

3.4.5. Determination of protein concentrations using bicinchoninic acid assay

The bicinchoninic acid assay (BCA assay) was performed according to Smith and colleagues (Smith et al. 1985) to determine the protein concentration of whole cell lysates used in the Smad phosphorylation assay (see 3.10.4). 2 µl of whole cell lysates and a standard series with defined amount of BSA protein were transferred to a 96-well plate. Subsequently, solution A and B were mixed in a volume ratio of 49 to 1 and 200 µl of this mixture were added per well. The 96-well plate was incubated for approximately 45 minutes at 56 °C and protein concentration was determined thereafter by measuring the absorbance at 550 nm using an ELISA reader.

Solution A: 6.75 g $NaHCO_3$
2.9 g NaOH
5 g BCA
2.85 g sodium tartrate
500 ml dH_2O

Solution B: 1.84 g $Cu(II)SO_4$
80 ml dH_2O

3.4.6. Mass spectrometry

Dr. Werner Schmitz determined the molecular weight for all recombinant proteins produced within this work using an Electrospray-Fourier-Transformation-Ion-Cyclotron-Resonance-Mass-Spectrometer (ESI-FTICR-MS, Bruker).

3.4.7. Western blotting

Western blotting was performed to determine specific proteins in whole cell lysates used in the Smad phosphorylation assay (see 3.10.4).
First, proteins were separated via SDS-PAGE (see 3.4.1) using a prestained molecular weight marker (SDS 7B2, Sigma) (see table 3.5). Subsequently, they were blotted semidry on a nitrocellulose membrane (Protran, Whatman). For this purpose, 3 layers of Whatman paper, membrane, SDS gel and again 3 layers of Whatman paper were rinsed with blotting buffer and placed in this order into a blot chamber (PerfectBlue Semi-Dry-Electroblotter, PEQLAB). Then the proteins were transferred from the SDS gel to the membrane applying 250 mA current per blot for 39 min. Thereafter, the membrane was stained with Ponceau S to verify the blotting process. The membrane was washed several times with TBS buffer to remove Ponceau S completely and incubated afterwards in blocking buffer for 1 h at RT to block all unspecific binding sites. The linkage of the first antibody (in blocking buffer) to the immobilized proteins on the membrane was carried out overnight at 4 °C. The next day, the membrane was washed three times for 5 min with blocking buffer to remove the unbound fraction of the first antibody. Thereupon, the membrane was incubated with an appropriate second antibody (in blocking buffer) coupled with horseradish peroxidase (HRP) for 1 h at

RT. After another washing step with blocking buffer, the protein detection was conducted in a darkroom. 10 ml of luminol solution was mixed with 44 µl enhancer and 10 ml H_2O_2 solution and applied to the membrane. After incubation for 1 min, the membrane was drained carefully, enveloped in transparent film, transferred with a radiographic film (A3, Konica Minolta) to a casket and sealed impervious to light. It remained there, depending on the chemiluminescent signal strength, for 10 sec – 30 min, then the radiographic film was developed (Compact 35, Protec). Finally, the molecular weight standards visible on the membrane were sketched in the radiographic film according to their position on the membrane. For examination, blots were scanned in and the strength of bands was calculated using the program ImageJ 1.41o (http://rsb.info.nih.gov/ij/).

Table 3.5 – Molecular weight marker for Western blotting

Protein	Molecular weight M_w [kDa]
α_2-Macroglobulin	180
β-Galactosidase	116
Lactoferrin	90
Pyruvate kinase	58
Fumarase	48.5
Lactic dehydrogenase	36.5
Triosephosphate isomerase	26.6

Ponceau S:
0.2 % (w/v) Ponceau S
3 % (w/v) TCA

Blotting buffer:
25 mM Tris/HCl
192 mM glycine
20 % (v/v) methanol

TBS buffer:
10 mM Tris/HCl, pH 7.5
150 mM NaCl

Blocking buffer:
5 % (w/v) BSA or nonfat dry milk
0.1 % (v/v) Tween-20
in TBS buffer

Luminol solution:
22.5 mg luminol (3-aminophthalhydrazide) (2.5 mM)
0.5 ml DMSO
49.5 ml 100 mM Tris/HCl, pH 8.5
store at 4 °C

Enhancer:
37 mg p-Coumaric acid (90 mM)
2.5 ml DMSO
store at 4 °C

H_2O_2 solution:
6.1 µl H_2O_2 (purchased as 30 % solution)
10 ml 100 mM Tris/HCl, pH 8.5
freshly prepared prior usage

3.5. Expression of recombinant proteins in *E.coli*

3.5.1. Culture medium

LB medium:
10 g/l bacto trypton
5 g/l bacto yeast extract
10 g/l NaCl
pH 7.5

TB medium:
13.3 g/l bacto trypton
26.6 g/l bacto yeast extract
4.4 ml/l glycerine
autoclave
80 ml 10x phosphate buffer and appropriate antibiotics were added to 720 ml sterile TB medium before usage

10x phosphate buffer:
0.17 M KH_2PO_4
0.72 M K_2HPO_4
autoclave

Agar plate:
15.0 g agarose
800 ml dH_2O
autoclave
following components were added after cooling to 50 °C:
200 ml 5x ENB medium
2.5 ml 40 % (w/v) glucose (sterile)
0.5 ml thiamine (c = 10 mg/ml) (sterile filtered)
1 ml antibiotics (optional)
pour liquid mixture in petri dishes,
store at 4 °C after solidification

5x ENB medium:
40 g/l nutrient broth
25 g/l bacto pepton
17.5 g/l NaH_2PO_4
7.5 g/l KH_2PO_4
25 g/l NaCl
autoclave

Antibiotics (1000x):
50 mg/ml ampicillin
34 mg/ml chloramphenicol (diluted in ethanol)
30 mg/ml kanamycin
12.5 mg/ml tetracyclin

3.5.2. Storage of *E.coli* cultures

E.coli bacteria can be stored on agar plates only for a limited time. For long term storage (up to 3 years) they should be preserved in glycerol stocks which are prepared as follows:
40 ml LB medium were inoculated with one individual clone and were shaken with 150 rpm (Certomat RM, B. Braun) until the optical density at 550 nm (OD_{550}) reached 1.5. The culture was centrifuged with 3000 rpm (Minifuge T, Heraeus) for 15 min. The pellet was resuspended in 1 ml LB medium, mixed with 1 ml of sterile (87 % v/v) glycerol and stored at – 20 °C in screw-cap glass vials.

3.5.3. Generation of competent *E.coli* cells

E.coli cells were made competent according to a protocol of Chung (Chung et al. 1989). Briefly, a single colony was inoculated to 5 ml LB medium and incubated overnight at 37 °C with 130 rpm. 1 ml of this culture was transferred to 100 ml LB medium and incubated again until the OD_{550} reached 0.5. The solution was chilled on ice for 20 min and cells were collected by centrifugation at 1200 g for 5 min at 4 °C. The pellet was resuspended in 10 ml of ice cold TSS solution and stored as aliquots (200µl each) at – 80 °C.

TSS solution: 85 % LB medium
10 % (w/v) PEG 8000
5 % DMSO
50 mM $MgCl_2$, pH 6.5

3.5.4. Transformation of competent *E.coli* cells

E.coli cells were transformed according to the work of Hanahan (Hanahan 1983). Competent cells (see 3.5.3) were thawed on ice and 10 µl of a ligation mixture (10-100 ng DNA) were added. The cells were incubated for 30 min on ice followed by a heat shock for 90 sec at 42 °C and cooled immediately at 0 °C for 1 – 2 min. 500 µl LB medium was added and incubated on a shaker for 1 h with 150 rpm. 150 µl of transformed cells were streaked on agarose plates and deposited over night at 30 °C. Control experiments were performed in the same way (positive control: 20 ng of non cutted plasmid; negative control: 100 ng of cutted vector treated with ligase).

3.5.5. Expression of BMP ligands

Bacterial expression strains were transferred from glycerol stock to an agar plate and incubated overnight at 37 °C. An individual clone was picked from the plate and incubated in 2 ml TB medium while shaking it with 130 rpm (Certomat RM, B. Braun) for 8 h at 37 °C. Consequently, it was added to 800 ml TB medium and agitated overnight with 130 rpm at 37 °C. This overnight culture was used for large scale fermentation.

6 – 12 shaking flasks containing 800 ml TB medium (plus 200 µl 10 % (v/v) Antifoam) were inoculated each with 40 ml overnight culture and cultured with 130 rpm at 37 °C until the OD_{550nm} reached 0.5 – 0.7. The protein expression was induced with 1 mM IPTG and executed for 4 h again with 130 rpm at 37 °C. The cells were harvested via centrifuging for 20 min with 5000 rpm at 4° C (JA10 rotor, J2-21 centrifuge, Beckman). Sediments were resuspended with TBSE buffer (400 ml in total), combined and centrifuged again for 20 min. The pellet was weighed and stored in 20 g portions at – 80 °C. Typical yields were 3 – 6 g pellet per liter culture medium (see also table 4.1).

TBSE buffer: 10 mM Tris/HCl, pH 8.0
150 mM NaCl
1 mM EDTA
0.5 mM PMSF
0.1 % (v/v) β-mercaptoethanol
PMSF and β-mercaptoethanol were added just before use

3.5.6. Expression of BMP receptors

E.coli bacteria for large scale fermentation were treated as described in section 3.5.5.
6 – 12 shaking flasks containing 800 ml TB medium (plus 200 µl 10 % (v/v) Antifoam) were inoculated each with 40 ml overnight culture and shaken with 130 rpm at 30 °C until the OD_{550nm} reached 0.5. The flasks were cooled down to room temperature (20 °C) and shaken overnight with 130 rpm at 20 °C after induction of protein expression with 1 mM IPTG. At the next morning, the cells were harvested via centrifuging for 10 min with 6000 rpm at 4° C (JA10 rotor, J2-21 centrifuge, Beckman). Sediments were resuspended with TBS buffer, combined and centrifuged again for 10 min. The pellet was weighed and stored in 8 g portions at – 80 °C. Typical yields were 3 – 10 g pellet per liter culture medium (see also table 5.1).

TBS buffer: 20 mM Tris/HCl, pH 7.5
150 mM NaCl

3.6. Purification of recombinant proteins

3.6.1. Purification of BMP ligands

Purification of inclusion bodies

After expression (see 3.5.5.), the cell pellet was defrosted in 10 volumes (w/v) TBSE buffer at 4 °C. Cells were sonicated (System 585, Ultraschallkopf Typ 512/1204, KLM) at 300 W for 5 min while cooling with ice. The protein deposited in inclusion bodies was separated from cell debris by centrifugation for 30 min with 11500 rpm at 4° C (JA14 rotor, J2-21 centrifuge, Beckman). The supernatant was discarded, the cell pellet was resuspended in TBSE buffer and sonicated again for 3 min. After repeating the centrifugation step the sediment was washed with 200 ml TBSE buffer containing 1 % (v/v) Triton X 100 and spinned down once again. To remove Triton X 100, the inclusion bodies were resuspended one more time in TBSE buffer, centrifuged and stored in 7 g portions at – 80 °C. Typical yields were ~ 350 mg per g harvested cells (see also table 4.1).

Protein extraction from inclusion bodies

First, inclusion bodies were resuspended in equal volume of Tris buffer. This solution was adjusted to 6 M urea by mixing the three-fold volume (in relation to the Tris buffer) of calibration buffer with the inclusion bodies solution. A 30-fold excess (relating to the Tris buffer) of extraction buffer was added and stirred (Ultra-Turrax T 25, IKA) to obtain a homogeneous solution. After centrifuging for 30 min with 11500 rpm at 20° C, the proteins in the supernatant were subjected to cation exchange chromatography.

Tris buffer:	20 mM Tris/HCl, pH 7.5
	1 mM DTT
Calibration buffer:	20 mM Tris/HCl, pH 7.0
	10 M urea buffer
	50 mM NaCl
	5 mM EDTA
	1 mM DTT

Extraction buffer:	20 mM Tris/HCl, pH 7.0
	6 M urea buffer
	50 mM NaCl
	5 mM EDTA
	1 mM DTT

Cation exchange chromatography (SP Sepharose FF)

Cation exchange chromatography was performed at ambient temperature. 20 ml of the SP Sepharose FF (GE Healthcare) were filled in a glass column and equilibrated with five bed volumes extraction buffer (flowrate: 5 ml/min). The protein solution extracted from inclusion bodies were loaded to the column (5 ml/min) and washed with three bed volumes extraction buffer (2.5 ml/min). The proteins were eluted by hydrostatic flow using elution buffer and collected in fractions of 10 ml. Protein concentration was measured photometrically, the protein containing fractions were combined and protein concentration was adjusted to 20 mg/ml using ultrafiltration (YM3 membrane, Amicon stirring chamber, Millipore). Finally, the proteins were used immediately either for refolding or were stored at – 80 °C.

Column:	Econo glass column 25 · 100 mm (BioRad)
Column matrix:	SP Sepharose FF (GE Healthcare)
Pump:	Minipuls 3 (Gilson)
Elution buffer:	20 mM Tris/HCl, pH 8.0
	6 M urea buffer
	500 mM NaCl
	5 mM EDTA
	1 mM DTT

Refolding of BMP ligands

Renaturation of BMP-2 was carried out by diluting the purified protein (see 3.6.1) to a final concentration of 200 µg/ml into BMP-2 refolding buffer. Usually 1 or 2 liters of buffer were prepared. Prior to use, the buffer was degassed, then BMP-2 was added dropwise while stirring gently the buffer. The refolding solution was stored in a dark place at 21 °C for 5 days. Refolding of BMP-2/6 was performed in a similar way as BMP-2. However, the final concentrations of BMP-2 and BMP-6 were 50 µg/ml and 100 µg/ml, respectively. Renaturation took place at 14 °C for at least 5 days.
During BMP-2/7 refolding, BMP-2 and BMP-7 was diluted to 50 µg/ml and 100 µg/ml as well. The solution was kept at 4 °C for 7 days.

BMP-2 and BMP-2/6 refolding buffer:	100 mM Tris/HCl, pH 8.0
	5 mM EDTA
	25 mM CHAPS
	1 M arginin
	5 mM cysteamin reduced
	0.5 mM cystamin oxidized
	degas and prechill as indicated
BMP-2/7 refolding buffer:	50 mM Tris/HCl, pH 8.0
	5 mM EDTA
	25 mM CHAPS
	2 M LiCl
	600 mM urea
	5 mM cysteamin reduced
	0.5 mM cystamin oxidized
	degas and prechill to 4 °C

Cation exchange chromatography (Fractogel EMD SO_3^- (S))

After renaturation, the refolding buffer was exchanged for 1 mM HCl via ultrafiltration as follows: The pH was adjusted to 3.0 by adding concentrated HCl. Then, the solution was transferred to a crossflow machine (Millipore) with an YM 10 membrane and concentrated to

200 ml. 900 ml of 1 mM HCl were added and concentrated again to 200 ml. This step was repeated for another three times. The protein solution was decanted, the crossflow was rinsed with 100 ml 1 mM HCl and combined with concentrated protein solution. Finally, the solution was dialysed twice against 5 litres of 1 mM HCl at 4 °C for 4 h.

20 ml Fractogel EMD SO_3^- (S) (bed height 4 cm) were filled in a glass column and equilibrated with 5 bed volumes loading buffer (flowrate: 1.5 ml/min). The dialysed protein solution was adjusted to 20 mM NaAc, pH 4.5 / 30 % Isopropanol with a final protein concentration of 1 mg/ml and loaded onto the EMD SO_3^- column at 14 °C. The column was washed with 3 bed volumes loading buffer and the proteins were eluted with a flowrate of 1.5 ml/min using the appropriate gradient described in table 3.6.

Table 3.6 – Elution gradient of the EMD SO_3^- column for different BMP ligands

BMP-2		BMP-2/6		BMP-2/7	
Time [min]	Fraction of elution buffer [%]	Time [min]	Fraction of elution buffer [%]	Time [min]	Fraction of elution buffer [%]
0	20	0	0	0	0
60	50	20	50	10	35
70	50	70	75	70	65
		80	100	80	100
		90	100	90	100

The eluate was collected in fractions of 1.5 ml, BMP dimer containing fractions were pooled and dialyzed twice against 100 volumes 0.1 % TFA for RP-HPLC analysis and afterwards once against 100 volumes dH_2O at 4 °C. Subsequently, the proteins were concentrated to 1 mg/ ml (YM10 membrane, Amicon stirring chamber) and centrifuged for 10 min with 4000 rpm at 4 °C to remove precipitated protein. The protein concentration was calculated via photometric scan, then, the protein was aliquoted, lyophilized and finally stored at – 80°C.

Column: Superperformance 10 (Merck)
Eco Glass Column 25 · 125 mm (Kronlab)

Column matrix: Fractogel EMD $SO3^-$ (S) (Merck)

Pump:	L6210 intelligent pump (Merck/Hitachi)
Detector:	GAT PHD 601; GAT-Linear (Gamma Analysen-Technik)
Fraction collector:	Model 203 (Gilson)
Loading buffer:	20 mM NaAc, pH 4.5 30 % isopropanol
Elution buffer:	20 mM NaAc, pH 4.5 30 % isopropanol 2 M NaCl

3.6.2. Purification of BMP receptors

Protein extraction from E.coli cells

After expression (see 3.5.6), the cell pellet was defrosted in 10 volumes (w/v) sonication buffer at 4 °C. Cells were sonicated (System 585, Ultraschallkopf Typ 512/1204, KLM) at 300 W on ice (8 times for 1 min). Cooling intervals of 30 sec between two sonication rounds were performed to prevent overheating of the sonication head. Soluble proteins were separated from cell debris by centrifugation for 20 min with 20000 rpm at 4 °C (JA20 rotor, J2-21 centrifuge, Beckman). The cell pellet was discarded and the supernatant was used immediately for immobilized metal ion affinity chromatography (IMAC).

Sonication buffer:	20 mM Tris/HCl, pH 7.9 500 mM NaCl 5 mM imidazole 1 mM PMSF

Immobilized metal ion affinity chromatography (IMAC) with Ni-chelating agarose

Metal ion affinity chromatography was performed at 4 °C to lower protease activity. A flowrate of 2.5 ml/min was used during all steps.

10 ml Chelating Sepharose FF (GE Healthcare) were filled in a glass column and washed with 100 ml ddH_2O. The column was charged with nickel ions using 100 ml of a 50 mM $NiCl_2$ solution and equilibrated with 100 ml loading buffer afterwards. A second column was filled with 2 ml Sephacryl S-100 (Pharmacia) and inserted in front of the main column as a filter.
The supernatant of the protein extraction was pumped across the pre-column on the main column. Due to its hexa-histidin tag mainly the BMP receptor fusion protein stuck to the nickel ions, all other proteins were swept away. The pre-column was discarded and the main column was rinsed with 50 ml washing buffer. After this, proteins were eluted and collected for in 10 ml fractions. Those who contained the right protein were combined and dialyzed against 5 litres EDTA buffer overnight at 4 °C (Visking 32/26, Roth). The main column was cleaned with 5 bed volumes of 100 mM EDTA, pH 8.0 and stored at 4 °C.

Column:	Econo glass column 25 · 100 mm (BioRad)
Column matrix:	Chelating Sepharose FF (Pharmacia)
Pre-column matrix:	Sephacryl S-100 (Pharmacia)
Pump:	Minipuls 3 (Gilson)
Detector:	2210 Recorder 2-Channel (LKB Bromma) 2238 Uvicord S II (LKB Bromma)
Fraction collector:	Model 203 (Gilson)
Loading buffer:	20 mM Tris/HCl, pH 7.9 500 mM NaCl 5 mM imidazole
Washing buffer:	20 mM Tris/HCl, pH 7.9 500 mM NaCl 60 mM imidazole

Elution buffer:	20 mM Tris/HCl, pH 7.9
	500 mM NaCl
	500 mM imidazole
EDTA buffer:	50 mM Tris/HCl, pH 7.5
	150 mM NaCl
	1 mM EDTA

Protein cleavage using the protease thrombin

A thrombin cleavage was carried out to divide the thioredoxin with histidin tag from the extracellular domain of the BMP receptors. First, the protein solution extracted from the IMAC process was dialyzed against 5 litres of thrombin cleavage buffer for at least 4 h at 4 °C. Subsequently, it was mixed up with 0.5 unit thrombin / mg fusion protein and incubated for 4 h at 30 °C. After completion, the mixture was dialyzed twice against 5 liters TBS buffer at 4 °C to remove $CaCl_2$ and thus to inactivate thrombin cleavage.

Thrombin cleavage buffer:	50 mM Tris/HCl, pH 7.5
	150 mM NaCl
	2.5 mM $CaCl_2$
Thrombin solution:	8.0 mg thrombin (T4648, Sigma)
	600 µl thrombin cleavage buffer
	600 µl glycerine
TBS buffer:	20 mM Tris/HCl, pH 7.4
	35 mM NaCl

Anion exchange chromatography (Fractogel EMD TMAE 650 (S))

An anion exchange chromatography was performed to separate the BMP receptors domains from the thioredoxin part.
A glass column was filled with 14 ml Fractogel EMD TMAE (S) and washed with 5 bed volumes of loading buffer. 150mg of protein obtained from the thrombin cleavage process

were loaded via an external loop using a Minipuls 3 pump (Gilson) on the TMAE column (flowrate 1.5 ml/min). Thereafter, the column was connected to the detector and washed with loading buffer with a speed of 1 ml/min until the protein detection reached baseline. Proteins were eluted accordingly to table 3.7 and collected in fractions to 1 ml. BMP receptor containing fractions were pooled and subjected for BMP-2 affinity chromatography.

Table 3.7 – Elution gradient of EMD TMAE (S) column for BMPR-IA_{ecd}

Time [min]	Elution buffer [%]
0	0
60	35
70	100
85	100
95	0

Column:	Superperformance 10 (Merck) Eco Glass Column 25 · 125 mm (Kronlab)
Column matrix:	Fractogel EMD TMAE 650 (S) (Merck)
Pump:	L6210 intelligent pump (Merck/Hitachi)
Detector:	GAT PHD 601; GAT-Linear (Gamma Analysen-Technik)
Fraction collector:	Model 203 (Gilson)
Loading buffer:	20 mM Tris/HCl, pH 7.4
Elution buffer:	20 mM Tris/HCl, pH 7.4 1 M NaCl

Affinity chromatography (BMP-2)

The BMP-2 affinity column was generated according to the guideline "Affinity Chromatography: Principles and Methods" from the company Pharmacia Biotech as follows:
3 g CNBr-activated sepharose 4B (Pharmacia) were soaked in 1 mM HCl for 30 min at 20 °C. The material was washed first with 300 ml 1 mM HCl, later on with 100 ml coupling buffer using a glas frit. The gel was resuspended in 25 ml coupling buffer using a 50 ml plastic tube (Greiner) and inactivated over night at 4 °C stirring constantly. After incubation, the material was equilibrated with 10 mM NaAc, pH 4.5. 20 mg BMP-2 were dissolved in 5 ml 10 mM NaAc, pH 4.5, added to the sepharose mix and stirred for at least 2 h at 4 °C. BMP-2 coupling was supervised every 30 min by centrifuging the sepharose with 1500 rpm and measuring the extinction of BMP-2 in the supernatant at 280 nm. After the decrease of protein extinction stopped, the supernatant was discarded, the pellet was washed with 100 ml 1 mM HCl and non-covalent bound BMP-2 was removed using 50 ml 4 M $MgCl_2$. After another washing process with 100 ml 1 mM HCl, the sepharose was equilibrated with washing buffer and incubated over night at 4 °C to saturate all remaining reactive groups in the matrix. On the next day, the sepharose was filled in a glass column, rinsed with HBS_{150} buffer and stored at 4 °C.

After anion exchange chromatography, the protein solution was dialyzed against HBS_{500} buffer overnight at 4 °C and concentrated to 1 – 2 ml via ultrafiltration. The BMP-2 affinity column was equilibrated with 50 ml HBS_{500} buffer (1 ml/min) and the protein mix was transferred directly to the column. Thereafter, the column was washed extensively with HBS_{500} buffer until no protein flow-through was detectable by the photometer. The flow-through was intercepted and concentrated again to 1 ml. Bound protein was eluted using 4 M $MgCl_2$ with a flowrate of 0.45 ml/min and collected in 4 ml fractions. The column was equilibrated again with HBS_{500} buffer and loaded with the flow-through. The whole procedure was repeated until no protein flow-through was measured. Fractions containing the desired protein were pooled, dialyzed twice against HBS_{150} buffer, concentrated to 1 mg protein / ml and stored at – 80° C.

Coupling buffer:	100 mM $NaHCO_3$, pH 8.3
	500 mM NaCl

Washing buffer:	100 mM Tris/HCl, pH 8.0 500 mM NaCl
Column:	Econo glass column 25 · 100 mm (BioRad)
Column matrix:	20 mg BMP-2 bound to CNBr-activated sepharose 4B (Pharmacia)
Pump:	Minipuls 3 (Gilson)
Detector:	2210 Recorder 2-Channel (LKB Bromma) 2238 Uvicord S II (LKB Bromma)
Fraction collector:	Model 203 (Gilson)
HBS_{150} buffer:	10 mM HEPES, pH 7.4 150 mM NaCl 3.4 mM EDTA (5 mM sodium azide, for storage purpose only)
HBS_{500} buffer:	10 mM HEPES, pH 7.4 500 mM NaCl 3.4 mM EDTA

3.6.3. Reverse phase high performance liquid chromatography (RP-HPLC)

To prepare the protein samples for mass spectrometry, a reverse phase high performance liquid chromatography was performed. A protein solution was mixed in a ratio 1:1 with TFA solution and loaded on the column using an injection loop (flowrate 0.8 ml/min). The loop was removed and the column was washed with TFA solution until the photometric protein detection reached again baseline. The protein was eluted applying the acetonitril gradient shown in table 3.8 and was collected in fractions of 0.8 ml. Protein containing fractions were combined, lyophilized and used for mass spectrometric measurements.

Table 3.8 – Elution gradient of the HPLC column

Time [min]	Acetonitril [%]
0	0
5	30
45	55
50	100
55	100

Column (analytical): Vydac-214TP, C4, 10µM pore diameter, 0.46 · 25 cm (MZ-Analysentechnik)

Column (semipreparative): Vydac-214TP, C4, 10µM pore diameter, 0.8 · 25 cm (MZ-Analysentechnik)

Pump: L6210 intelligent pump (Merck/Hitachi)

Detector: GAT PHD 601; GAT-Linear (Gamma Analysen-Technik)

Fraction collector: Model 203 (Gilson)

TFA solution: 0.1 % (v/v) TFA in ddH_2O

Elution buffer: Acetonitril

3.6.4. Gel filtration chromatography

Gel filtration chromatography was performed for the purification of antibody-receptor complexes. After equilibration of the superdex 200 column with gelfiltration buffer, the antibody-receptor solution was concentrated to 100 µl and loaded on the column using an injection loop with the same capacity. The column was rinsed with gelfiltration buffer (flowrate 0.5 ml/min) and the eluate was collected in fractions to 0.5 ml. Fractions containing the antibody-receptor complex were pooled, concentrated and used for crystallization.

Column:	Superdex 200 HR10/30 (Pharmacia)
Pump:	L6210 intelligent pump (Merck/Hitachi)
Detector:	GAT PHD 601; GAT-Linear (Gamma Analysen-Technik)
Fraction collector:	Model 203 (Gilson)
Gelfiltration buffer:	10 mM HEPES, pH 7.4 150 mM NaCl (5 mM sodium azide, for storage purpose only)

3.7. Biosensor analysis using the BIAcore technique

Interaction analysis was carried out using a BIAcore™ 2000 System (GE Healthcare, Biacore). Prof. Dr. Walter Sebald performed all measurements.

The BIAcore technique is based on the method of surface plasmon resonance (SPR) in order to measure the interactions between biomolecules in real time. One of the reactant was immobilised on the dextran surface of a sensor chip via biotin streptavidin coupling, the binding partner (analyte) solved in HBS_{500} buffer was perfused across this dextran surface. The binding of the analyte to the immobilized reactant (association) can be detected as an increase of mass via an optical scale. This interaction can be displayed as time-dependent change of resonance units (RU), whereas 1 RU is correlated with a mass increase of 1 pg/mm^2. One measuring cycle is composed of 3 phases: (1) the association, (2) the equilibrium binding phase at which association and dissociation is in balance and (3) the dissociation. After finishing the measurements the sensor chips were regenerated with 4 M $MgCl_2$, washed and stored at 4 °C.

The sensorgrams were evaluated using the software BIAevaluation 2.4 based on a 1:1 Langmuir binding model for BMPR-IA_{ecd}/BMP ligand interaction and on a 1:2 binding model for BMP ligand/BMPR-IA_{ecd} interaction. All measurements were corrected for non-specific interactions by subtracting a control sensorgram recorded for flow cell 1. Apparent binding constants (K_D) were obtained from the dose dependence of equilibrium binding and from the kinetic rate constants for complex formation (k_{on}) and dissociation (k_{off}) respectively. The mean standard deviations for all K_D values were < 50 %.

HBS_{500} buffer:	10 mM HEPES, pH7.4
	500 mM NaCl
	3.4 mM EDTA

3.8. Preparation and crystallization of antibody-receptor complexes

The preparation and crystallization of the AbyD1556/BMPR-IA_{ecd} complex was already accomplished during the author´s diploma thesis (Harth 2006). Briefly, all components were rebuffered in complex buffer using ultrafiltration (Zentricon tubes, Millipore). The 1:1 antibody-receptor complex was formed by addition of a 1.1-fold molar excess of BMPR-IA_{ecd} and subjected to gel filtration using a superdex 200 HR10-30 (GE Healthcare). The final protein concentration was 16.4 mg/ml in complex buffer. Initial screening for crystallization was performed using a sparse matrix setup obtained from successful crystallization conditions reported for antibody/protein complexes in the RCSB databank. Crystals were obtained in hanging drops at room temperature over a reservoir solution. Hanging drops were composed of 2 µl protein solution and 1 µl reservoir solution. Crystals of a final size of approximately 150 µm · 150 µm · 40 µm grew within 7 days.

Complex buffer:	10 mM HEPES, pH 7.4
	150 mM NaCl
Reservoir solution:	100 mM Tris/HCl pH 7.0
	20 % (w/v) PEG 8000
	10 % (w/v) Glucose

3.9. X-ray diffractometry

3.9.1. Measurement of X-ray diffraction data

Together with Dr. Alexander Kotzsch, diffraction datasets were acquired on our X-ray home source (Rigaku MicroMax007 with Osmic HighRes VariMax mirrors and a RAXIS-IV++ image plate system, X-stream 2000 cooling system) at 100 K.

Protein crystals were harvested from the hanging drop using nylon loops (CrystalCap Copper, Hampton Research) magnetized on copper pins and quick-freezed in liquid nitrogen. The copper pin was attached to an inverse assembled φ-axis goniometer and the crystal was centered to the focus of the beamline. To test the quality of the crystal, diffraction data at an angular degree of 0° and 90° with a 1° rotation were recorded for 120 to 300 s each. If the crystal diffracted up to a resolution of ~ 3.5 Å, a whole data set was recorded with a step size of 0.5° to 1° for 5 – 30 min.

3.9.2. Processing and analysis of X-ray diffraction data

Together with Prof. Dr. Thomas Müller, diffraction data were processed with the software CrystalClear 1.3.6 (Rigaku). To resolve the presence of noncrystallographic symmetry, the software packages phenix.xtriage (Adams et al. 2010) and GLRF (Tong and Rossmann 1997) were used to check for the presence of pseudotranslation and NCS symmetry. The complex structure of AbyD1556/BMPR-IA_{ecd} was solved by molecular replacement using the software packages CNS (Brunger 2007) and Phaser (McCoy et al. 2007). The structure of a human Fab fragment with high affinity for tetanus toxoid (PDB entry 1AQK) (Faber et al. 1998) was used as a search model in this process due to its high similarity on amino acid sequence level in comparison to AbyD1556. In addition, the structure of BMPR-IA_{ecd} bound to BMP-2 (PDB entry 1REW) (Keller et al. 2004b) was employed as a search template for the receptor ectodomain. Finally, structures were refined with Refmac Version 5.02 (Murshudov et al. 1997) and rebuilt manually via Quanta2006 (Accelrys).

3.10. Determination of protein activity in eukaryotic cell-based assays

3.10.1. General handling of cell cultures and overview of culture media

All working steps handling eukaryotic cells were carried out in a laminar airflow cabinet. Hands and working surface were cleaned with 70 % (v/v) ethanol prior work. Solutions and working tools were sterilized (see 2.2.10), the last were also flame-treated before use.
Cell lines ATDC 5, IH-1 and INA-6 were cultivated at 37 °C, 95 % humidity and 5 % CO2, C2C12 and MPC-11 at 10 % CO2. Growth mediums are listed in table 3.9. To prevent

contamination, antibiotics were added to culture medium (100 units/ml penicillin G and 100 µg/ml streptomycin). Subculturing was performed according to manufacturer protocol. To split adherent cells, they were washed with 1x PBS buffer, trypsinized and transferred to new culture boxes.

Table 3.9 – List of cell lines and their culture medium

Cell lines	Culture medium
ATDC5	DMEM + HAM´s F12 (1:1), 5% FCS, 2 mM glutamate
C2C12	DMEM, 10 % FCS, 4 mM glutamate, 1mM sodium pyruvate
IH-1	RPMI 1640, 10% heat inactivated human serum, 2 mM glutamate, 0.1 ng/ml IL-6
INA-6	RPMI 1640, 10% FCS, 2 mM glutamate, 2 ng/ml IL-6

20x PBS buffer:

160 g NaCl
4 g KCl
28.8 g Na_2HPO_4
4.8 g KH_2HPO_4
adjust pH 7.4, then autoclave

3.10.2. Cell counting via trypan blue staining

Cell number was determined using the vital staining with trypan blue. A cell suspension was mixed in a ratio of 1:1 with trypan blue solution (0.5 % (w/v) trypan blue in isotonic NaCl solution) and incubated for 5 min at RT. Cells were counted using a Neubauer counting chamber and a light microscope. All four areas of the chamber were evaluated. The cell concentration was computed using equation 2.2. The specific chamber factor of the Neubauer counting chamber is 10^4.

Equation 2.2: cell number · specific chamber factor / 4 = amount of cells / ml

3.10.3. Alkaline phosphatase assay

To quantify the activity of alkaline phosphatase and therefore to deduce the biological activity of BMP ligands, 10 000 cells/well of C2C12 or 12 000 cells/well of ATDC 5 were seeded in a

96 well plate and incubated overnight. On the next day, the cells were transferred to serum starved medium (DMEM, 2 % (v/v) fetal calf serum) and stimulated with varying concentrations of several ligands for 72 h. After cells were washed with PBS buffer and lysed with 100 µl of ALP buffer 1 while shaking for 1 h at RT, enzymatic reaction was initiated by adding 100 µl ALP buffer 2. Then, alkaline phosphatase activity was determined by measuring the absorbance at 405 nm using an ELISA reader.

ALP buffer 1: 100 mM glycine, pH 9.6
1 mM $MgCl_2$
1 mM $ZnCl_2$
1 % (v/v) NP-40

ALP buffer 2: 100 mM glycine, pH 9.6
1 mM $MgCl_2$
1 mM $ZnCl_2$
2 mg/ml p-nitro-phenylphosphate

3.10.4. Smad phosphorylation assay

To measure the phosporylation of Smad proteins, 200 000 cells/well of C2C12 or 250 000 cells/well of ATDC 5 were seeded in a 6 well plate and incubated overnight. After starvation for 24 h with serum free DMEM medium, cells were stimulated with varying concentration of BMP ligands for 30 min. Therafter, cells were washed with PBS, detached with a cell scraper, lysed with 20 µl lysis buffer for 20 min on ice and frozen afterwards at – 20 °C. Protein concentration was determined using a BCA assay (see 3.4.5), then, 30 µg of total protein amount were loaded on a SDS gel running a SDS-PAGE. Finally, phosporylated Smad proteins were made visible by western blotting (see 3.4.7).

Lysis buffer: 25 mM Tris/HCl pH 7.6
150 mN NaCl
1 % (v/v) NP-40
1 % (v/v) sodium deoxycholate
0.1 % (v/v) SDS
store at 4 °C

3.10.5. ^{3}H-Thymidine incorporation assay

To evaluate the potency of BMP ligands to inhibit cell proliferation, INA6 cell were seeded in 200 µl culture medium in 96 well plates with a density of 5 000 cells/well supplemented with increasing concentrations of BMP ligands. IH-1 cells were treated likewise, but in this case, 20 000 cells/well were used. After 72 h, 10 µl of ^{3}H-thymidine mix was added to each well. The cells were immobilized after 24 h on fiber mats (Skatron Instruments A⁄S, Lier, Norway) and dried for 1 h at 60 °C. ^{3}H-thymidine incorporation was determined using a RITA counter (radioactive intelligent thin layer analyzer RITA, Raytest).

^{3}H-thymidine mix: 25 µM ^{3}H-thymidine (GE Healthcare/Amersham)
47.5µM thymidine solved in PBS

3.10.6. IH-1 apoptosis assay

IH-1 apoptosis assay was performed as described in (Hjertner et al. 2001). 50 000 IH-1 cells per well were seeded in 200 µl culture medium in 24 well-plates supplemented with varying concentrations of BMP ligands and incubated for 72 h. Then, viability and apoptosis of IH-1 cells were determined by flow cytometric analysis of annexin V-FITC bind and PI uptake (APOPTEST-FITC kit; Nexins Research, Hoeven, Netherlands). Cells were washed once in phosphate-buffered saline, resuspended in 300 µl binding buffer, and incubated in the dark with 0.25 µl annexin V-fluorescein isothiocyanate (FITC) at 4 °C. After 1 h, Propidium iodide (PI) diluted in binding buffer with an endconcentration of 2 µg/ml was added and cells were evaluated using a FACScan flow cytometer (Becton Dickinson, San Jose, CA). For this, cells were classified as either PI- or annexin V-positive or -negative. All PI-positive cells were considered dead (upper 2 quadrants of dot plots), PI-negative and annexin V-positive cells were considered apoptotic (lower right quadrant), and remaining cells (lower left quadrant) were considered viable.

4. Expression, biochemical characterization and biological analysis of BMP heterodimers

4.1. Expression and purification of BMP ligands

Generation, expression and purification of BMP-2 was performed basically according to a protocol established by the work of Ruppert and colleagues (Ruppert et al. 1996). The purification processes for BMP-2/6 and BMP-2/7 heterodimers are based on this standard protocol but were developed further in this work to match the characteristics of the heterodimeric proteins.

4.1.1. BMP-2

Cloning and expression

The mature part of human BMP-2 (comprising residues 283 – 396 plus an N-terminal extension of Met-Ala) was cloned into the QKA vector using NcoI and BamHI restriction sites which permitted the integration of the coding sequence after the promoter/operator region T5/LacPO (see fig. 4.1 A).

A)

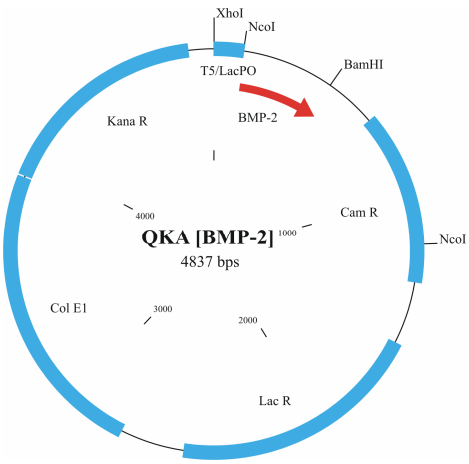

B)

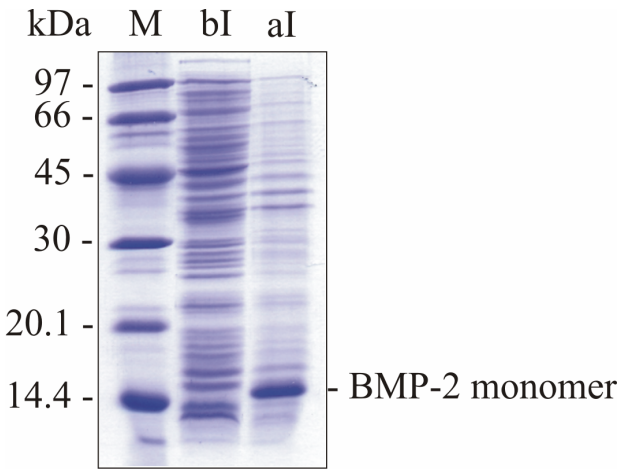

Fig. 4.1 – **A)** Expression vector QKA [BMP-2] – Mature part of human BMP-2 was inserted via restriction sites XhoI and BamHI and was expressed in MM294 cells. **B)** Induction control of BMP-2 – SDS-PAGE (reduced) with protein marker (M) and cell samples before (bI) and after 4 h induction (aI).

For protein expression, the QKA [BMP-2] vector was transformed into MM294 cells. Protein expression was induced by adding 1 mM IPTG to exponentially growing cells. Then, cells were shaken for 4 h at 37 °C and finally harvested. Protein expression was controlled via SDS-PAGE (see fig. 4.1 B). The gel displays a strong band after induction at about 15 kDa correlating to the size of the BMP-2 monomer construct. The yield was approximately 6.1 g wet weight per liter culture medium (for summary: see table 4.1).

Protein extraction from inclusion bodies and Cation exchange chromatography (SP Sepharose FF)

Recombinant expressed proteins were mostly deposited in *E.coli* cells in an insoluble form called inclusion bodies due to misfolding (Baneyx and Mujacic 2004). Therefore, cells were sonicated and centrifuged to separate the inclusion bodies containing BMP-2 from cell debris and other soluble proteins. Subsequently, BMP-2 was extracted from inclusion bodies using 6 M urea. Most of BMP-2 could be solubilized and was recovered on the supernatant (see fig. 4.2). Nonetheless, a small part remained in the cell pellet despite varying extraction conditions. As first purification step, the supernatant was subjected to cation exchange chromatography using SP Sepharose. At pH 7.0, BMP-2 bound effectively to the column and was eluted by increasing the pH to 8.0 and the salt concentration to 500 mM NaCl. Elution fractions containing the BMP-2 monomer were identified by means of SDS-PAGE analysis. These fractions were combined, concentrated to 20 mg per ml buffer and used for protein refolding together with either BMP-6 or BMP-7. The yield after this step was ~360 mg protein per g harvested cells (see table 4.1).

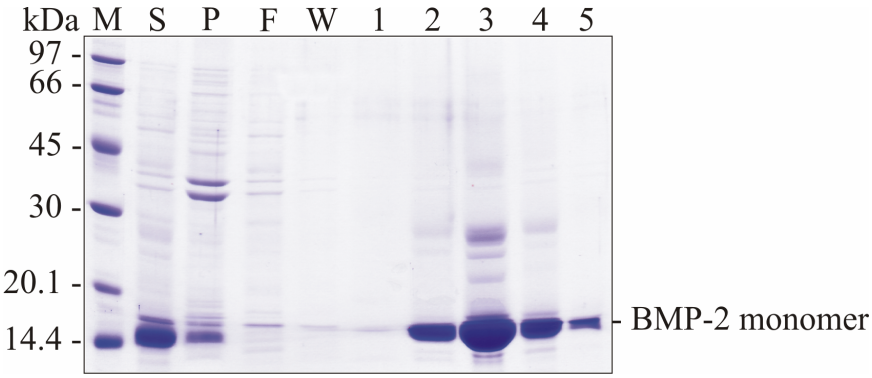

Fig. 4.2 – Cation exchange chromatography of BMP-2 using SP Sepharose FF – SDS-PAGE (reduced) with protein marker (M), supernatant (S), pellet (P) after urea extraction, flowthrough (F), wash (W) and elution fractions (1-5).

4.1.2. BMP-2/6

Cloning and expression

The gene representing the mature part of human BMP-6 (consisting of residues 375 – 513 with an N-terminal elongation of Met-Ala-Pro-Thr) was cloned into the QKA vector in the same manner like BMP-2 (see fig. 4.3 A). For expression, the QKA [BMP-6] vector was transformed into MM294 cells. After induction, the BMP-6 protein was expressed in large amounts (see fig. 4.3 B). The yield of cells after fermentation was with ~5.3 g wet weight per liter culture medium similar to that of BMP-2 with (see table 4.1).

A) **B)**

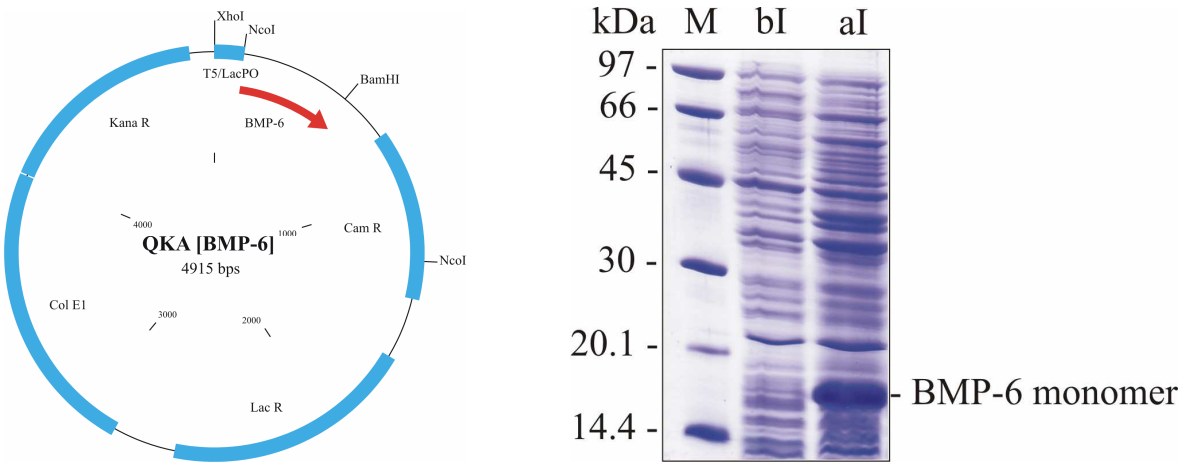

Fig. 4.3 – A) Expression vector QKA [BMP-6] – Mature part of human BMP-6 was inserted via restriction sites XhoI and BamHI and was expressed in MM294 cells. **B)** Induction control of BMP-6 – SDS-PAGE (reduced) with protein marker (M) and cell samples before (bI) and after 4 h induction (aI).

Protein extraction from inclusion bodies and Cation exchange chromatography (SP Sepharose FF)

Protein extraction and cation exchange chromatography for BMP-6 was performed as described for BMP-2. Results are summarized in fig. 4.4. Protein containing fractions were pooled, concentrated and subjected to refolding. The yield after this step was around 390 mg protein per g harvested cells (see table 4.1).

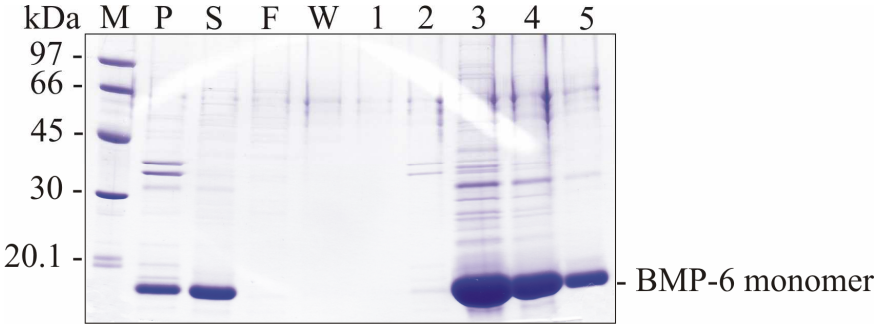

Fig. 4.4 – Cation exchange chromatography of BMP-6 using SP Sepharose FF – SDS-PAGE (reduced) with protein marker (M), pellet (P) after urea extraction, supernatant (S), flowthrough (F), wash (W) and elution fractions (1-5).

Refolding of BMP-2/6 heterodimer

The BMP-2/6 heterodimer could be refolded successfully under the same conditions as the BMP-2 homodimer. However, the concentration of BMP-6 monomer was doubled in relation to BMP-2 because BMP-6 tends to build aggregates of high-molecular weight during the renaturation process (see lane 1 and 3 in fig. 4.5). In SDS-PAGE analysis, the BMP-2/6 band can be clearly distinguished from that of BMP-2 and BMP-6 because of its intermediate molecular weight facilitating the control of renaturation.

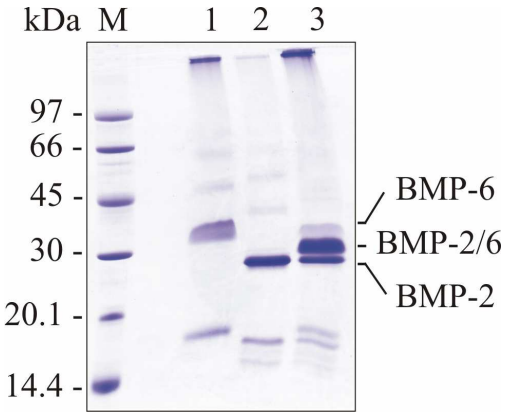

Fig. 4.5 – Refolding of BMP-2/6 – SDS-PAGE (non reduced) of the BMP-2/6 refolding process. The BMP-2/6 heterodimer (lane 3) runs between BMP-6 (lane 1) and BMP-2 (lane 2) due to its intermediate molecular weight.

Cation exchange chromatography (Fractogel EMD $SO3^-$)

To isolate the BMP-2/6 heterodimer, the refolding mixture was subjected to cation exchange chromatography employing a Fractogel EMD $SO3^-$ column. First, the refolding buffer was

exchanged by 1 mM HCl using ultrafiltration. In the next step, the protein solution was adjusted to 20 mM NaAc, pH 4.5, 30 % (v/v) isopropanol and pumped on the column. After extensive washing with loading buffer, the protein was eluted by increasing the salt concentration in the buffer.

BMP-2/6 elutes together with BMP-6 in one peak at circa 1.2 M NaCl. BMP-2 is effectively separated in a second peak at 1.3 M NaCl (see fig. 4.6 A) as seen after SDS-PAGE analysis (see fig. 4.6 B). Fractions containing BMP-2/6 and BMP-6 were used for further purification trials.

A)

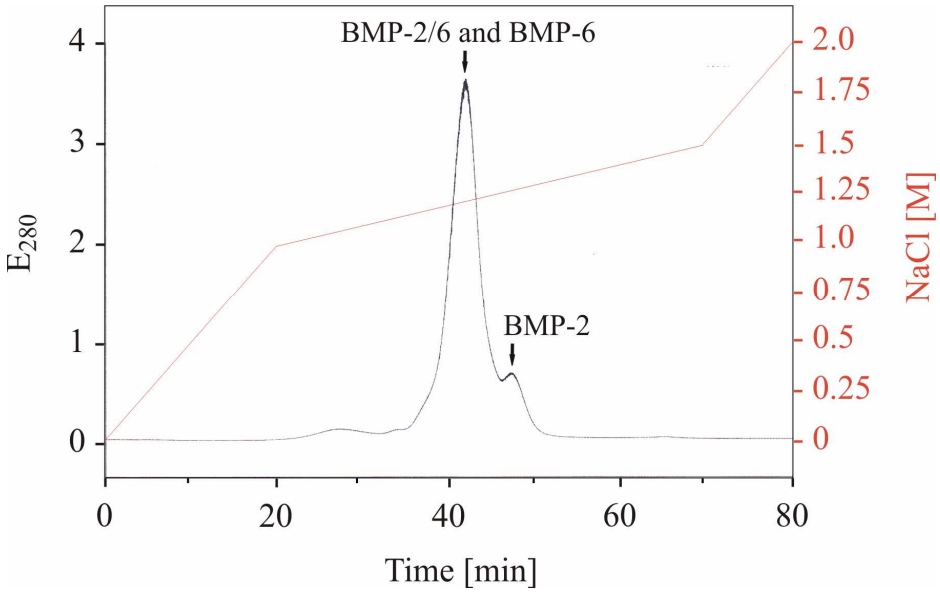

B)

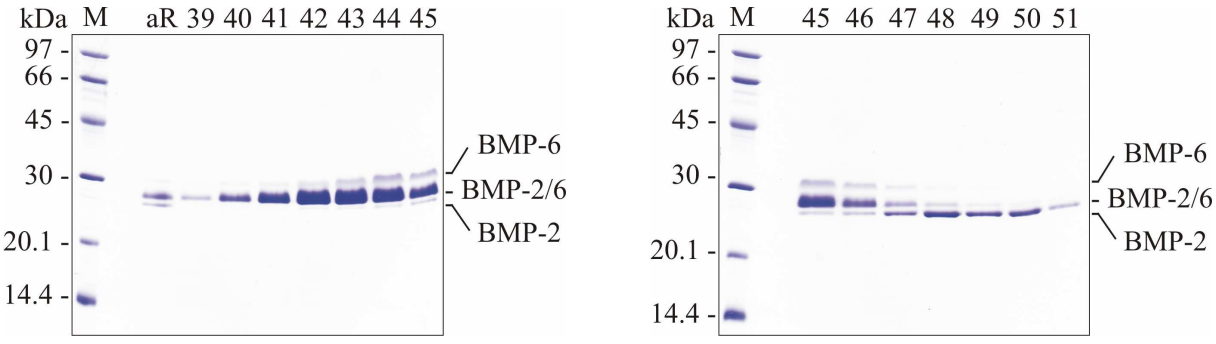

Fig. 4.6 – Cation exchange chromatography for BMP-2/6 using a Fractogel EMD SO_3^- (S) column –
A) Elution profile (black) – BMP-2/6 elutes together with BMP-6 in the first peak at 1.2 M NaCl, BMP-2 dimers elute in the second peak at approximately 1.3 M NaCl. The salt gradient is plotted in red.
B) SDS-PAGE (non reduced) with protein marker (M) and protein samples from after refolding (aR) and elution fractions 39 – 51. BMP-2/6 together with BMP-6 are visible in fractions of the first peak (lane 39 – 46), whereas BMP-2 can be separated from it in the second peak (lane 45 – 51). Elution fractions 39 – 44 were used for further experiments.

Several other chromatography steps were performed to purify the BMP-2/6 fraction from BMP-6 contamination. Ion exchange chromatography using weak cation exchangers (Fractogel EMD COO^- and Hi-Trap CM Sepharose FF, GE Healthcare) as well as Heparin Sepharose 6 FF chromatography due to the heparin binding properties of the N-terminus in BMP-2 (Ruppert et al. 1996) were tested, but BMP-6 could not be efficiently separated from BMP-2/6 (data not shown). Since the portion of BMP-6 is rather small compared to BMP-2/6 and BMP-6 seems to be not biological active in several cell-based assays due to the lack of a carbohydrate moiety crucial for ActR-I mediated signalling (Saremba et al. 2008), this minor impurities were tolerated. In a final step, BMP-2/6 was dialyzed against dH_2O, lyophilized and stored at – 80 °C.

A final examination of protein purity was carried out via SDS-PAGE and RP-HPLC analysis (see fig. 4.7). Under reducing conditions both BMP-2 and BMP-6 monomers are clearly visible in similar amount indicating the assembly of true BMP-2/6 heterodimers. Under non reducing conditions only a faint band for BMP-6 is distinguishable above the BMP-2/6 band. Moreover, BMP-2/6 elutes as a single peak in RP-HPLC analysis indicating the high purity of BMP-2/6 protein.

A) **B)**

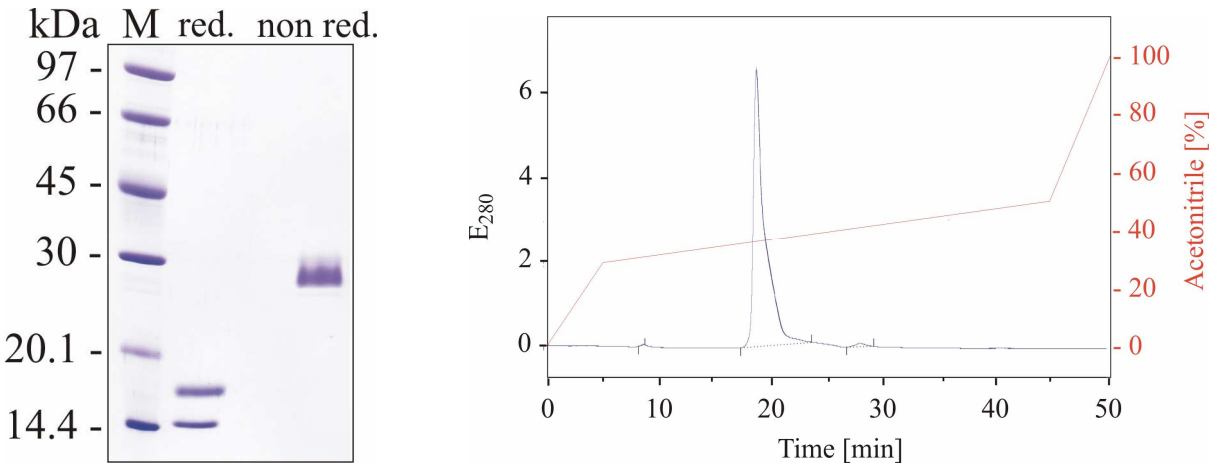

Fig. 4.7 – RP-HPLC of BMP-2/6 – **A)** SDS-PAGE of the purified BMP-2/6 heterodimer under reduced (red.) and non reduced (non red.) conditions that is used for RP-HPLC. **B)** Elution profile (black) – BMP-2/6 elutes as a single peak after 19 min. The acetonitrile gradient is plotted in red.

The yield of all purification steps are summarized in table 4.1. The final yield of BMP-2/6 was 20.1 mg per 50 mg BMP-2 and 100 mg BMP-6 monomer used during renaturation. This

resembles a transformation rate of ~13 % of BMP monomers (in total) into heterodimers during the refolding process.

Mass spectrometric analysis of BMP-2/6

BMP-2/6 was also subjected to mass spectrometry as an additional quality control. In the original data, signals from BMP-2/6 are only visible with their different grade of protonation indicating a high degree of protein purity (see fig. 4.8 A). After deconvolution procedure, the theoretical molecular weight could be validated (see fig. 4.8 B) confirming the production of active BMP-2/6 heterodimers.

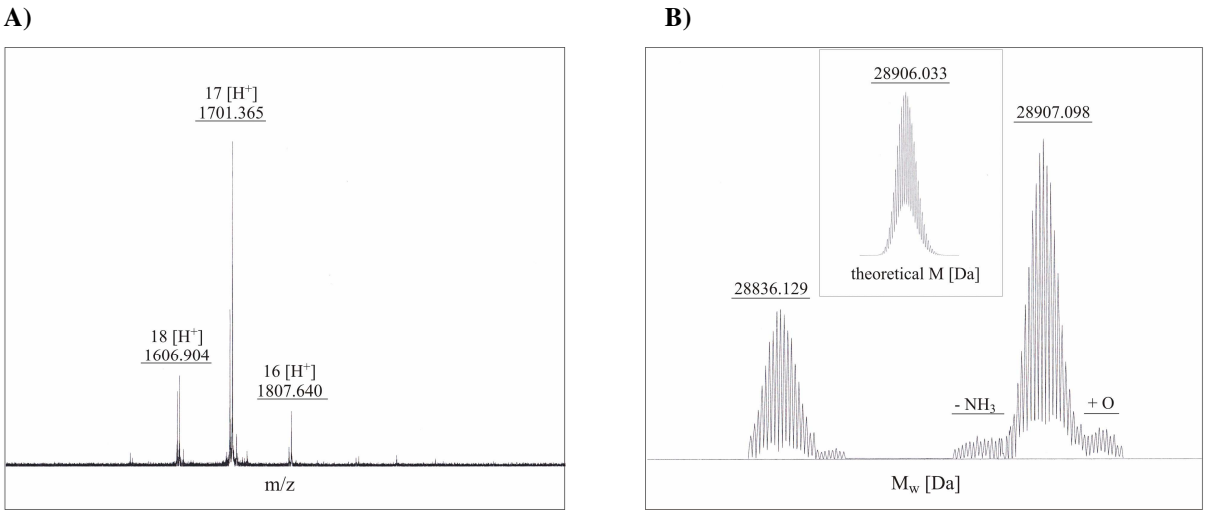

Fig. 4.8 – Mass spectrometric analysis of BMP-2/6 – **A)** Original data visualized by the mass-to-charge ratio m/z. **B)** Data of the 17-fold charged ions after deconvolution depicted with the corresponding molecular weight M_w. A truncated version of BMP-2/6 lacking the N-terminal alanine (M_W: 28836.129 Da) residue is also visible.

4.1.3. BMP2/7

Cloning and expression

The cDNA of the mature part of human BMP-7 (residue 293 – 431) was optimized for expression in *E.coli* and synthesized by GENEART (Regensburg, Germany). The BMP-7 gene was transferred from pPCR-Script vector to pET28b expression vector using the flanking NcoI and BamHI restriction sites (see fig. 4.9 A). For expression, the pET28b [BMP-7] vector was transformed into Rossetta (DE3) pLysS cells.

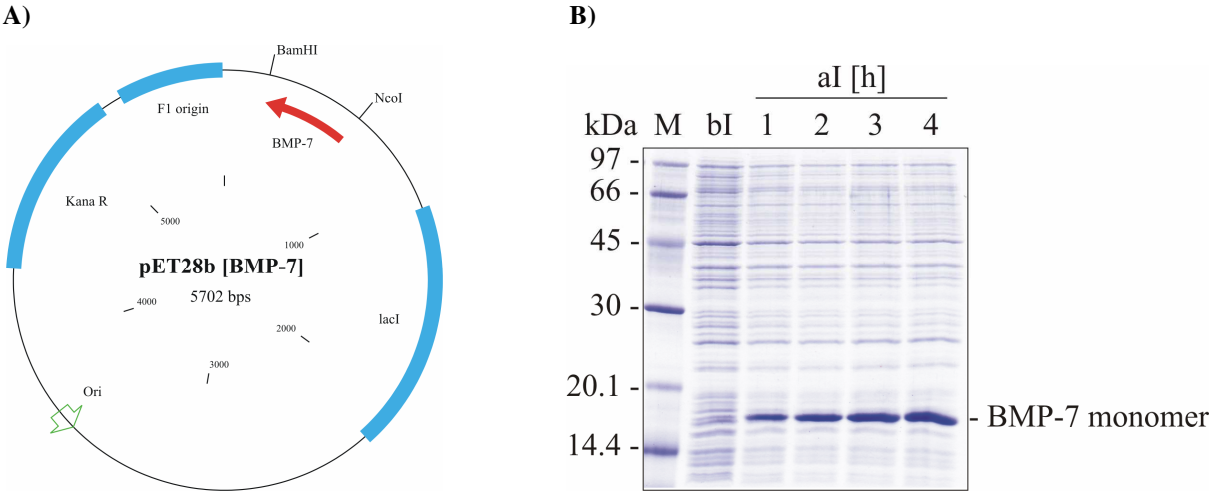

Fig. 4.9 – A) Expression vector pET28b [BMP-7] – Mature part of human BMP-7 was inserted via restriction sites NcoI and BamHI and was expressed in Rossetta (DE3) pLysS cells. **B)** Induction control of BMP-7 – SDS-PAGE (reduced) with protein marker (M), cell samples before (bI) and after 1, 2, 3, 4 h induction (aI [h]).

Protein expression was induced by adding 1 mM IPTG and cells were then agitated for 4 h at 37 °C. Cells were harvested and protein expression was controlled by SDS-PAGE (see fig. 4.9 B). The gel exhibits a strong band already after 1 h of incubation at the predicted molecular weight for the BMP-7 construct, reaching its maximum after 4 h. The harvested cell mass was ~3.4 g per liter culture medium, similar to the yields obtained in BMP-2 and BMP-6 expression (for summary: see table 4.1).

Protein extraction from inclusion bodies and Cation exchange chromatography (SP Sepharose FF)

Protein extraction and cation exchange chromatography for BMP-7 was performed in the same way as described above for BMP-2 and BMP-6. Results are summarized in fig. 4.10.

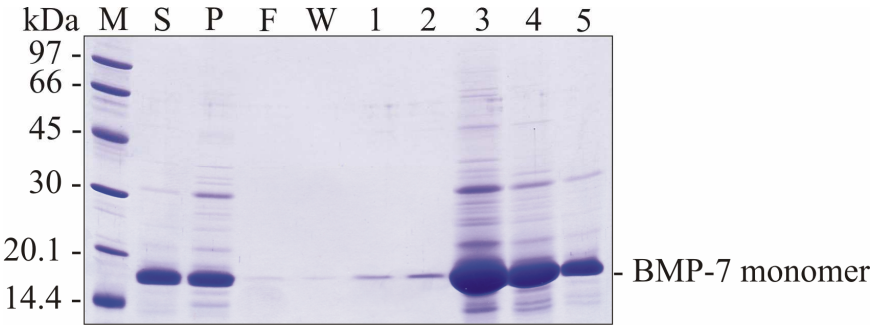

Fig. 4.10 – Cation exchange chromatography of BMP-7 using SP Sepharose FF – SDS-PAGE (reduced) with protein marker (M), supernatant (S), pellet (P), flowthrough (F), wash (W) and elution fractions (1-5).

Protein containing fractions were pooled, concentrated and subjected to refolding. The yield of BMP-7 after this step was ~180 mg protein per g inclusion body. This amount was roughly four-fold higher than that for BMP-2 and BMP-6 indicating a very effective expression system (see table 4.1).

Refolding of BMP-2/7 heterodimer

In the beginning, numerous trials for the generation of an active BMP-7 homodimer were conducted. Preliminary analysis with formed BMP-7 homodimers revealed that BMP-7 was not biological active in BIAcore measurements (data not shown). Moreover, BMP-7 tended to form large insoluble high-molecular weight aggregates. To prevent this, BMP-2 was added as a refolding helper to stabilize the renaturation process for BMP-7. Therefore, various approaches to refold a functional BMP-2/7 heterodimer were performed. However, a clear and positive result for BMP-2/7 refolding, as seen in the case of BMP-2/6, could not be achieved (see fig. 4.11).

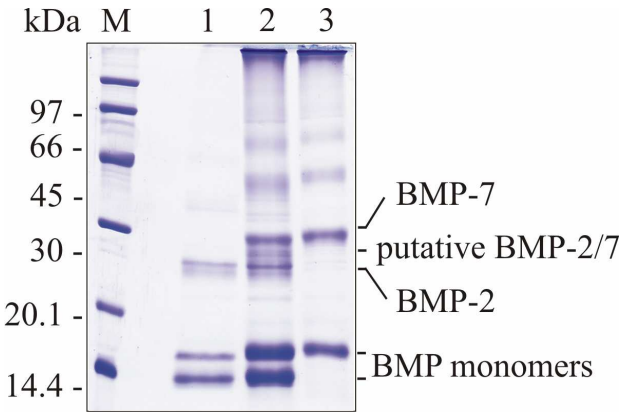

Fig. 4.11 – SDS-PAGE (non reduced) of the BMP-2/7 refolding process – The putative BMP-2/7 heterodimer (lane 2) runs between BMP-2 (lane 1) and BMP-7 (lane 3) due to its intermediate molecular weight. Most of the BMP proteins remain in their monomeric state.

In SDS-PAGE analysis, only a faint band for a possible BMP-2/7 protein could be observed between the band for BMP-2 and BMP-7 homodimers. In addition, most protein remained in its monomeric state or built aggregates. Only a small part formed dimers. Since several trials to increase the amount of BMP-2/7 showed no significant effect, a cation exchange chromatography was carried out to verify whether an active BMP-2/7 heterodimer was generated at all.

Cation exchange chromatography (Fractogel EMD SO3⁻)

The cation exchange chromatography was accomplished in the same way as described for BMP-2 and BMP-2/6. The elution chromatogram displayed that two protein fractions could be separated from each other (see fig. 4.12 A). A first SDS-PAGE examination of the non reduced protein showed no significant differences between these two fractions (see 4.12 B, C).

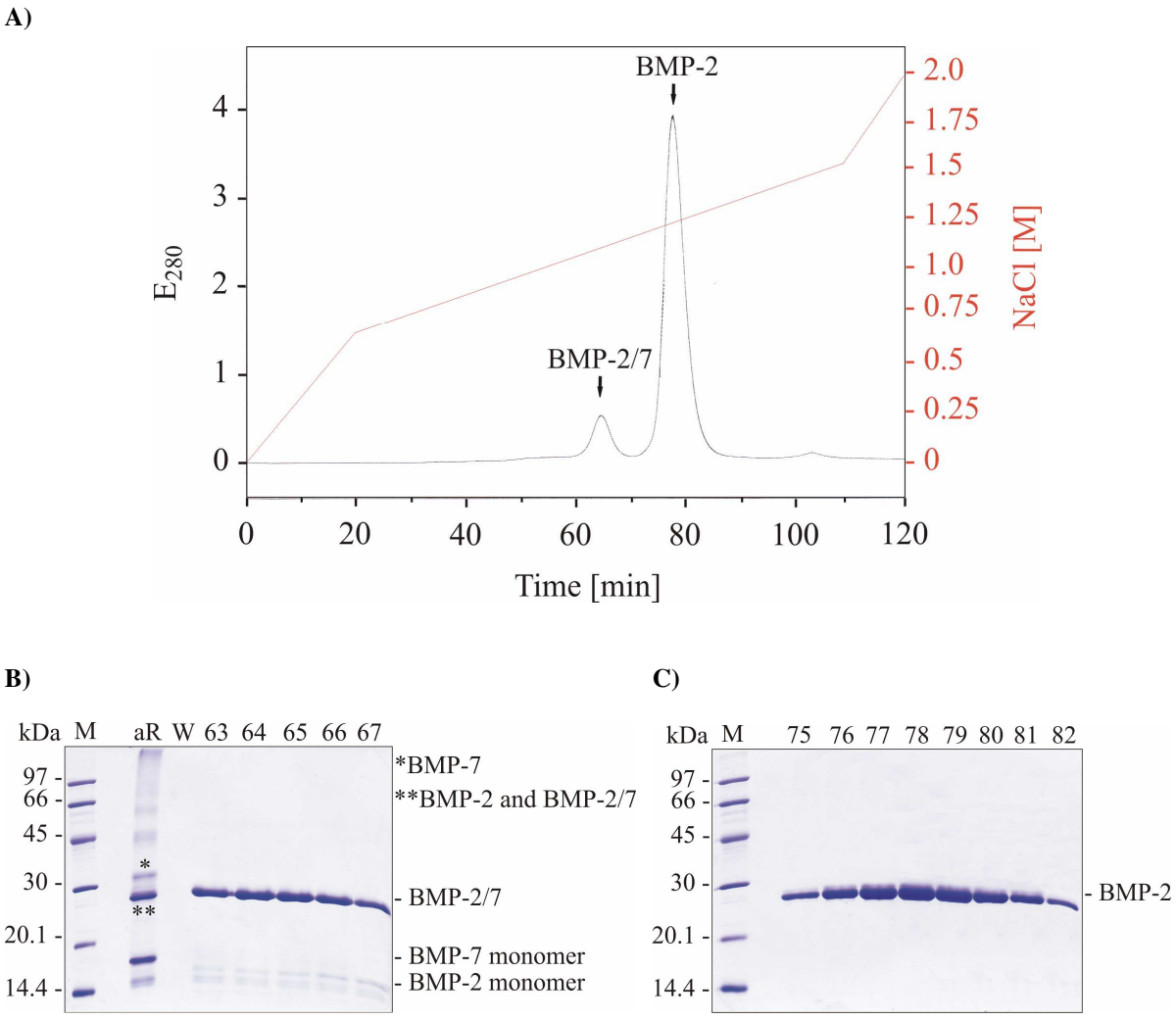

Fig. 4.12 – Cation exchange chromatography for BMP-2/7 using a Fractogel EMD SO_3^- (S) column – **A)** Elution profile (black) – BMP-2/7 elutes in the first peak at 1.1 M NaCl, BMP-2 dimer elutes in the second peak at 1.25 M NaCl. The salt gradient is plotted in red. **B)** SDS-PAGE (non reduced) with protein samples from the protein marker (M), after refolding (aR), flowthrough and wash (W) and elution fractions 63 – 67 of the first peak. **C)** SDS-PAGE (non reduced) with protein samples from elution fractions 75 – 82 of the second peak.

A detailed investigation employing the reduced protein revealed that the first elution peak consisted only of BMP-2/7 and the second one of BMP-2 (see 4.13). BMP-7 homodimer or multimers were not visible in the elution profile. Probably, they precipitated and stuck

irreversible to the column since no protein could be detected in the flowthrough during loading and washing cycle.

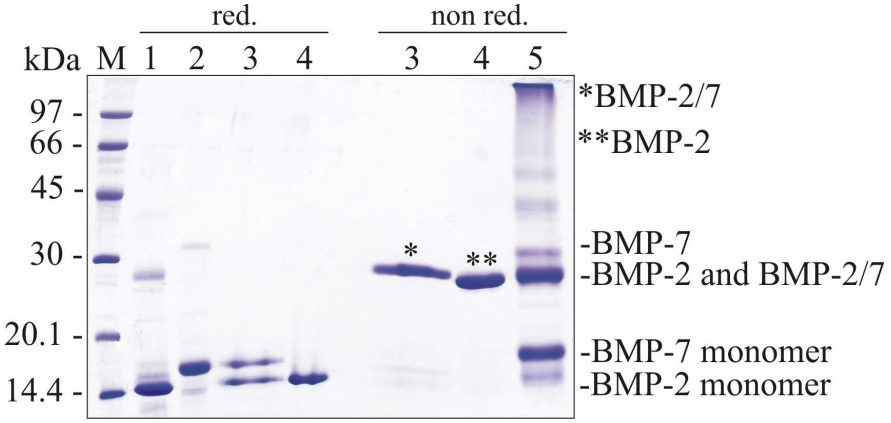

Fig. 4.13 – SDS-PAGE to summarize the results from **fig. 4.12** – The combined fractions from the first peak at 1.1 M NaCl (lane 3, right) under non reduced conditions (non red.) comprise the BMP-2/7 heterodimer. Under reduced conditions (red.) the BMP-2 and BMP-7 monomers are clearly visible (lane 3, left). Fractions from the second peak at 1.25 M NaCl (lane 4) contain only the BMP-2 homodimer. During the refolding process (lane 5), the BMP-2 and BMP-2/7 band run at the same height, therefore they are indistinguishable during this stage. BMP-2 (lane 1) and BMP-7 (lane 2) monomers are shown as reference points.

This result finally showed that the assumption was wrong that BMP-2/7 migrates in between BMP-2 and BMP-7 in SDS-PAGE analysis as seen for BMP-2/6 (for comparison see fig. 4.5). In fact, the BMP-2/7 heterodimer runs together with BMP-2 (see fig. 4.13, lane 5). Moreover, changes in the composition of SDS gels towards a better separation of BMP-2/7 from BMP-2 were not successful (data not shown). Thus, only a detailed examination applying a cation exchange chromatography step can confirm the amount of BMP-2/7 protein formed during renaturation, making an optimization of BMP-2/7 refolding conditions very difficult. Due to these problems, the yield of BMP-2/7 after this step was very low, resulting in only 3 mg per 300 mg BMP monomers used in total for refolding. This resembles a transformation rate of only 1 % of monomers into heterodimers during the refolding process. This rate can be likely increased, when a better assay is available.

Despite the issues mentioned, the BMP-2/7 obtained during this process was very pure validated by a final SDS-PAGE and RP-HPLC analysis (see fig. 4.14).

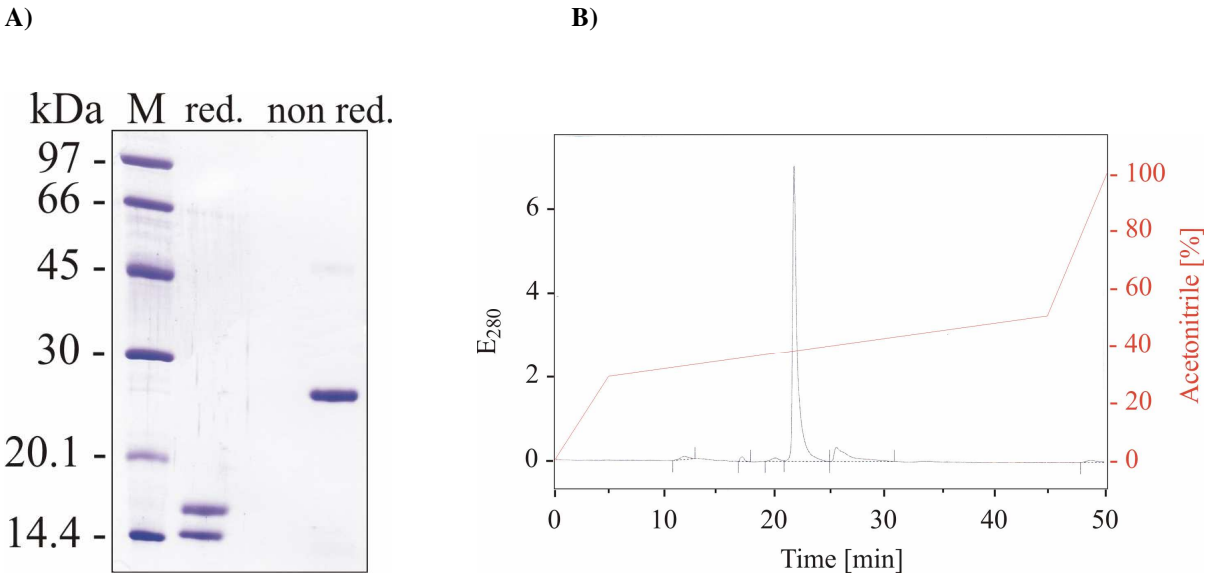

Fig. 4.14 – RP-HPLC of BMP-2/7 – **A)** SDS-PAGE of the purified BMP-2/7 heterodimer under reduced (red.) and non reduced (non red.) conditions that is used for RP-HPLC. **B)** Elution profile (black) – BMP-2/7 elutes as a single peak after 21.7 min. The acetonitrile gradient is plotted in red.

Mass spectrometric analyis of BMP-2/7

In addition, BMP-2/7 was also analyzed by mass spectrometry as an additional quality control. Signals from BMP-2/7 in the original data are only visible with their different grade of protonation indicating a high degree of protein purity (see fig. 4.15 A). After deconvolution procedure, the theoretical molecular weight could be verified (see fig. 4.15. B), confirming the production of active BMP-2/7 heterodimers.

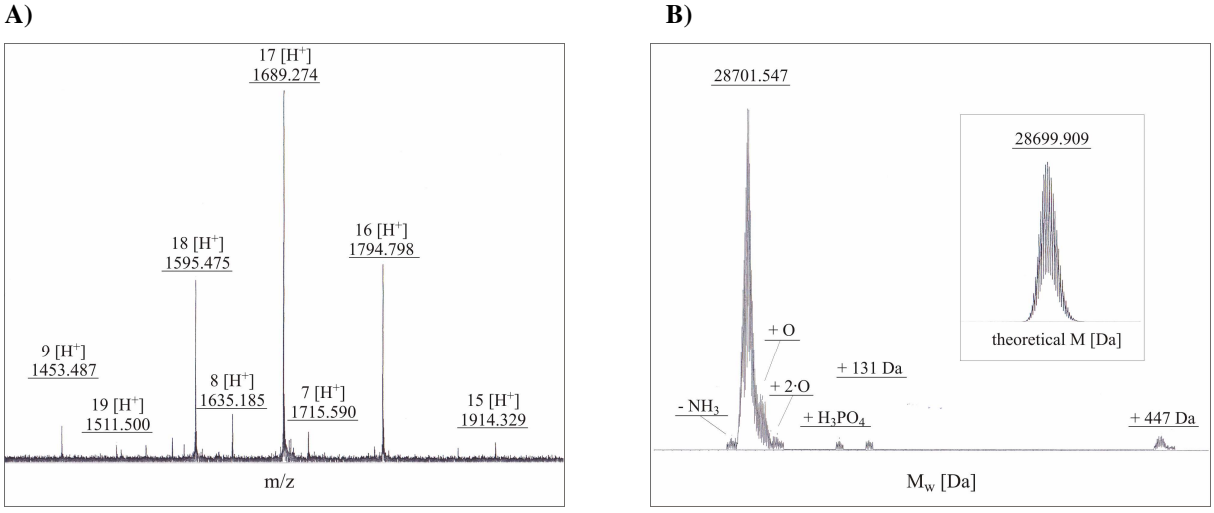

Fig. 4.15 – Mass spectrometric analysis of BMP-2/7 – **A)** Original data visualized by the mass-to-charge ratio m/z. **B)** Data of the 18-fold charged ions after deconvolution depicted with the corresponding molecular weight M_w.

4.1.4. Summary of BMP ligand generation

During this work, two heterodimers, namely BMP-2/6 and BMP-2/7, could be successfully generated, expressed in *E.coli* and purified to homogeneity.

The yield of every stage is reviewed in table 4.1 and 4.2. BMP-2 was only used for heterodimer formation; a BMP-2 homodimer was not produced separately.

To test the biological activity of BMP-2/6 and BMP-2/7 in comparison to other BMP ligands, BIAcore measurements as well as several cell-based assays were performed. The results for these experiments are described in the next chapters.

Table 4.1 – Yields of BMP ligands during the purification process

	Yield of BMP monomers			Yield of refolded BMP dimers	
BMP ligand	Wet weight of cells after fermentation [g/L medium]	Wet weight of inclusion bodies after sonication [mg/g cells]	SP Sepharose chromatography [mg/g IB]	Monomer used during refolding [mg/L medium]	EMD $SO3^-$ chromatography [mg/L buffer]
2	6.14	363.3	41.1	200	84[a]
6	5.3	392.2	56.5	-	-
7	3.37	308.7	181.7	-	-
2/6	-	-	-	50 (BMP-2) 100 (BMP-6)	20.1
2/7	-	-	-	100 (BMP-2) 200 (BMP-7)	3.0

[a] Reference value (Christian Söder, personal communication)

Table 4.2 – Molecular weights (M_w) of BMP ligands determined by mass spectrometry

BMP ligand	M_w [Da]	Theoretical M_w [Da]	Difference [Da]	Modifications
2	25937.448[a]	25937.688	- 0.240	-
2/6	28907.098	28906.033	1.065	-
	28836.129	28835.998	0.131	- Ala (N-terminal)
2/7	28701.547	28699.909	1.638	-

[a] Reference value (C. Söder, personal communication)

4.2. BIAcore interaction analysis of ligand receptor interplay

To test the biological activity of BMP-2/6 and BMP-2/7 in comparison to other BMP ligands, BIAcore measurements were performed. For this, BMP ligands (BMP-2, BMP-2/6, BMP-2/7 and BMP-7) were immobilized on the surface of a BIAcore sensor chip and the ectodomains of various type I and type II receptors in different concentrations were perfused across this surface. Sensorgram examples for BMPR-IA, ActR-I and ActR-IIB bound to immobilized BMP-2 and BMP-2/6 are given in fig. 4.16. All measurements are summarized in table 4.3.

The binding constant K_D obtained for BMPR-IA bound to BMP-2 (K_D: 20.9 nM) are in line with previous published results indicating a reproducible experimental setup (Keller 2004a: K_D ~ 48 nM). The BMP heterodimers display similar K_D values like BMP-2 for BMPR-IA binding (see table 4.3). Regarding the kinetic constants, the k_{off} values (= off rate constants of dissociation) of BMP heterodimers are smaller than that of BMP-2. Accordingly, the corresponding k_{on} values (= on rate constants of association) are slower in BMP heterodimers compared with BMP-2 resulting finally in the same K_D values. Therefore, systematic changes in the kinetic constants are clearly apparent suggesting non homogenous binding sites in BMP heterodimers.

The binding constant K_D for ActR-I binding could not be determined exactly in both BMP-2 and BMP-2/6 due to low binding affinity. However, the sensorgrams for BMP-2 and BMP-2/6 exhibit a same level of resonance units suggesting the same binding behavior to ActR-I (see fig. 4.16 C, D). In addition, the apparent binding constants K_D for interaction with ActR-II and ActR-IIB display the same level for both BMP homo- and heterodimers (see table 4.3).

Although the binding constants for receptor binding were the same in all tested BMPs, differences in the total amount of resonance units in case of the binding of BMPR-IA and ActR-IIB to BMP-2 and BMP-6 were clearly visible (see fig. 4.16 A, B and E, F). However, it is not clear whether the smaller amount of resonance units is due to the total capacity of the bound heterodimers or caused by the binding to only one BMP-subunit. For that reason, the fact of lower resonance units was not examined further in BIAcore measurements.

In conclusion, the BMP heterodimers produced in this work exhibited the same binding affinities to type I and type II receptors as homodimers. To examine the biological activity of heterodimers more thoroughly, additional cell assays were accomplished (see chapter 4.3).

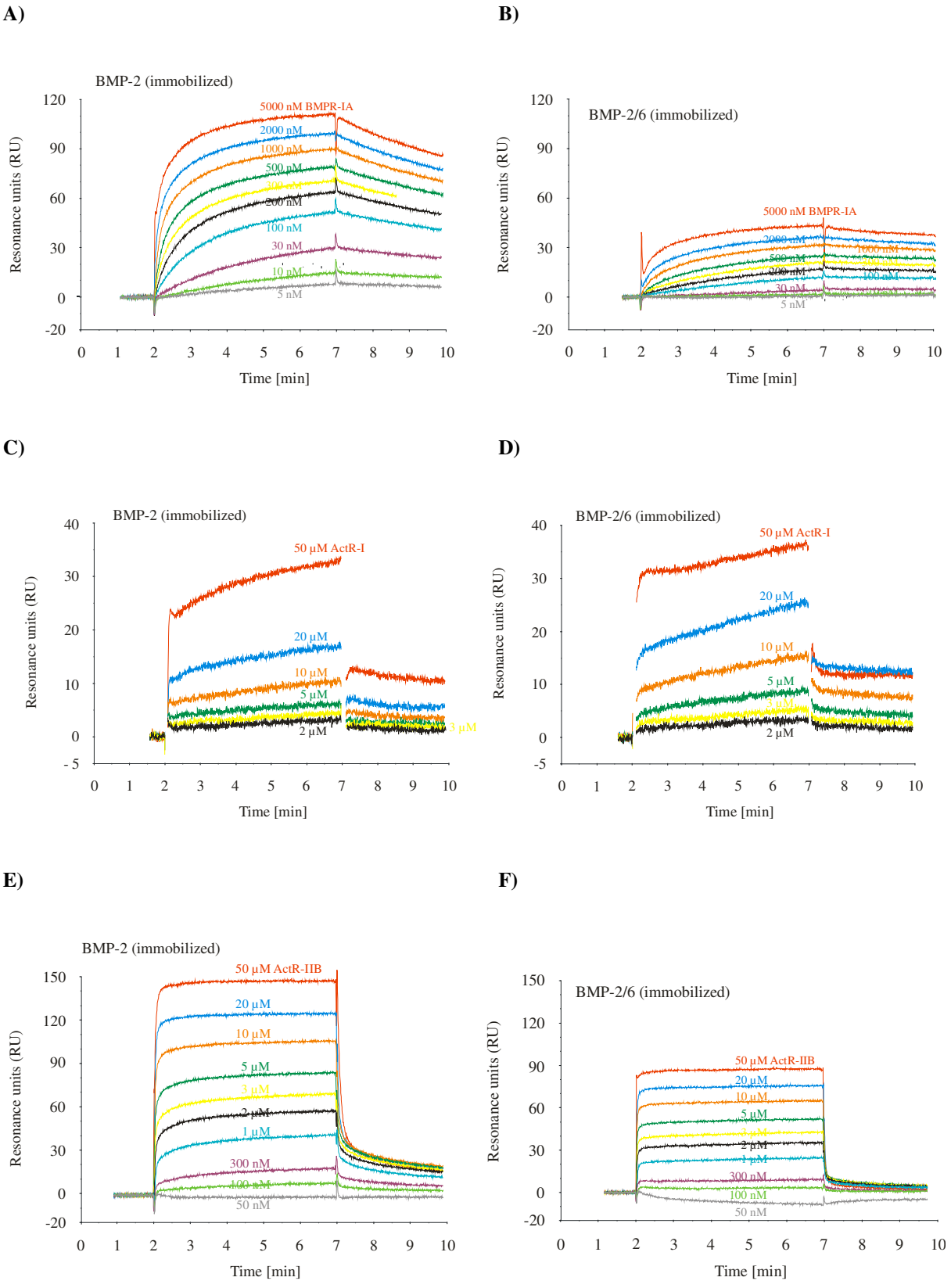

Fig. 4.16 – BIAcore sensograms of the interaction of receptor ectodomains with immobilized BMP ligands.

A, B) BMPR-IA$_{ecd}$ bound to immobilized BMP-2 and BMP-2/6.

C, D) ActR-I$_{ecd}$ bound to immobilized BMP-2 and BMP-2/6.

E, F) ActR-IIB$_{ecd}$ bound to immobilized BMP-2 and BMP-2/6.

Table 4.3 – Summary of BIAcore interaction analysis of BMP receptor ectodomains bound to immobilized BMP ligands

Proteins (immobilized)	Analyte (perfused)					
	BMPR-IA$_{ecd}$			ActR-I$_{ecd}$	ActR-II$_{ecd}$	ActR-IIB$_{ecd}$
	k_{off} [10^{-3} s^{-1}]	k_{on} [10^{4} M^{-1} s^{-1}]	K_D[a] [nM]	K_D[b] [µM]		
BMP-2	1.99	10.17	20.9 +/- 7.9	n.d.[c]	3.5	3.0
BMP-2/6	1.38	20.78	42.9 +/- 41.3	n.d.	3.8	-
BMP-2/7	0.37	4.98	7.3 +/- 0.7	-	-	2.1
BMP-7	10.67	9.17	202 +/- 151	-	-	1.0

[a] Dissociation binding constant K_D was derived from calcutating $K_D = k_{off} / k_{on}$.

[b] Apparent binding constant K_D was obtained from the dose dependence of equilibrium binding.

[c] Binding could not be determined because equilibrium was not reached.

4.3. Biological activity in cell assays

In addition to BIAcore measurements, the biological activity of BMP-2/6 and BMP-2/7 were tested in a variety of cell-based *in-vitro* assays with the focus on type I receptor selection.
In the first experiments, their ability to induce the expression of alkaline phosphatase was extensively studied in chondrocytic and myogenic cell lines. Later on, their capability to inhibit cell proliferation and to induce apoptosis was examined in myeloma cells. Finally, their competence to phosphorylate Smad proteins was analyzed.

4.3.1. Alkaline phosphatase assay

ALP assay using C2C12 cells

Katagiri and colleagues demonstrated that BMP-2 promotes the production of alkaline phosphatase (ALP) in the murine myoblast cell line C2C12 (Katagiri et al. 1994). Since that, the ALP assay evolved to a standard method to test the biological activity of BMP ligands in

living cells. Consequently, the BMP-2/6 and BMP-2/7 heterodimers were evaluated and compared with other BMPs first in C2C12 cells.

Briefly, 10 000 cells/well were seeded in a 96 well plate and incubated overnight. On the next day, the cells were transferred to serum starved medium (DMEM, 2 % (v/v) fetal calf serum) and stimulated with varying concentrations of several BMP ligands for 72 h. Cells were lysed and the amount of alkaline phosphatase was measured by the cleavage of para-Nitrophenyl-phosphate (pNPP) into yellow para-nitrophenol. This process could be quantified by measuring the absorbance at 405 nm.

BMP-2 produced in *E.coli* cells induced ALP production in a dose dependent manner in C2C12 cells (see fig. 4.17). The calculated EC_{50} value is in line with the results established in previous works (e.g. Weber et al. 2007: ~ 10 – 15 nM). Heterodimeric BMP-2/6 and BMP-2/7 induced efficiently ALP activity. Both proteins exhibit an at least two- to three-fold lower EC_{50} value compared to BMP-2. This finding is in agreement with the work of Israel and others (Israel et al. 1996) showing that heterodimeric BMP-2/7 produced in eukaryotic CHO cells achieved a specific activity about 20-fold higher than BMP homodimers in ALP assays using the mouse stromal cell line W-20-17.

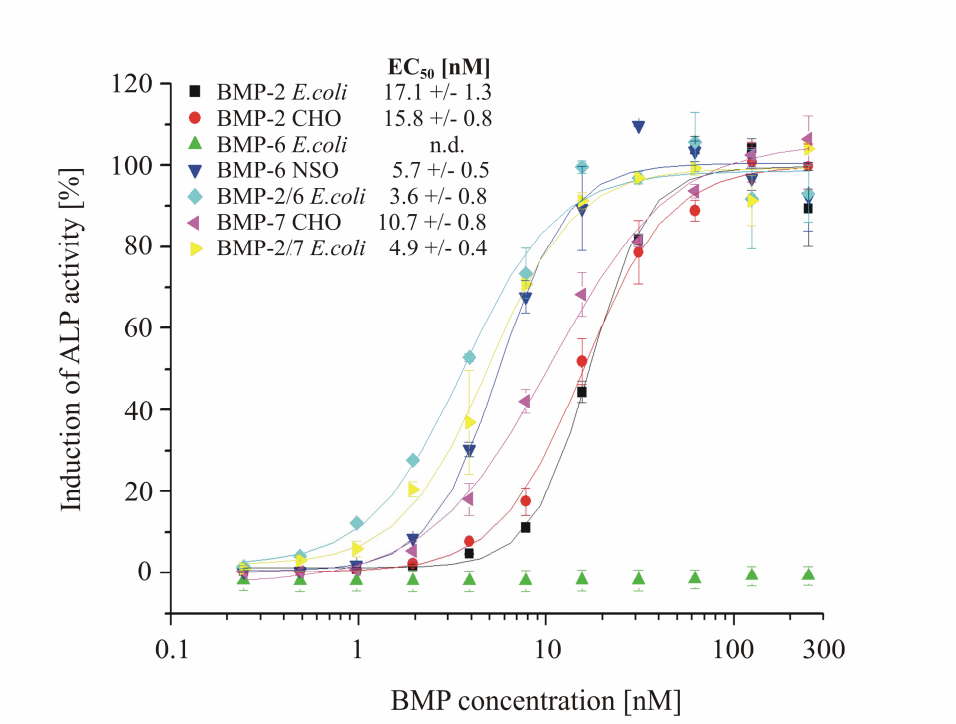

Fig. 4.17 – Determination of alkaline phosphatase (ALP) activity in C2C12 cells – BMP ligands induce ALP activity in a dose dependent manner except for BMP-6 produced in *E.coli* cells. In this case, an EC_{50} was not determinable (n.d.).

While the source of BMP-2 proteins (both from *E.coli* and eukaryotic CHO cells) is not crucial to their activity, only BMP-6 derived from NSO cells was functional, BMP-6 from *E.coli* induced no ALP signal at all as shown previously (Saremba et al. 2008). Remarkably, BMP-6 from NSO cells was nearly as active as the heterodimers from *E.coli* and more active than BMP-7 CHO and the BMP-2 proteins.

C2C12 cells contain the type I receptors ActR-I and BMPR-IA, but not BMPR-IB (Akiyama et al. 1997; Ebisawa et al. 1999). Therefore, we addressed the question which of these receptors might be involved in the efficient signalling of the heterodimers. Two antibodies raised against BMPR-IA$_{ecd}$ – AbyD1556 and AbyD1564 – were added together with BMP ligands to C2C12 cells and ALP assays were repeated in the same way described above.
Both antibodies prevented efficiently the induction of ALP (see figure 4.18 and 4.19). Only minor differences in their potency for different ligands as well as among each other were detectable. These experiments illustrate clearly that BMPR-IA is involved in forming the receptor signalling complex, whether in collaboration with other receptor I subtypes or exclusively remains to be determined. The antibodies blocked signalling even in the BMP-6/7 subgroup which signals mainly via ActR-I (Ebisawa et al. 1999).

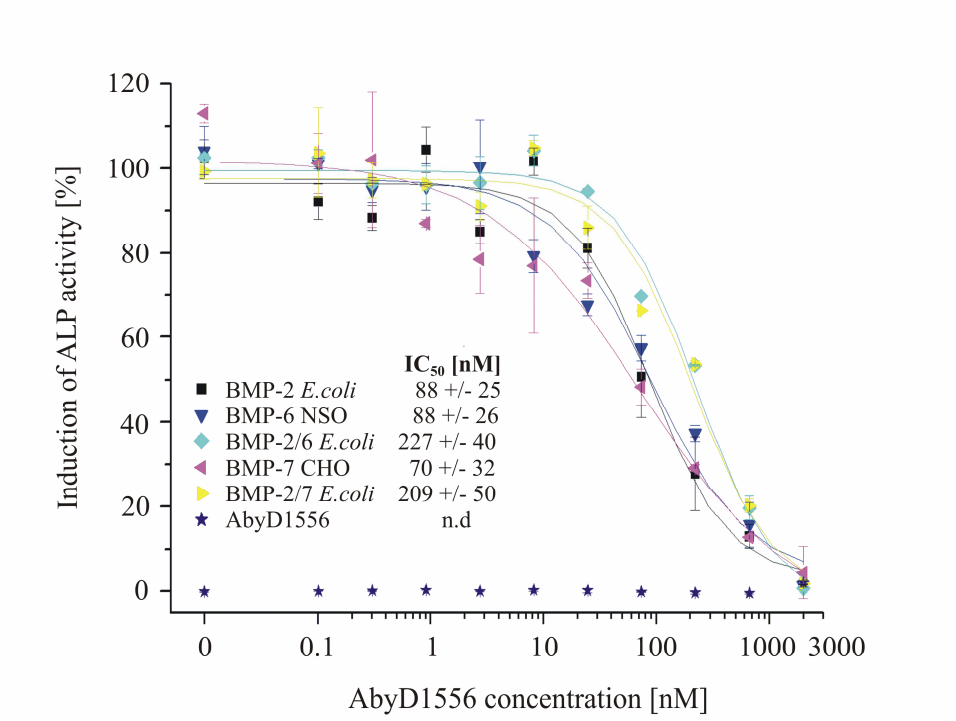

Fig. 4.18 – Determination of alkaline phosphatase (ALP) activity in C2C12 cells – AbyD 1556 blocks BMPR-IA thus inhibiting the induction of ALP activity via BMP ligands in a dose dependent manner. Concentration of BMP ligands were the same at all measuring points correlating with the EC_{50} value established in fig. 4.17 for every single ligand. AbyD 1556 alone elicit no effect on ALP activity, therefore an IC_{50} was not determinable (n.d.).

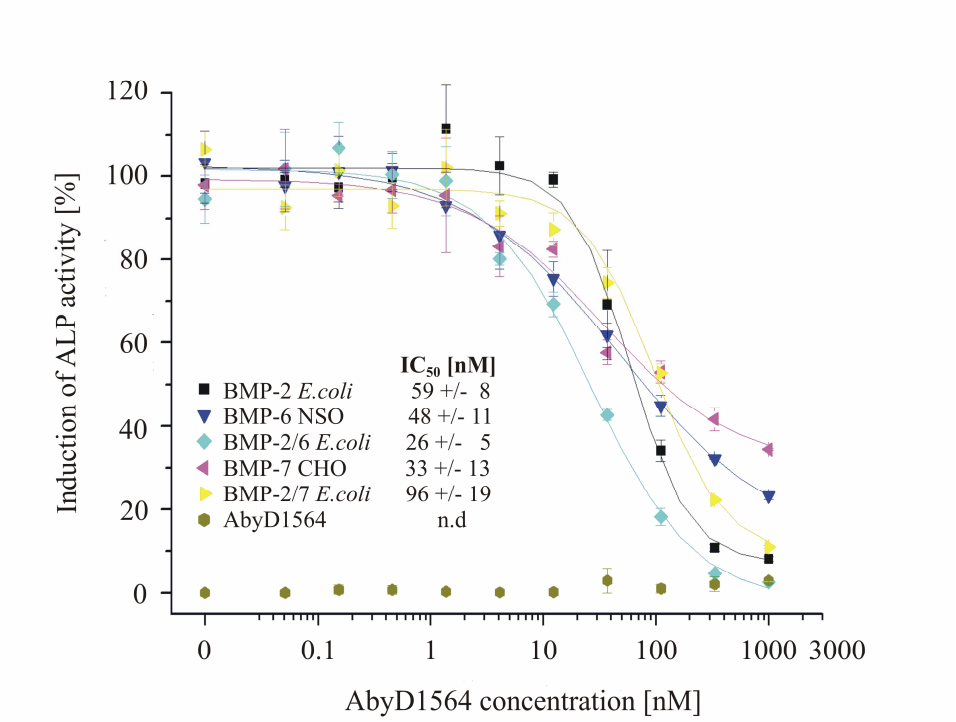

Fig. 4.19 – Determination of alkaline phosphatase (ALP) activity in C2C12 cells – AbyD 1564 blocks BMPR-IA thus inhibiting the induction of ALP activity via BMP ligands in a dose dependent manner. Concentration of BMP ligands were the same at all measuring points correlating with the EC_{50} value established in fig. 4.17 for every single ligand. AbyD 1564 alone elicit no effect on ALP activity, therefore an IC_{50} was not determinable (n.d.).

Unfortunately, effective antibodies against ActR-I were not available, thus its involvement in ALP induction could not be examined thoroughly. To circumvent this problem, another cell line which expresses only ActR-I as type I receptor was examined (see chapter 4.3.2.).

ALP assay using ATDC5 cells

The same experiments described above were performed using the murine chondrocytic cell line ATDC5 which has also the ability to produce ALP upon BMP stimulation (Nakamura et al. 1999).

Again, all BMPs, except for BMP-6 from *E.coli*, induced ALP activity in a dose dependent manner (see fig. 4.20). Remarkably, the activity of BMP heterodimers is five- to ten-fold higher than that of the BMP homodimers. In addition, heterodimers exhibit significant lower EC_{50} values by the factor of around 20 in the ATDC5 cells compared with the results from the C2C12 cell experiments (see fig. 4.17 for comparison). Homodimers showed also an increased activity. However, this was not as pronounced as seen in the case of BMP-2/6 and BMP-2/7.

This finding is in agreement with the work of Israel and others (Israel et al. 1996) They showed that heterodimeric BMP-2/7 produced in eukaryotic CHO cells achieve a specific activity about 20-fold higher than BMP homodimers in ALP assays using the mouse stromal cell line W-20-17. In addition, EC_{50} values for ligands BMP-2 (CHO), BMP-6 (NSO) and BMP-7 (CHO) derived from the company R+D systems are in agreement with their postulated activity strengthen the results obtained for BMP-2/6 and BMP-2/7 (see www.rndsystems.com for comparison).

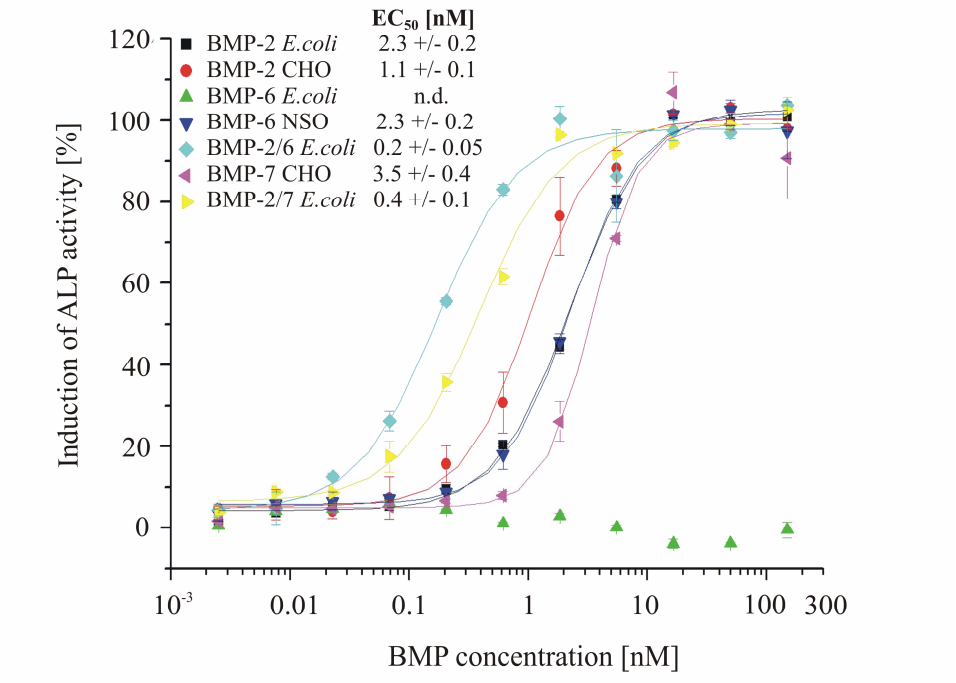

Fig. 4.20 – Determination of alkaline phosphatase (ALP) activity in ATDC5 cells – BMP ligands induce ALP activity in a dose dependent manner except for BMP-6 produced in *E.coli* cells. In this case, an EC_{50} was not determinable (n.d.).

Experiments with BMPR-IA inhibiting antibodies were also performed in ATDC5 cells which exhibit the same type I receptor composition as C2C12 cells (Akiyama et al. 2000). Here, BMPR-IA and ActR-I are found in similar amounts, whereas BMPR-IB is missing.

Both antibodies were able to block ALP induction mediated by BMP ligands even though not as efficiently as monitored in C2C12 cells (see Fig. 4.21 and 4.22). However, when applied alone, the antibodies inhibited also an intrinsic signal probably mediated by BMP-4 which is produced in ATDC5 cells (Akiyama et al. 2000). This circumstance makes it very difficult to address the real contribution of different receptor subtypes to ALP signalling or the objective efficiency of the two BMPR-IA inhibiting antibodies. Therefore, this cell line was not further used for additional ALP inhibiting assays.

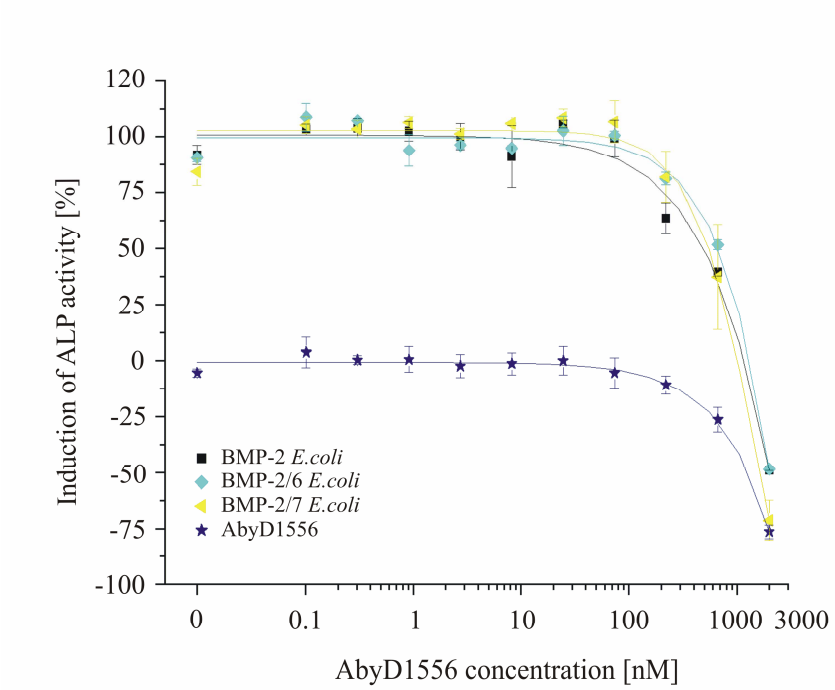

Fig. 4.21 – Determination of alkaline phosphatase (ALP) activity in ATDC5 cells – AbyD 1556 blocks BMPR-IA thus inhibiting the induction of ALP activity via BMP ligands in a dose dependent manner. Concentration of BMP ligands were the same at all measuring points correlating with the EC_{50} value established in fig. 4.20 for every single ligand. AbyD 1556 alone elicit a noticeable inhibiting effect on ALP activity, therefore IC_{50} values for ligands were impossible to determine.

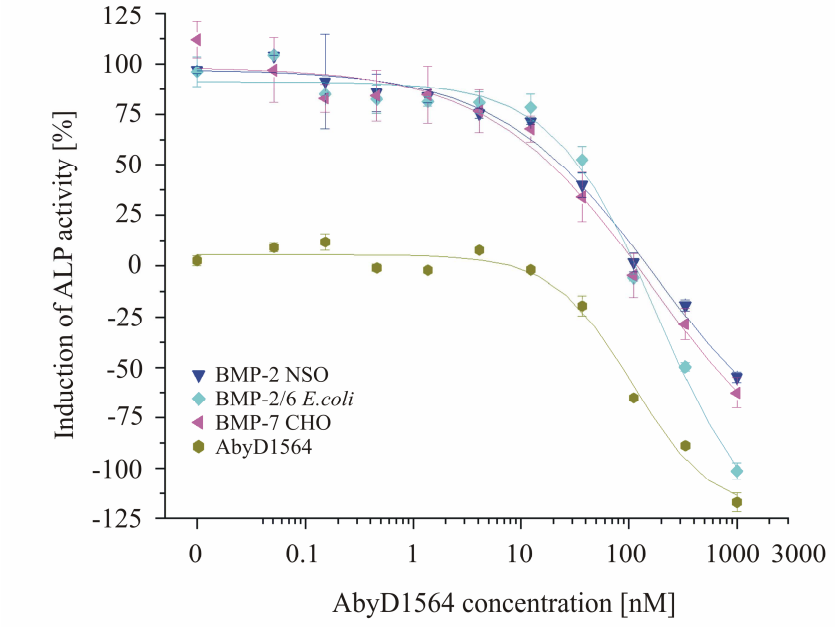

Fig. 4.22 – Determination of alkaline phosphatase (ALP) activity in ATDC5 cells – AbyD 1564 blocks BMPR-IA thus inhibiting the induction of ALP activity via BMP ligands in a dose dependent manner. Concentration of BMP ligands were the same at all measuring points correlating with the EC_{50} value established in fig. 4.20 for every single ligand. AbyD 1564 alone elicit a noticeable inhibiting effect on ALP activity, therefore IC_{50} values for ligands were impossible to determine.

4.3.2. ^{3}H-Thymidine incorporation assay

As already mentioned in chapter 4.3.1, the effect of the type I receptor ActR-I in ALP assays could not be examined thoroughly because of the lack of suitable inhibiting antibodies directed versus ActR-I. To circumvent this problem, the cell line INA-6 which expresses only mRNA for ActR-I was examined. It could be demonstrated previously that only BMPs from the BMP-6/7 subclass were able to inhibit cell proliferation and to induce apoptosis due to their receptor affinities (Ro et al. 2004). BMP-2 was unable to do so probably because of the lack of its main signalling receptors BMPR-IA and BMPR-IB. However, the issue of BMP heterodimers who comprises both ligand subtypes was not addressed. Therefore, a ^{3}H-Thymidine incorporation assay using BMP-2/6 and BMP-2/7 to check their ability to inhibit proliferation of INA-6 cells was performed (see chapter 3.10.5).

BMP-6 and BMP-7 were able to inhibit cell proliferation as expected (see fig. 4.23). BMP-6 derived from *E.coli* is inactive in INA-6 cells as described before (data not shown) (Saremba et al. 2008). The heterodimers and BMP-2 from *E.coli* or CHO cells exhibited an activity which was more than 100-fold lower than that of BMP-6 and BMP-7 from animal cells. The IC_{50} values of BMP heterodimers and BMP-2 were between 60 and 300 nM. However, it is unclear, whether these differences between the IC_{50} values are meaningful, since the applied concentrations are at the limit of solubility for these proteins.

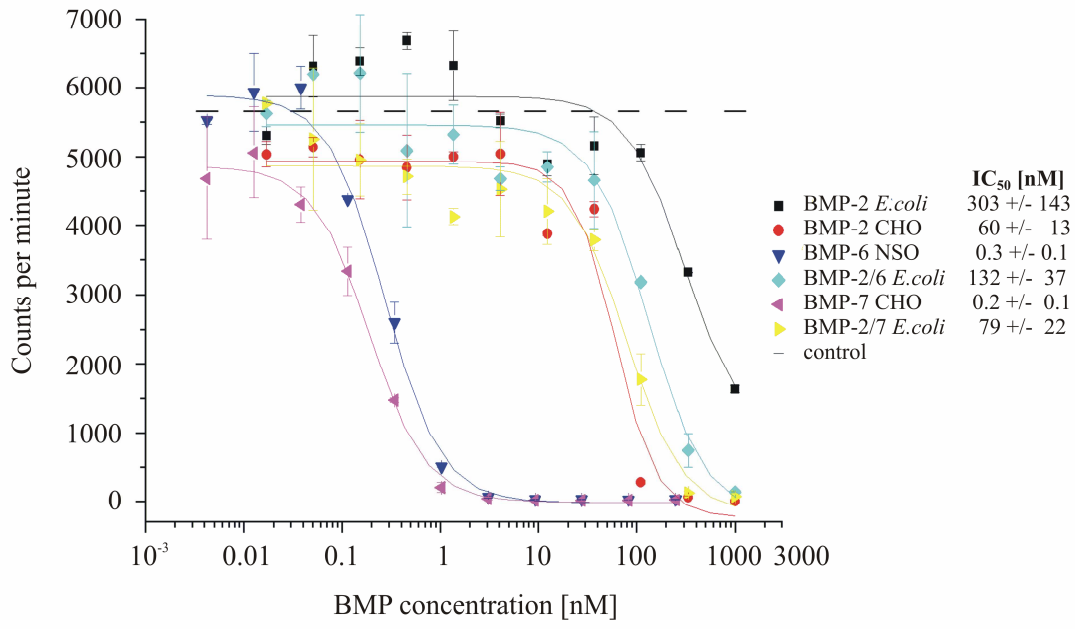

Fig. 4.23 – Determination of ^{3}H-Thymidine incorporation in INA-6 cells – BMP ligands inhibit cell proliferation in a dose dependent manner.

The results of the INA-6 assay strongly suggest that ActR-I alone is not sufficient to mediate a high biological activity of the heterodimeric BMP-2/6 and BMP-2/7. Furthermore, it would be interesting to see, whether glycosylated heterodimers produced in animal cells exhibit a higher activity than both the glycosylated BMP-6 and BMP-7 and the heterodimers produced in *E.coli* (see discussion).

^{3}H-Thymidine incorporation assays were also carried out in IH-1 cells expressing all three relevant receptor subtypes BMPR-IA, BMPR-IB and ActR-I (Ro et al. 2004).
Here, the finding was a different one compared to the results obtained in INA-6 cells (see fig. 4.24). The effect of BMP-2 (CHO) and both heterodimers on cell proliferation was drastically increased and reached about the same EC_{50} levels as BMP-7 (CHO) and BMP-6 (NSO). The level of BMP-7 (CHO) did not change in comparison to the results in INA-6 cells, whereas the effect of BMP-6 (NSO) was slightly lower. BMP-2 (*E.coli*) showed also an enhanced activity by the factor of 30 and even BMP-6 (*E.coli*) exhibited an effect, although at very high doses which are at the limit of solubility for BMP proteins.

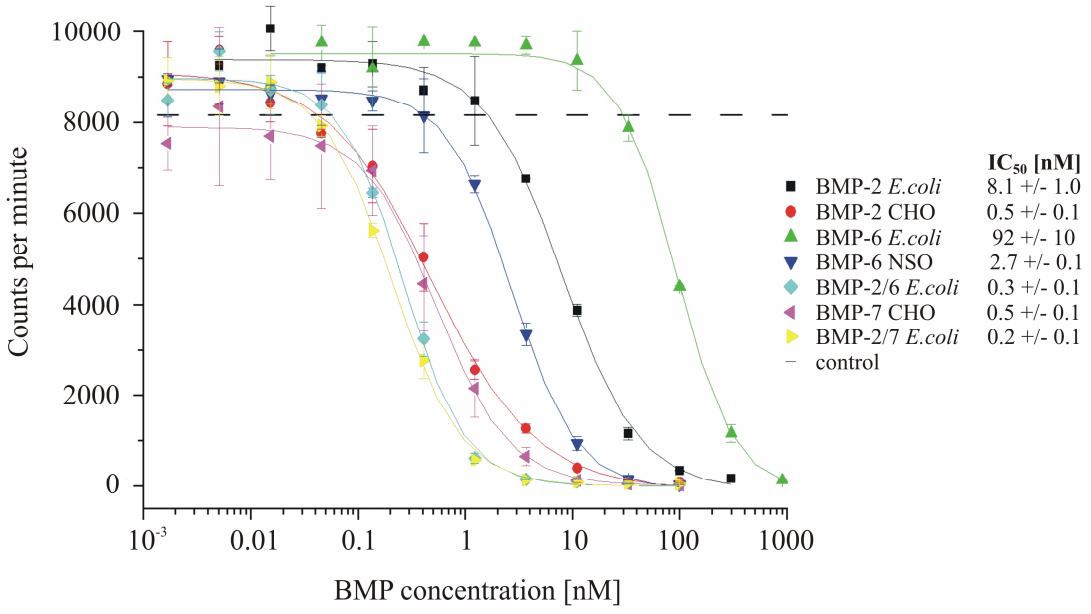

Fig. 4.24 – Determination of ^{3}H-Thymidine incorporation in IH-1 cells – BMP ligands inhibit cell proliferation in a dose dependent manner.

Taken together, it is most likely that the effect of increased BMP potency to inhibit cell proliferation is mainly achieved by an additional signalling via BMPR-IA and/or BMPR-IB. However, a direct involvement and contribution of BMPR-IB to the signalling could not be proved with this experimental setting. It is more likely that BMPR-IA is responsible for the

increased BMP-2 and BMP heterodimer activity since BMPR-IA is the main signalling receptor as already confirmed in ALP experiments in C2C12 cells (see fig. 4.18 and 4.19). In addition, BMP heterodimers showed again an enhanced activity as compared to their homodimer counterparts as already observed in ALP experiments.

4.3.3. IH-1 apoptosis assay

Beside the ability to inhibit cell proliferation, BMP ligands were also tested regarding their capability to induce apoptosis. For these experiments, BMPs were used at three different, but representative concentrations: at their EC_{50} level, examined in ^{3}H-Thymidine incorporation assays (see fig. 4.24), 100-fold below as well above this level (EC_{50} / 100 and 100 · EC_{50}). As one example, valuation is shown for non treated cells and cells treated with BMP-2/7 (see fig. 4.25).

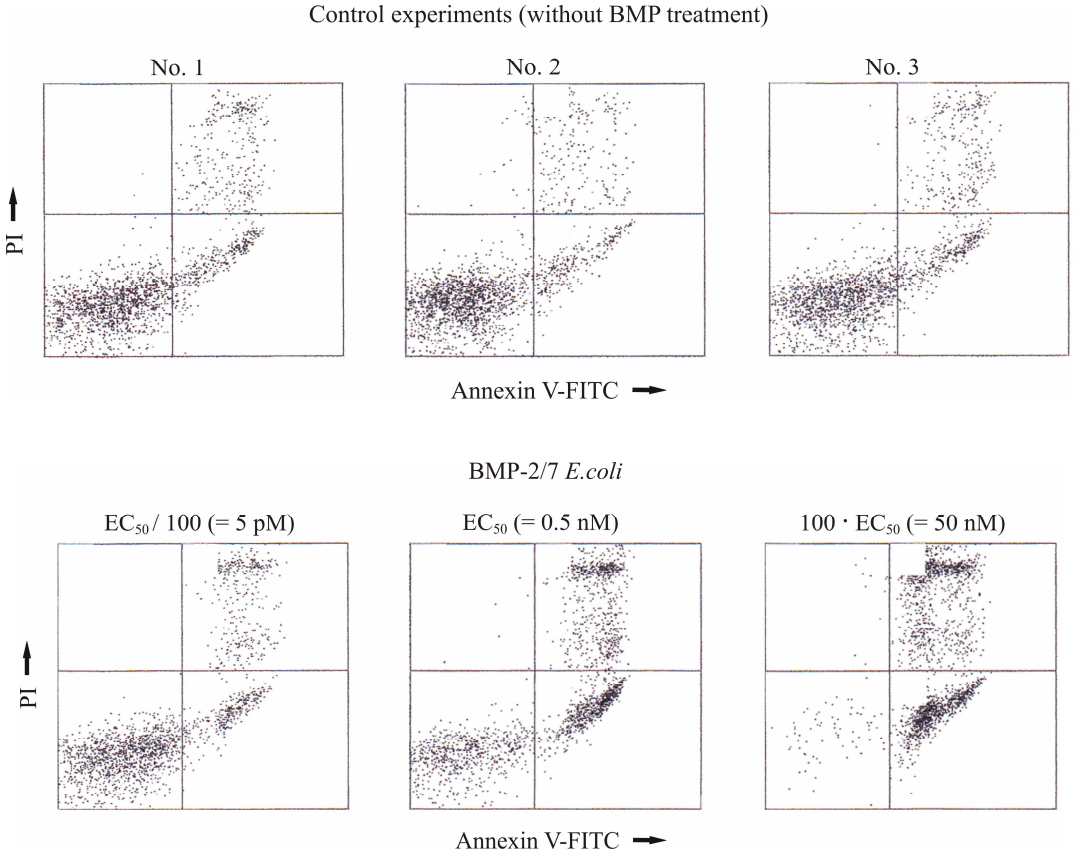

Fig. 4.25 – BMP induced apoptosis in IH-1 cells – For FACS analysis, cells were classified as either PI- or annexin V-positive or -negative. All PI-positive cells were considered dead (upper 2 quadrants of dot plots), PI-negative and annexin V-positive cells were considered apoptotic (lower right quadrant), and remaining cells (lower left quadrant) were considered viable. Typical dot plots for control (upper panel) and BMP-2/7 treated cells (lower panel) are shown. BMP concentrations were chosen according to the results in figure 4.24.

Cell viability was determined by annexin V-FITC / propidium iodide (PI) flow cytometry. All PI positive cells were considered dead (upper 2 quadrants of dot plots), PI negative and annexin V positive cells were considered apoptotic (lower right quadrant), and remaining cells (lower left quadrant) were considered viable. The amount of viable cells was constant in the control experiments (see fig. 4.25 upper row), whereas it decreased tremendously with increasing BMP-2/7 concentrations (see fig. 4.25 lower row). The results for all BMPs used in IH-1 apoptosis assay are summarized in fig. 4.26.

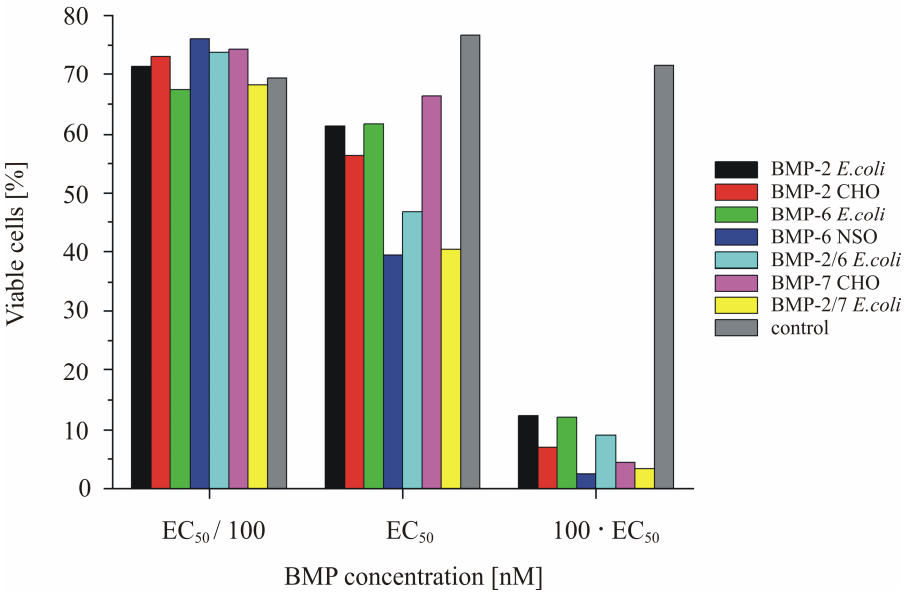

Fig. 4.26 – BMP induced apoptosis in IH-1 cells – **B)** Results of all tested BMP ligands are summarized here. All BMP ligands induce apoptosis in IH-1 cells at high dose concentrations (100 · EC_{50}). At EC_{50}-level, all BMPs exhibit an effect on cell viability, which is pronounced in BMP-6 (NSO), BMP-2/6 and BMP-2/7 stimulated cells, whereas all other BMPs were less effective. At very low concentrations (EC_{50} / 100) no effect was visible. (Note: For BMP-6 *E.coli*, the high dose concentration was only 10-fold above the EC_{50}-value.)

At very low BMP concentrations (EC_{50} / 100) the amount of viable cells remained unaffected in all cases. At very high dose rates (100 · EC_{50}) viability was completely abolished by all BMPs. Though all BMPs reduced the amount of viable cells at intermediate concentrations (EC_{50}) compared to low doses experiments, only BMP-6 (NSO), BMP-2/6 and BMP-2/7 showed considerable effects. A detailed analysis applying smaller intervals in BMP concentrations could result in a better estimation of BMP doses necessary for inducing apoptosis.

Nonetheless, all BMPs were capable to induce apoptosis in IH-1 cells; even though their potency varied extremely corresponding to their respective EC_{50} values in ^{3}H-Thymidine incorporation assays (see fig. 4.24).

4.3.4. Smad phosphorylation assay

All cell assays, that have been described so far, monitor BMP responses quite late after receptor assembly and activation (e.g. ALP induction, cell proliferation and cell apoptosis). Therefore, the phosphorylation of Smad proteins as a more immediate and well described effect upon receptor activation was examined in addition. The phosphorylation of Smad proteins is already detectable in western blot analysis 5 – 10 min after BMPs were added to C2C12 or ATDC5 cells (Jannes Ulbrich, personal communication). BMPs use the Smad 1,5,8 subclass to activate specific target genes in the cell nucleus (Massague et al. 2005). The potency of heterodimeric BMPs to phosphorylate Smad proteins were tested in ATDC5 and C2C12 cells during a 30 minute incubation period (see fig. 4.27).

BMP-2 and BMP-6 were able to induce Smad phosphorylation in both cell lines in a dose dependent manner with EC_{50} values of ~ 100 pM (BMP-2 *E.coli*) and 840 pM (BMP-6 NSO) in ATDC5 cells (see fig. 4.27 A, B). The EC_{50} values determined in C2C12 cells were about two times lower (see fig. 4.27 C, D). As seen already in ALP assays, the BMP heterodimer BMP-2/6 and BMP-2/7 were considerable more active compared to their respective BMP homodimers with EC_{50} values of 10 – 20 pM in both cell lines.

In conclusion, the BMP-2/6 and BMP-2/7 heterodimers produced in *E.coli* exhibited a higher biological activity in the short-term smad phosphorylation assay and in long-term ALP induction assays than their homodimeric counterparts. This suggests that the heterodimeric BMP proteins are more efficient in the early steps of BMP signalling which means receptor binding and assembly.

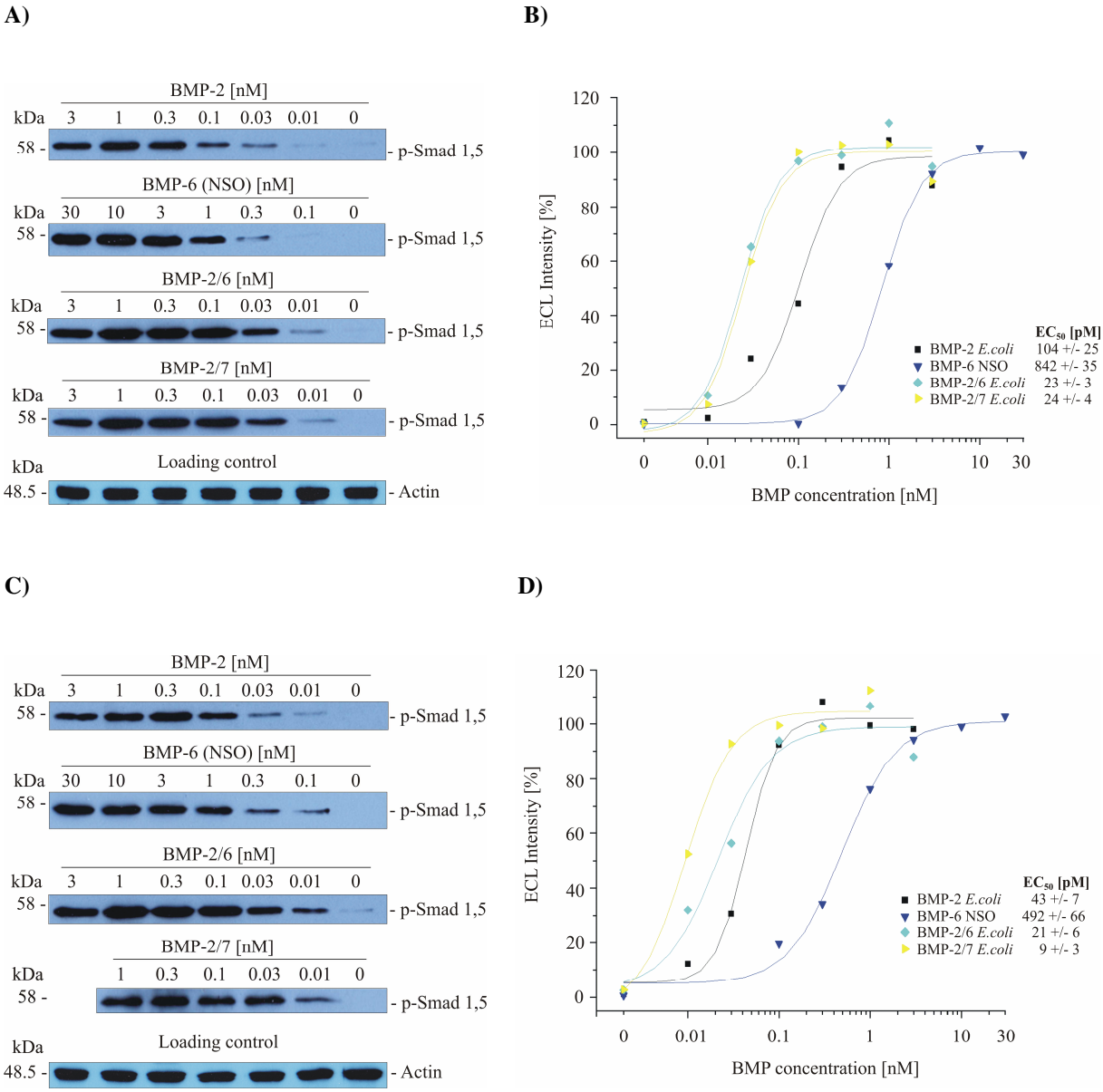

Fig. 4.27 – Determination of Smad phosphorylation activity in ATDC5 (A, B) and C2C12 cells (C, D) – **A, C)** Western blot analysis demonstrates the Smad phosphorylation inducing properties of BMP-2 (*E.coli*), BMP-6 (NSO) and both BMP heterodimers 2/6 and 2/7. The expression of actin is shown as loading control. **B, D)** The strength of western blot bands (shown in A and C) were processed, evaluated and summarized in a scatter plot to determine the potency (EC_{50} value) of BMPs to induce Smad phosphorylation.

5. Structural and functional analysis of an antibody/BMPR-IA$_{ecd}$ complex

5.1. Preparation of BMPR-IA$_{ecd}$ wildtype and mutants

Generation, expression and purification of BMPR-IA$_{ecd}$ protein was performed according to a protocol established by Kirsch and colleagues (Kirsch et al. 2000a). The position of amino acids altered in BMPR-IA$_{ecd}$ mutants were selected on the basis of results of the structure analysis of the antibody/BMPR- IA$_{ecd}$ complex (see section 5.3). The mutants were produced in the same way as the BMPR-IA$_{ecd}$ wildtype.

Cloning and expression

The extracellular domain of BMPR-IA (residues 24 – 152 of the precursor protein) including a N-terminal extension of GSGAMA was cloned into the modified pET32a vector via NcoI and Bpu11021 restriction sites resulting in a thioredoxin fusion protein (see fig. 5.1A).

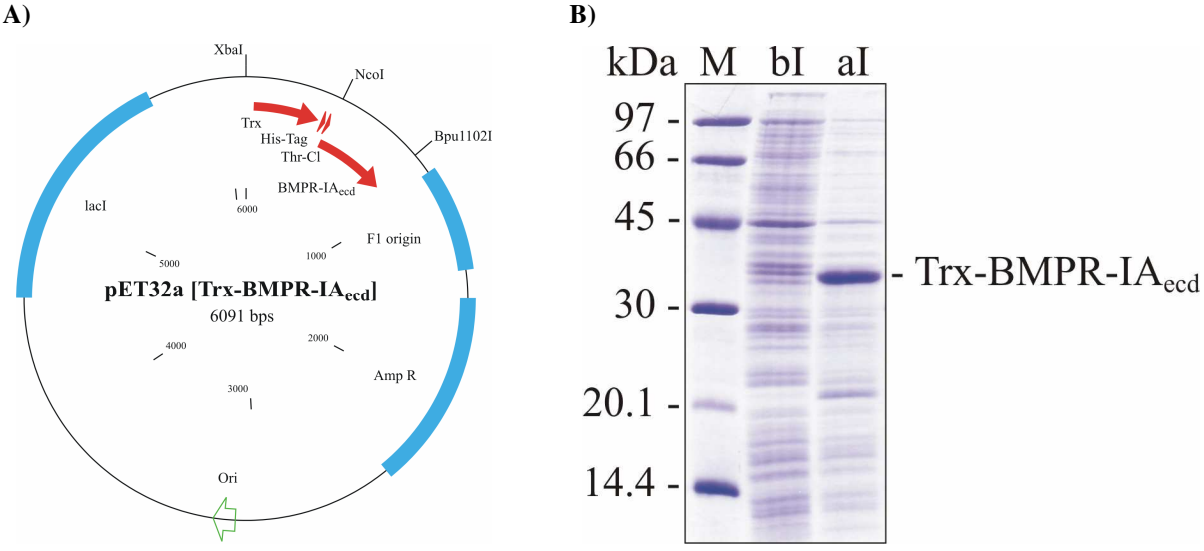

Fig. 5.1 – A) Expression vector pET32a [Trx-BMPRIA$_{ecd}$] – Extracellular domain of BMPR-IA was inserted via restriction sites NcoI and Bpu1102. BMPR-IA$_{ecd}$ was expressed as thioredoxin (Trx) fusion protein including a hexahistidin tag (His-Tag) and a thrombin cleavage site (Thr-Cl) in AD494 (DE3) cells. **B)** Induction control of Trx-BMPR-IA$_{ecd}$ – SDS-PAGE (reduced) with protein marker (M), cell samples before (bI) and after 16 h induction (aI).

The final expression construct comprised the thioredoxin protein, a hexahistidin tag, a thrombin cleavage site and the $BMPRIA_{ecd}$ part. For expression, the pET32a [Trx-$BMPRIA_{ecd}$] vector was transformed into AD494 (DE3) cells.
Protein expression was induced with 1 mM IPTG and cells were shaken for 16 h at 20 °C afterwards. Then, cells were harvested and protein expression was monitored via SDS-PAGE (see fig. 5.1 B). The gel exhibits a strong band after induction above 30 kDa, which corresponds to the size of the $BMPRIA_{ecd}$ construct. The protein yield varied depending on the $BMPRIA_{ecd}$ mutant between 2.81 and 10.67 gram per liter culture medium (for summary, see table 5.1).

Protein extraction and immobilized metal ion affinity chromatography (IMAC) using Ni-chelating agarose

After harvesting, cells were disrupted via sonication and soluble proteins were separated from cell debris by centrifugation. Most of the thioredoxin-$BMPRIA_{ecd}$ fusion protein was located in the supernatant (see fig. 5.2). However, a small part remained in the cell pellet irrespective of repeated sonication cycles. Consequently, the supernatant was loaded on a column filled with Ni-chelating agarose and an immobilized metal ion affinity chromatography (IMAC) was performed as first purification step. $BMPRIA_{ecd}$ bound to the column due to its hexahistidin tag and could be eluted with 500 mM imidazole afterwards. Elution fractions containing the thioredoxin-$BMPRIA_{ecd}$ fusion protein were identified by means of SDS-PAGE analysis. These fractions were combined and dialyzed against EDTA buffer to remove adherent nickel ions. The yield after this step ranged from 12.45 to 37.92 milligram protein per gram harvested cells (see table 5.1).

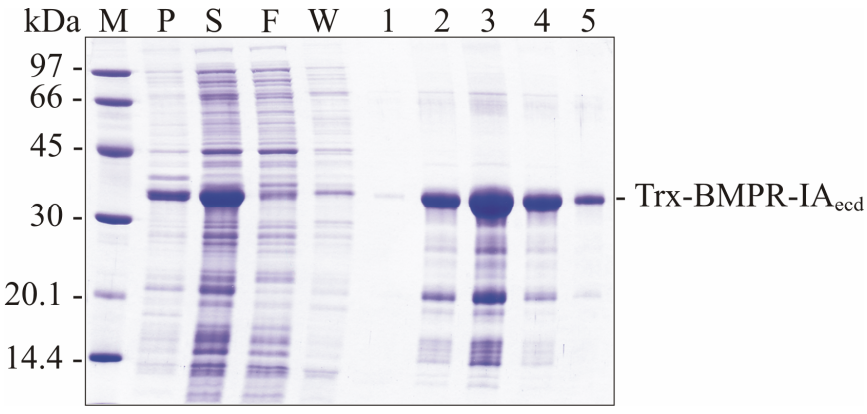

Fig. 5.2 – Immobilized metal ion affinity chromatography of Trx-BMPR-IA_{ecd} using Ni-chelating agarose – SDS-PAGE (reduced) with pellet (P), supernatant (S), flowthrough (F), wash (W) and elution fractions (1-5).

Protein cleavage employing the protease thrombin

The protein solution from the IMAC purification step (see above) was dialyzed against thrombin cleavage buffer. Afterwards, 0.5 units of thrombin per milligram thioredoxin-$BMPRIA_{ecd}$ fusion protein were added. Protein cleavage was monitored by SDS-PAGE analysis (see fig. 5.3). Under reducing conditions thioredoxin and $BMPRIA_{ecd}$ exhibit a different running performance although they have almost the same molecular weight (14 084 kDa and 14 660 kDa, respectively). $BMPRIA_{ecd}$ runs at approximately 20 kDa, whereas thioredoxin displays a running behavior as expected. However, this difference was also observed in previous studies (e.g. Weber et al. 2007), therefore confirming our experimental setup. Under non reducing conditions both proteins run as one band at circa 14 kDa as anticipated. After complete cleavage, the protein solution was dialyzed twice against the buffer for the next purification step.

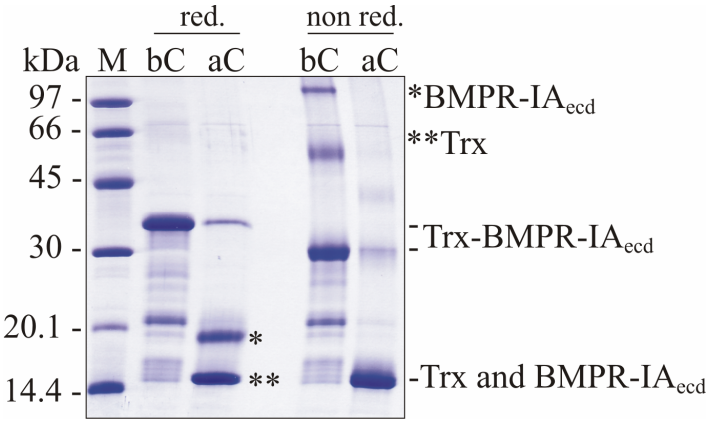

Fig. 5.3 – Thrombin cleavage of Thioredoxin-BMPR-IA_{ecd} – SDS-PAGE with protein samples before (bC) and after cleavage (aC) under either reducing (red.) or non reducing conditions (non red.). Thioredoxin and BMPR-IA_{ecd} are clearly distinguishable from each other under reducing conditions whereas they run almost as one band under non reducing conditions.

Anion exchange chromatography using Fractogel EMD TMAE 650 (S)

To separate biological active $BMPRIA_{ecd}$ monomers from the cleaved thioredoxin part and from inactive multimers, an anion exchange chromatography step was accomplished.
Applying a gradient with increasing NaCl concentration, $BMPRIA_{ecd}$ monomer eluted in a single peak at 0.2 M NaCl (see fig. 5.4 A). Applying SDS-PAGE analysis (see fig. 5.4 B, C), the monomer containing fractions 27 – 30 were combined and dialyzed against HBS_{500} buffer

for BMP-2 affinity chromatography. The yield of $BMPRIA_{ecd}$ proteins had the dimension of 0.38 – 2.66 milligram per gram harvested cells (see table 5.1).

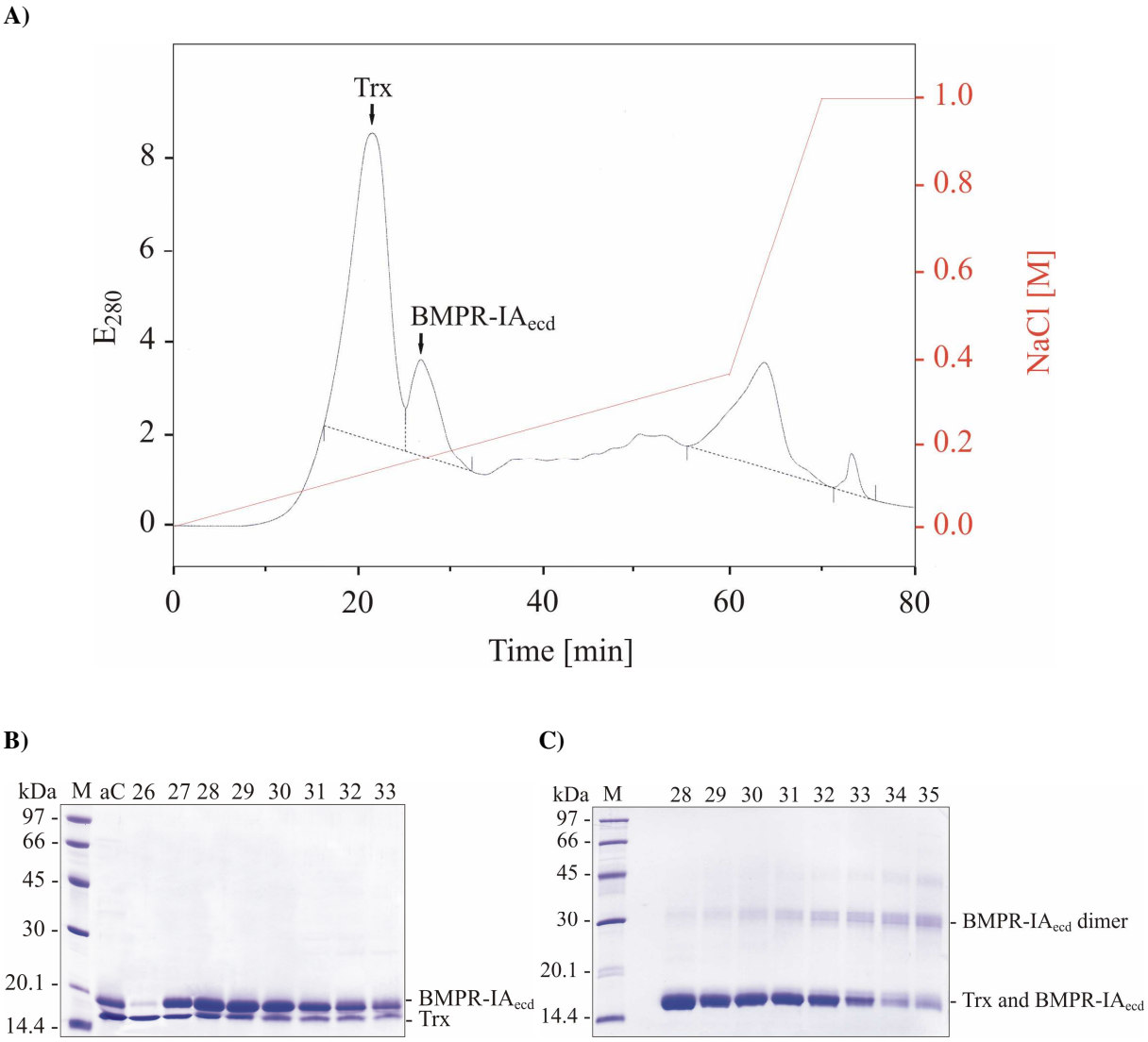

Fig. 5.4 – Anion exchange chromatography for $BMPR\text{-}IA_{ecd}$ using an EMD TMAE 650 (S) column – **A)** Elution profile (black) – Thioredoxin (Trx) elutes mainly in the first peak, $BMPR\text{-}IA_{ecd}$ monomers elute in the second peak at 26.7 min. The salt gradient is plotted in red. **B)** SDS-PAGE (reduced) with protein samples after thrombin cleavage (aC) and fractions 26 – 33. **C)** SDS-PAGE (non reduced) with protein samples from elution fractions 28 – 35. A gradual agglutination process resulting in dimers and multimers is clearly visible beginning with fraction 31. Fractions 27 – 30 were combined and used for further purification.

BMP-2 affinity chromatography

To test whether the $BMPR\text{-}IA_{ecd}$ protein was biological active, BMP-2 affinity chromatography as last purification step was performed. In a first step, a BMP-2 affinity column was generated with a maximal capacity of approximately 3 mg $BMPRIA_{ecd}$ protein.

Then, the $BMPRIA_{ecd}$ solution extracted from the anion exchange chromatography step was concentrated to 1 – 2 ml by ultrafiltration and loaded on the BMP-2 affinity column. $BMPRIA_{ecd}$ was eluted with $MgCl_2$, protein containing fractions were combined and dialyzed against HBS150 buffer. The protein flowthrough was concentrated again and reloaded on the regenerated column. This process was executed until protein binding to the column was not detectable anymore. Finally, $BMPRIA_{ecd}$ was concentrated to 1 mg protein / ml buffer and stored at – 80°C.

Two $BMPRIA_{ecd}$ mutants, F60A and F85A, were unable to bind to the BMP-2 affinity column most likely due to an altered structural architecture as a result of mutation. For these proteins, a preparative RP-HPLC was carried out as last purification step.

Protein purity was determined via SDS-PAGE and RP-HPLC analysis (see fig. 5.5). $BMPRIA_{ecd}$ runs in the SDS gel as single band both under reducing and non reducing conditions. Moreover, it elutes as a single peak in RP-HPLC indicating the high purity of $BMPRIA_{ecd}$ protein. The yield of all produced $BMPRIA_{ecd}$ mutants are summarized in table 5.1. It ranges from 0.01 mg to 0.41 mg protein / gram harvested cells.

A) **B)**

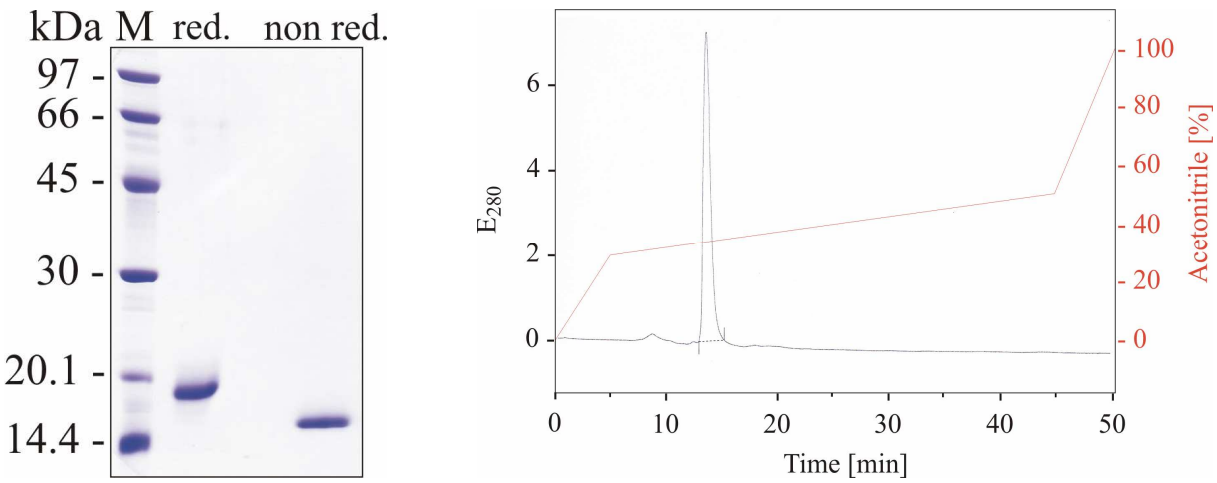

Fig. 5.5 – Affinity chromatography of $BMPR\text{-}IA_{ecd}$ using a BMP-2 column – **A)** SDS-PAGE of the combined elution fractions of $BMPR\text{-}IA_{ecd}$ under reduced (red.) and non reduced conditions (non red.). **B)** RP-HPLC elution profile (black) of $BMPR\text{-}IA_{ecd}$ – $BMPR\text{-}IA_{ecd}$ elutes as a single peak after 13.5 min. The acetonitrile gradient is plotted in red.

Table 5.1 – Yields of BMPR-IA$_{ecd}$ mutants during the purification process

BMPR-IA$_{ecd}$ mutants	Wet weight of cells after fermentation [g/L medium]	Ni-chelat affinity chromatography [mg/g cells]	TMAE anion exchange chromatography [mg/g cells]	BMP-2 affinity chromatography [mg/g cells]
Wildtype	3.90	32.46	2.44	0.24
F60A	4.97	21.96	0.93	0.01[a)]
I62A	3.75	36.89	2.14	0.29
E64A	2.81	37.92	1.21	0.15
D67A	4.56	28.05	0.64	0.14
M78A	3.61	24.62	0.88	0.09
K79A	7.31	15.25	0.48	0.19
E81A	7.56	14.89	0.80	0.10
F85A	8.00	14.93	0.57	0.04[a)]
K92A	6.22	31.74	1.79	0.21
Q94A	4.28	32.01	1.76	0.41
R97A	10.67	12.45	0.38	0.08
I99A	6.11	22.00	2.66	0.06

a) The final purification step for F60A and F85A was a preparative RP-HPLC.

Mass spectrometric analyis of BMPR-IA$_{ecd}$

As an additional quality control, BMPR-IA$_{ecd}$ was subjected to mass spectrometry. Signals from BMPR-IA$_{ecd}$ in the original data are only visible with their different grade of protonation indicating a high degree of protein purity (see fig. 5.6 A). After deconvolution procedure, the theoretical molecular weight could be validated (see fig. 5.6 B).

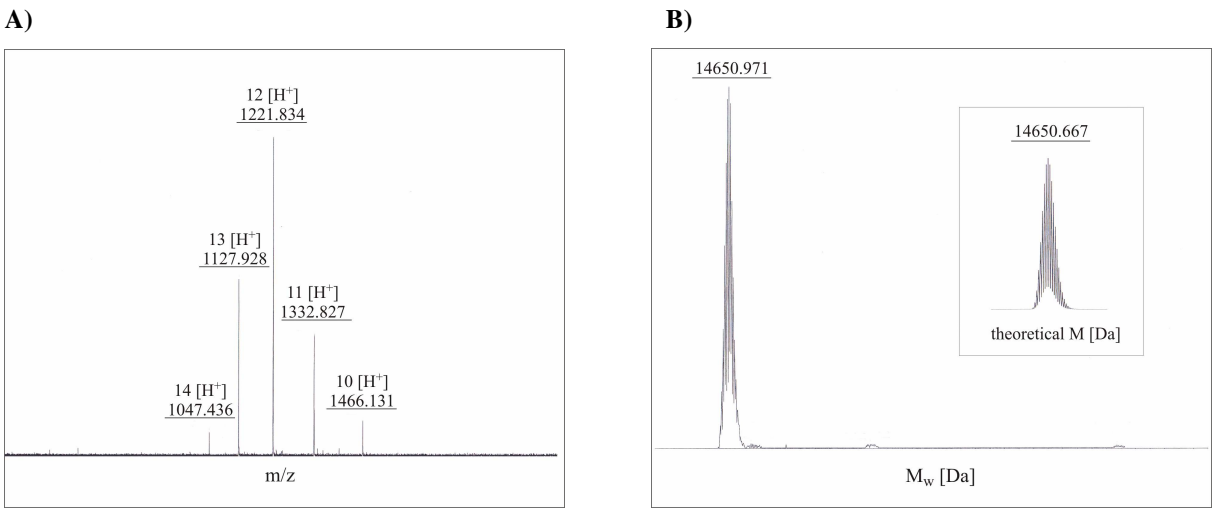

Fig. 5.6 – Mass spectrometric analysis of BMPR-IA$_{ecd}$ – **A)** Original data visualized by the mass-to-charge ratio m/z. **B)** Data of the 12-fold charged ions after deconvolution depicted with the corresponding molecular weight M_w.

The mass spectrometry data for all BMPR-IA$_{ecd}$ mutants are listed in table 5.2. All mutants are in agreement with their theoretical molecular weight. However, for four mutants – F60A, K79A, K92A and Q94 – also a truncated form without the N-terminal GSGAMA extension could be detected. Since this extension cannot be found in the native form of BMPR-IA$_{ecd}$ and the N-terminus displays a high structural flexibility in structural analyis (Kirsch et al. 2000b; Keller et al. 2004b), the lack of these amino acids should not exhibit any negative impacts in interaction analysis studies (see section 5.3.4).

Table 5.2 – Molecular weights (M_w) of BMPR-IA$_{ecd}$ mutants determined by mass spectrometry

BMPR-IA$_{ecd}$ mutants	M_w [Da]	Theoretical M_w [Da]	Difference [Da]	Modifications
Wildtype	14 650.971	14 650.667	0.304	
F60A	14 574.754	14 574.636	0.118	
	14 100.736	14 100.446	0.290	- GSGAMA (N-terminal)
I62A	14 608.563	14 608.620	- 0.057	
E64A	14 592.635	14 592.662	- 0.027	
D67A	14 606.651	14 606.677	- 0.026	
M78A	14 590.649	14 590.664	- 0.015	
K79A	14 593.625	14 593.609	0.016	
	14 119.411	14 119.420	-0.009	- GSGAMA (N-terminal)
E81A	14 592.892	14 592.662	0.230	
F85A	14 574.857	14 574.636	0.221	
K92A	14 593.883	14 593.609	0.274	
	14 119.688	14 119.420	0.268	- GSGAMA (N-terminal)
Q94A	14 593.869	14 593.646	0.223	
	14 119.721	14 119.458	0.263	- GSGAMA (N-terminal)
R97A	14 565.847	14 565.603	0.244	
I99A	14 608.796	14 608.620	0.176	

5.2. Complex preparation and crystallization

The preparation and crystallization of antibody/BMPR-IA$_{ecd}$ complexes were already accomplished during the author's diploma thesis (Harth 2006). Briefly, a binary complex of AbyD1556 bound to BMPR-IA$_{ecd}$ was formed by mixing AbyD1556 with a 1.1-fold molar excess of BMPR-IA$_{ecd}$. The protein complex was purified by gel filtration using a Superdex200 column. Fractions containing the antibody-receptor complex in equimolar stoichiometry were combined and the protein solution was concentrated up to 16.4 mg/ml using ultrafiltration. Single crystals of the AbyD1556/BMPR-IA complex could be grown

from hanging drop setups at room temperature over a reservoir solution of 100 mM Tris-HCl pH 7.0, 20% (w/v) PEG 8000 and 10% (w/v) glucose. Drops were composed of 2 µl protein solution and 1 µl reservoir solution. Protein crystals grew to a final size of approximately 150x150x40µm within 7 days (see fig. 5.7).

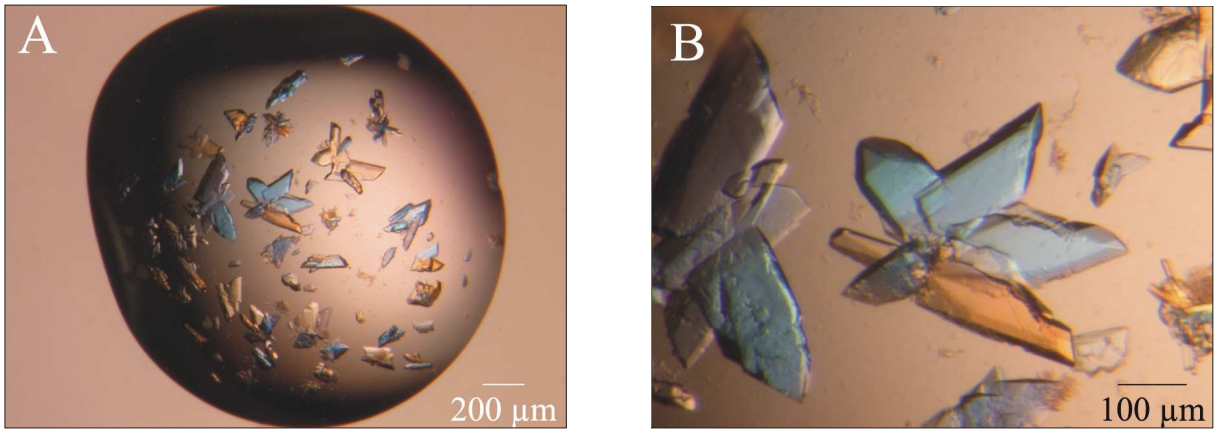

Fig. 5.7 – A) Crystals of the binary AbyD 1556/BMPR-IA$_{ecd}$ complex in a hanging drop vapor system – Crystallization condition is 100 mM Tris-HCl pH 7.0, 20% (w/v) PEG 8000 and 10% (w/v) glucose. The hanging drop is composed of 2 µl protein solution (c= 16.4 mg/ml) and 1 µl reservoir solution. Protein crystals grew to a final size of approximately 150 x 150 x 40 µm within 7 days. **B)** Magnification of a single protein crystal from the same drop. Picture is taken from (Harth 2006).

5.3. Structural analysis and characterization of an antibody/BMPR-IA$_{ecd}$ complex

5.3.1. Measurement of diffraction data sets

A native dataset of the AbyD1556/BMPR-IA$_{ecd}$ complex was acquired from a single crystal shown in fig. 5.7 on our X-ray home source. Crystals suitable for data acquisition diffracted to a resolution limit of up to 2.7Å (see fig. 5.8) and had the primitive monoclinic space group $P2_1$ with unit cell parameters of a = 89.32 Å, b = 129.25 Å, c = 100.24 Å and $\alpha = \gamma = 90°$ and $\beta = 92.27°$.

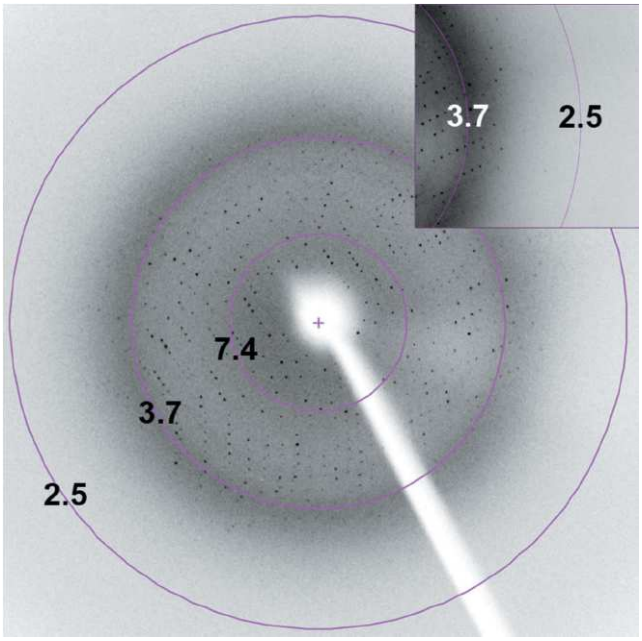

Fig. 5.8 – X-ray diffraction pattern of an AbyD 1556/BMPR-IA$_{ecd}$ crystal shown in fig. 5.7. – Illumination period was 3 min per 0.5° angular degree. The crystal diffract to a resolution limit of up to 2.7Å. The resolution limits (in Å) are indicated by magenta circles. Picture is taken from (Harth et al. 2010a).

Diffraction data were indexed and integrated using the software CrystalClear 1.3.6 (Rigaku). A complete dataset (95.3% completeness for the resolution range 30.4 to 2.7Å) and an R_{sym} of 0.08 could be obtained. A first analysis of the unit cell content by calculating the Matthew's coefficient (Matthews 1968) suggested the presence of three or four AbyD1556/BMPR-IA$_{ecd}$ complexes in the asymmetric unit. The Matthew's coefficient for three complexes was V_m = 3.06 Å^3/Da (= 60 % solvent content) and for four complexes V_m = 2.29 Å^3/Da (= 46 % solvent content), respectively. Since SDS-PAGE analysis of the crystals clearly suggested a 1:1 ratio of AbyD1556 and BMPR-IA$_{ecd}$ in the crystals (Harth 2006), a different packing with free and BMPR-IA$_{ecd}$ bound AbyD1556 seemed unlikely. While pseudotranslation could not be detected from analysis of the native Patterson map applying the program phenix.xtriage (Adams et al. 2010), two twofold axes could be identified from a self rotation calculation using the program GLRF (Tong and Rossmann 1997) on the κ = 180° section, which were perpendicular to each other and were oriented at about 45° with respect to the crystallographic twofold (see fig. 5.9). Considering the additional absence of any peaks in the κ = 120° section, the crystal is very likely to contain four AbyD1556/BMPR-IA$_{ecd}$ complexes in the asymmetric unit, which was confirmed in further experiments described below.

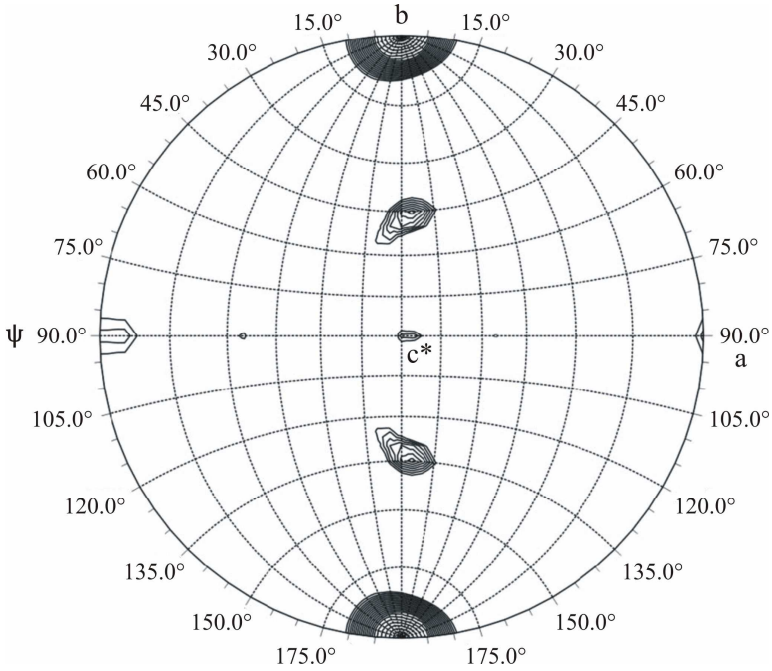

Fig. 5.9 – Section of a self-rotation using the software GLRF at κ = 180° – In addition to the crystallographic twofold observed at the top and bottom of the plot, two noncrystallographic twofold that are perpendicular to each other and share an angle of about 45° with the crystallographic twofold axes are seen. Picture is taken from (Harth et al. 2010a).

Initial phasing was performed by molecular replacement using the software packages CNS (Brunger 2007) and Phaser (McCoy et al. 2007). The structure of a human Fab fragment with high affinity for tetanus toxoid (PDB entry 1AQK) (Faber et al. 1998) was used as a search model for AbyD1556, the structure of BMPR-IA_{ecd} bound to BMP-2 (Keller et al. 2004b) as a search template for the receptor ectodomain. The structure was then refined in an iterative procedure using Refmac Version 5.02 (Murshudov et al. 1997) and via manual rebuilding using Quanta2006 (Accelrys). Statistics for data acquisition and structure refinement are compiled in table 5.3.

Table 5.3 – Data acquisition and structure refinement

Crystals and data processing	AbyD1556/BMPR-IA$_{ecd}$ complex
Beamline	home source
Wave length	1.5418 Å
Space group	$P2_1$
Unit cell	a = 89.32, b =129.25 Å, c = 100.24 Å
	$\alpha = \gamma = 90°$, $\beta = 92.27°$
Resolution	30.4 – 2.70 Å
	(2.80 – 2.70 Å)[a)]
Number of reflections collected	155123 (15796)
Number of unique reflections	59539 (6237)
Completeness	95.3 (97.8) %
Multiplicity	2.6 (2.6)
R_{sym} for all reflections	8.0 (34.1) %
<Intensity/σ>	8.2 (2.7)
χ^2	0.98 (1.19)
Refinement statistics	
Rcryst	22.8 (28.8) %
Rfree (test set 5%)	28.2 (34.2) %
r.m.s. deviation	
Bonds	0.021 Å
Angles	2.010°
Torsion period 1	7.914°
Torsion period 2	35.745°
Torsion period 3	21.882°
Torsion period 4	22.536°
Average *B*-Factor	67.1 Å^2
Coordinate error (based on R_{free})	0.41 Å
NCS groups	3 (heavy chain, light chain, receptor)
TLS groups	20 (1 for each C_H, C_L, V_H, V_L and BMPR-IA)
Procheck analysis[b)]	
Residues in most favored region	86.2% (1475)
Residues in additional allowed region	13.4% (229)
Residues in generously allowed region	0.4% (7)
Residues in disallowed region	0.0% (0)

a) Statistical analysis for the highest resolution shell is shown in parentheses.

b) The number of the residues used in the analysis is given in parentheses.

5.3.2. General description of the AbyD1556/BMPR-IA$_{ecd}$ complex

Four AbyD1556/BMPR-IA$_{ecd}$ complexes in the asymmetric unit of the crystal could be identified (see section 5.3.1). The overall structure of one of these complexes is shown in fig. 5.10.

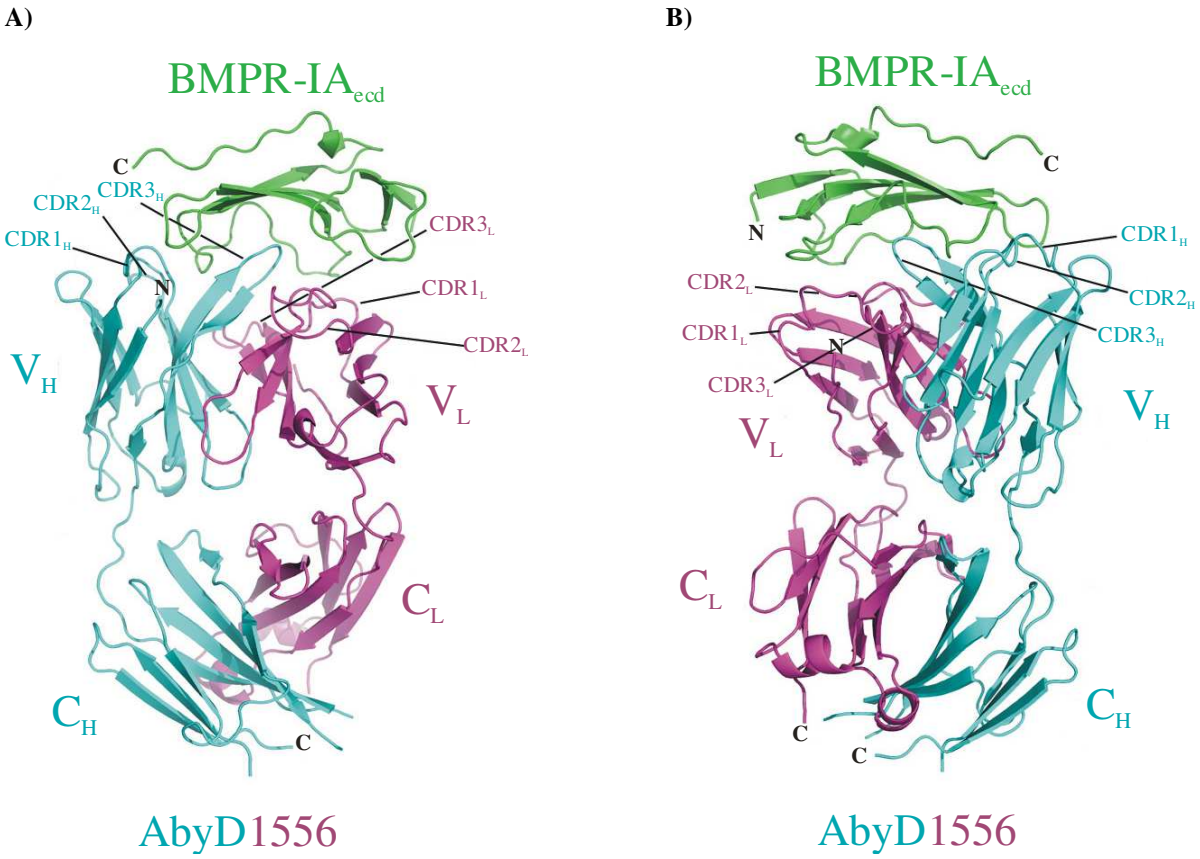

Fig. 5.10 – A) Ribbon representation of the Fab-receptor complex of BMPR-IA$_{ecd}$ bound to AbyD1556. The receptor ectodomain (Pro34 - Val118) is shown in green, the heavy chain (H) of AbyD1556 is shown in cyan, the light chain (L) is marked in magenta. Complementary determining regions (CDRs), constant (C) and variable (V) regions are indicated. **B)** Same molecule as in **A)** but rotated by 150° around the y-axis. Scheme is from (Harth et al. 2010b).

A comparison of the four complexes in the asymmetric unit suggested that all four of the AbyD1556/BMPR-IA$_{ecd}$ complexes were almost identical, as a global fitting yielded r.m.s. deviations of 0.5 to 0.6Å for all Cα-atom positions. However, a detailed analysis revealed that the substructures, i.e. the Fab fragment or the receptor ectodomain, were identical within the accuracy of the acquired data. Backbone as well as sidechain atoms of the four Fab fragments in the asymmetric unit superimposed almost perfectly with most pairings exhibiting an r.m.s.d. of 0.3 Å or less, superpositioning of the four BMPR-IA receptor

ectodomains yields an r.m.s.d. of 0.17 Å or less. However, when the Fab fragments were structurally aligned, a comparison of the bound BMPR-IA ectodomains showed that the receptor proteins shifted slightly in the four complexes in the asymmetric unit (see fig. 5.11 A – D).

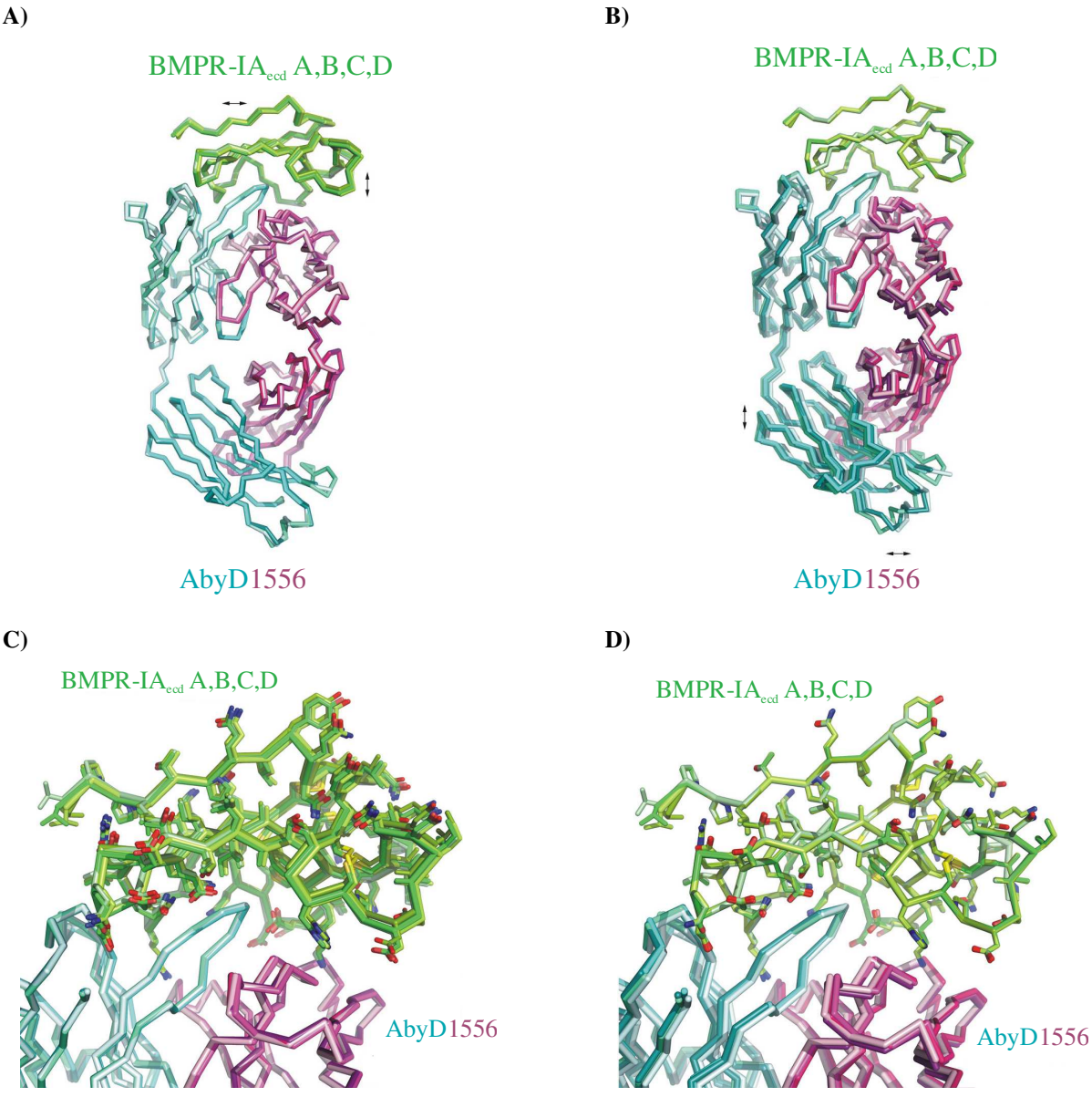

Fig 5.11 – Structural alignment of the four Fab/BMPR-IA complexes of the asymmetric unit. **A)** The four structures of BMPR-IA$_{ecd}$ (A,B,C,D) are shown in different shades of green, similarly the Fab heavy and variable regions of the four Fab molecules of the asymmetric unit are indicated in different shades of cyan and magenta. Only the Cα-trace is shown. Structural superposition was performed using all Cα-atoms of the four Fab molecules thereby showing slight, but significant differences in the location of the four BMPR-IA molecules (~1Å). **B)** As in **A)** but structural alignment was performed on the Cα-atoms of BMPR-IA. **C)** As in **A)** but side chains of the four BMPR-IA molecules of the asymmetric unit are shown, illustration the positional shifts of the BMPR-IA molecules in the Fab binding site. **D)** As in **B)** but with structural alignment performed on the Cα-atoms of the four BMPR-IA molecules. Figure is taken from (Harth et al. 2010b)

In the AbyD1556/BMPR-IA$_{ecd}$ complex 1 of the asymmetric unit, the BMPR-IA moiety is shifted by 0.8 to 1 Å towards the heavy chain, compared to the three other Fab/receptor ectodomain complexes of the asymmetric unit. Both the Fab fragment and the receptor ectodomain seemed to act as rigid bodies, thus these differences showed that small reorientation of BMPR-IA within the binding epitope of the antibody protein were possible.

Upon complex formation, about 1110Å^2 of solvent-accessible surface area of the antibody and 1230Å^2 of the BMP receptor ectodomain were buried. As expected from other antigen-antibody structures, the complementary determining region (CDR) 3 of the heavy chain contributed by far the largest amount to the buried surface area (570Å^2), as the CDR 3 of the variable heavy domain (V_H) was in the centre of the antibody-antigen interface (see fig. 5.12).

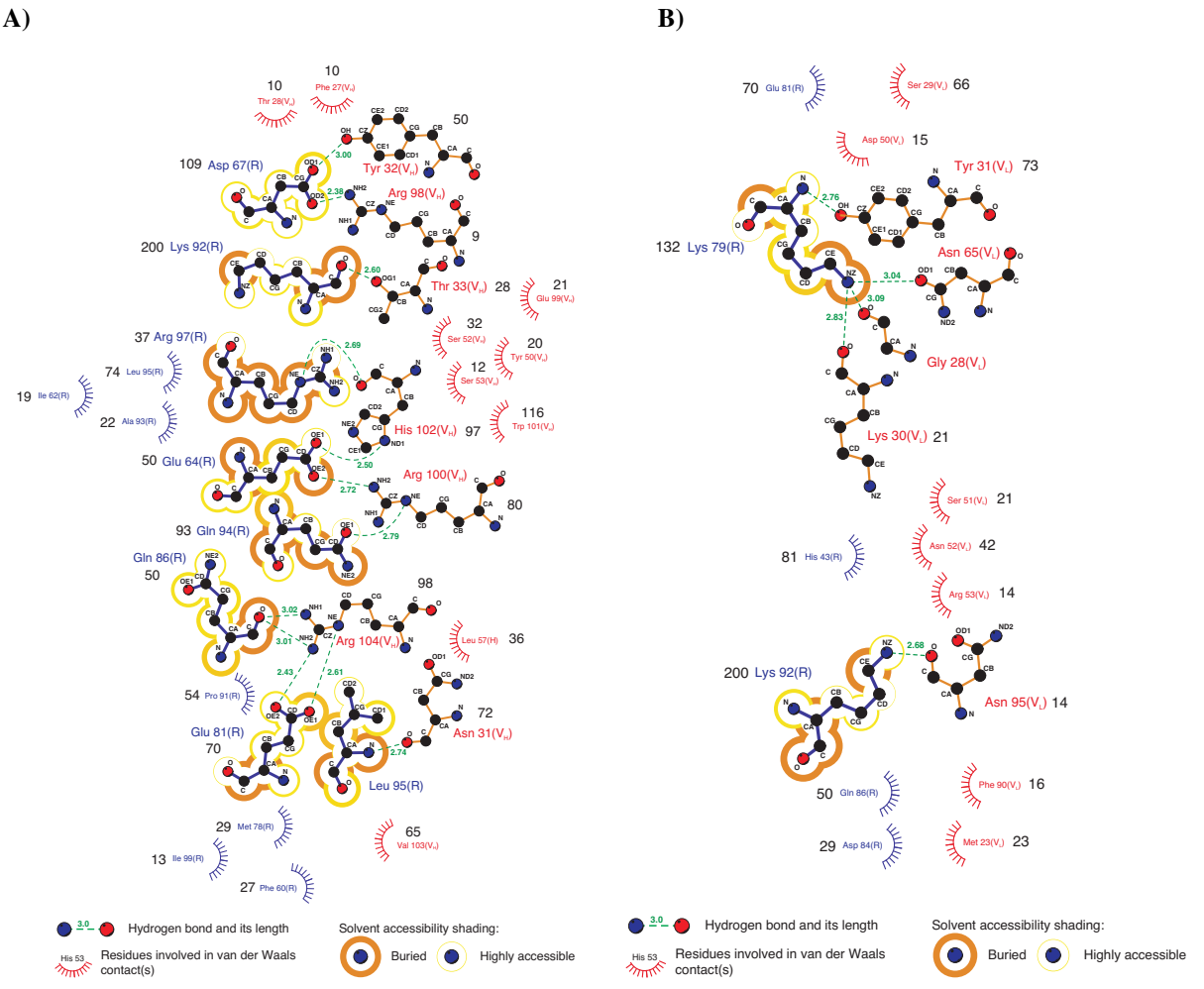

Fig. 5.12 – A) Ligplot analysis of the interaction of the variable heavy (V_H) domain of AbyD1556 with BMPR-IA. Hydrogen bonds are indicated as green stippled lines, with distances between the acceptor and donor atom shown. The buried surface area upon complex formation is given in Å^2 next to the residue name (written in black). Residues of AbyD1556 are written in orange and annotated with VH, residues of BMPR-IA are shown in blue and labeled with R. **B)** As in **A)** but for the interaction of the variable light (V_L) domain of AbyD1556 with BMPR-IA. Figure is from (Harth et al. 2010b).

In the light chain CDR 1 and 2 contributed significantly (165 and 95Å^2) to the antibody interface, whereas CDR 3 did not seem to be much involved in the binding (buried surface area 59 Å^2), due to the location of CDR3 of the variable light domain (V_L) at the periphery of the BMPR-IA binding site (see 5.12 B).

In total, the CDRs of the light chain contributed only 319 Å^2 of surface area to the interface, in contrast to the CDRs of the heavy chain, which all together delivered almost 800 Å^2 of interface area. One possible explanation for the uneven contribution of the V_H and V_L segments to the interface is in the location of BMPR-IA$_{ecd}$ on top of the antigen-binding site of AbyD1556. The V_L segment is placed opposite of the β1β2-loop and the C-terminal end of β-strand 4 of BMPR-IA, whereas the V_H segment covers most of the three-stranded central β-sheet and a large part of the β4β5-loop of the receptor ectodomain (see fig. 5.13 A).

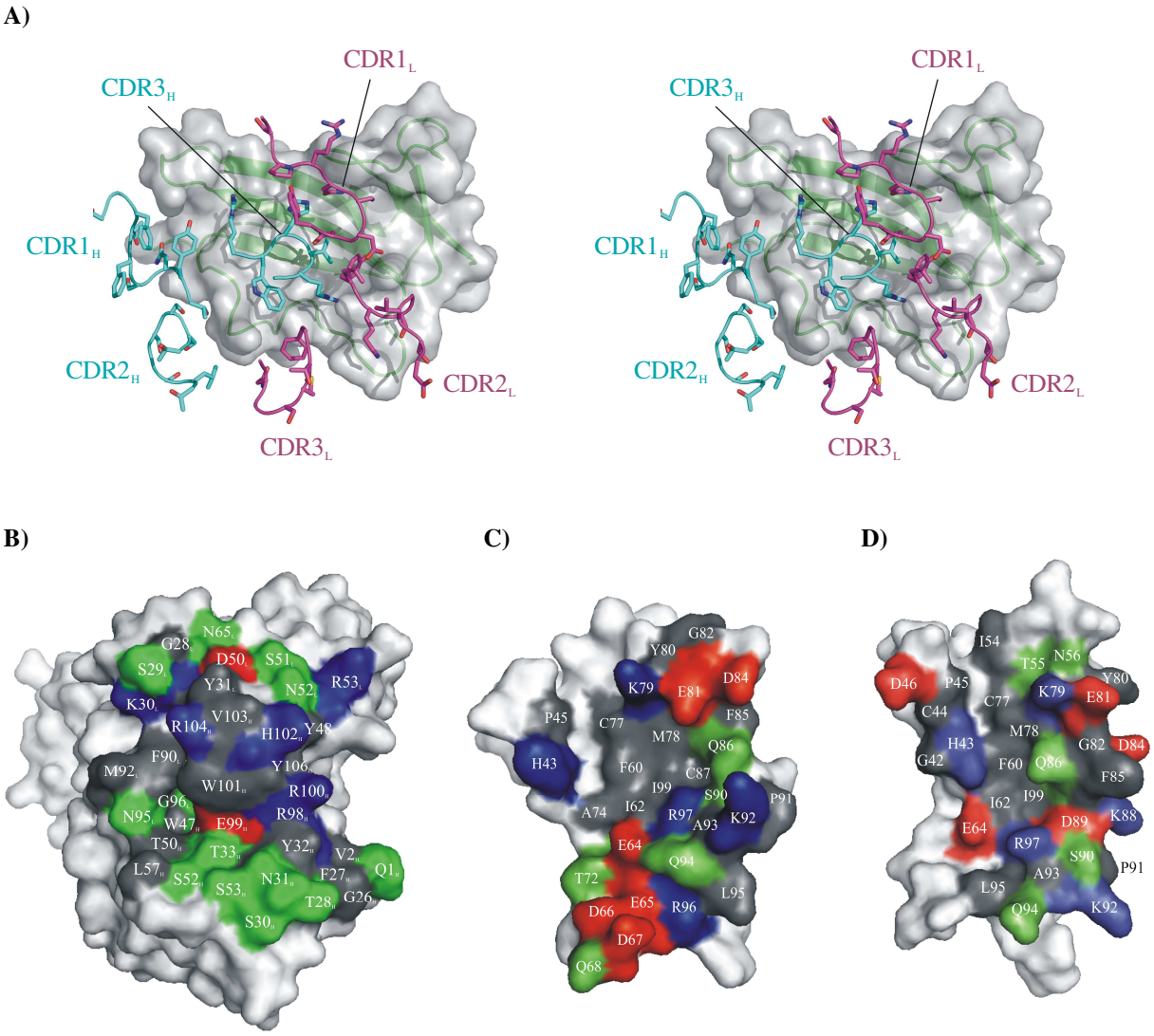

Fig. 5.13 – A) Stereo view of the binding epitope of BMPR-IA in the AbyD1556/BMPR-IA complex. The positions of the six CDR binding loops are shown highlighting the central location of CDR 3 of the heavy chain

of AbyD1556. Besides CDR3 of the heavy chain only the CDRs 1 and 2 of the light chain make significant contact with BMPR-IA. **B, C)** Open book view of the binding epitopes of AbyD1556 **(B)** and BMPR-IA$_{ecd}$ **(C)** – The binding epitope is color-coded with hydrophobic amino acid residues (A, C, F, G, I, L, M, P, V, W, and Y) in dark gray, acidic residues in red (D, E), basic residues in blue (H, K, R) and polar but uncharged residues in green (N, Q, S, T). **D)** The binding epitope of BMPR-IA for binding to BMP-2 showing that both epitopes are highly similar and exhibit almost perfect overlap. The orientation of BMPR-IA in **C)** and **D)** are identical. Scheme is modified according to (Harth et al. 2010b).

In the case of BMPR-IA, the interfacial residues of the AbyD1556/BMPR-IA$_{ecd}$ complex were almost evenly distributed over the slightly concave site of the three-stranded β-sheet consisting of the β-strands β3, β4 and β5, but the AbyD1556-binding epitope also involved several residues from the β1β2- and the β4β5-loops. A comparison with BMPR-IA$_{ecd}$ bound to BMP-2 (PDB entry 1REW) (Keller et al. 2004b) revealed that the binding epitopes on BMPR-IA overlap heavily in both complexes (see fig. 5.13 B – D). Even the amount of interface area involved for BMPR-IA was quite similar (BMPR-IA$_{AbyD1556}$ 1230Å^2 vs. 1200Å^2 for BMPR-IA$_{BMP-2}$). A closer inspection, however, exhibited also differences to which extent individual residues participate in the interface (see fig. 5.12). In the BMP-2/BMPR-IA$_{ecd}$ complex the β1β2-loop of the receptor ectodomain is more tightly packed into the interface in comparison to the AbD1556/BMPR-IA$_{ecd}$ complex, whereas in the latter β-strand 3 and the C-terminal end of the β4β5-loop of BMPR-IA are most strongly buried.

Seventeen hydrogen bonds between AbyD1556 and BMPR-IA$_{ecd}$ documented the quite polar character of the antibody/receptor interaction (see fig. 5.15, table 5.4).

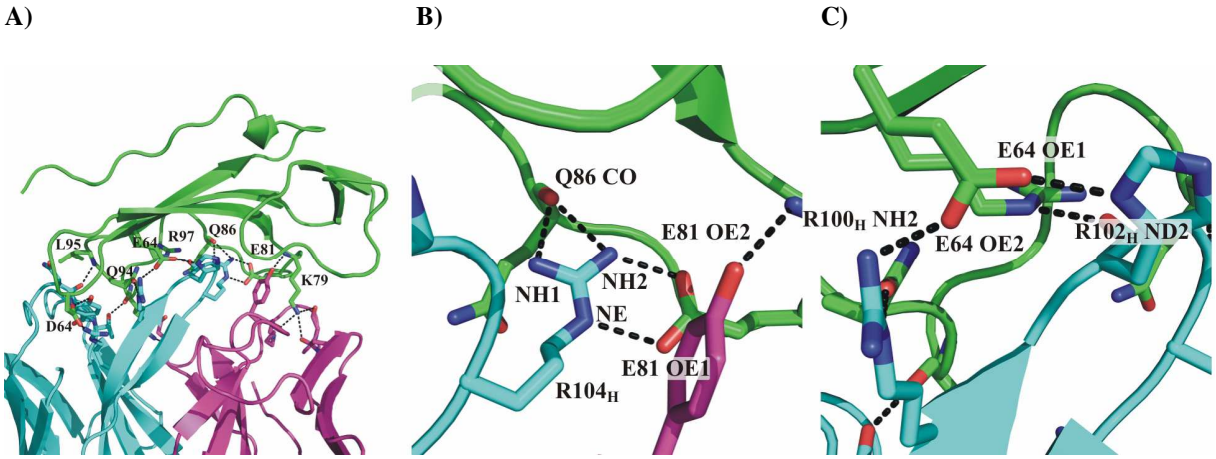

Fig. 5.15 – Hydrogen bond network in the AbyD1556/BMPR-IA interface – **A)** Overview of the hydrogen bonding between AbyD1556 (shown in cyan and magenta for the heavy and light chain, respectively) and BMPR-IA$_{ecd}$ (green). Only residues involved in H-bonds across the interface are shown. **B**) Zoom into the H-bond cluster around Glu81 of BMPR-IA and **C**) around Glu64. Figure is taken from (Harth et al. 2010b).

Table 5.4 – Geometry of H-bonds in the AbyD1556/BMPR-IA interface

BMPR-IA$_{ecd}$	AbyD1556	Distance Å	Angle NOC[a)]	H-bond[b)]
E64 (OE1)	H102$_H$[c)] (ND1)	2.50	140	SC–SC
E64 (OE2)	R100$_H$ (NH1)	2.72	106	SC-SC
D67 (OD1)	Y32$_H$ (OH)	3.00	113	SC-SC
D67 (OD2)	R98$_H$ (NH2)	2.38	139	SC-SC
K79 (N)	Y31$_L$ (OH)	2.76	119	MC-SC
K79 (NZ)	G28$_L$ (O)	3.09	104	SC–MC
K79 (NZ)	K30$_L$ (O)	2.83	100	SC-MC
K79 (NZ)	N65$_L$ (OD1)	3.04	155	SC-SC
E81 (OE1)	R104$_H$ (NE)	2.61	127	SC-SC
E81 (OE2)	R104$_H$ (NH2)	2.43	125	SC–SC
Q86 (O)	R104$_H$ (NH1)	3.02	94	MC-SC
Q86 (O)	R104$_H$ (NH2)	3.01	94	MC-SC
K92 (O)	T33$_H$ (OG1)	2.60	104	MC-SC
K92 (NZ)	N95$_L$ (O)	2.68	130	SC-MC
Q94 (OE1)	R100$_H$ (NE)	2.79	104	SC-SC
L95 (N)	N31$_H$ (O)	2.74	110	MC-MC
R97 (NE)	H102$_H$ (O)	2.69	131	SC-MC
mean value		2.76	132	
S.D.		0.22	21	

The numbers in parentheses are the distances between donor and acceptor atoms and N–O–C angles in the AbD1556/BMPR-IA interface of complex 1 in the asymmetric unit.

a) N, O, C are the donor-acceptor atoms; from general statistics (Xu et al. 1997) this angle is 149° ± 15° for MC–MC hydrogen bonds and 129° ± 18° for SC–MC and SC–SC H-bonds;

b) MC (main chain) and SC (side chain) donor/acceptor atoms;

c) H and L denote heavy and light chain of AbyD1556, respectively.

Most hydrogen bonds to the antibody involved the β4β5-loop segment of BMPR-IA (eight H-bonds for residues Glu81 to Arg96), which also carries the main binding determinants for the binding to BMP-2 (Keller et al. 2004b). This suggests that either amino acid composition or the conformation of the β4β5 loop render this segment "sticky" for protein-protein interactions. Two residues in the antibody/receptor complex formed hydrogen bond clusters or networks. From the guanidinium group of Arg104 of the Fab heavy chain, four H-bonds emanate to the carboxylate group of BMPR-IA Glu81, forming a bi-dentate salt bridge and two further H-bonds are formed with the backbone carbonyl of BMPR-IA Gln86 (fig. 5.15 B).

The large number of H-bonds, together with the fact that these residues were rather deeply buried inside the interface, indicated that Arg104 of the AbyD1556 and possibly also Glu81 of BMPR-IA might represent so-called hot spots of binding. The second independent H-bond network was centered on BMPR-IA Glu64, whose side chain carboxylate group formed hydrogen bonds with the side chain of Arg100 and His102 of the heavy chain of AbyD1556 (fig. 5.15 C). Both latter side chains are pre-oriented in the interface either by additional H-bond, i.e. Fab Arg100 to Gln94 of BMPR-IA or by hydrophobic contacts, i.e. Fab His102 forming contacts to BMPR-IA Ile62 and Tyr48 of the light chain of AbyD1556.

5.3.3. Comparison of the structures of BMPR-IA in complex with AbyD1556 and BMP-2

Due to the overlapping epitopes of the Fab AbyD1556 and BMP-2 on BMPR-IA, one can consider the Fab AbyD1556 binding epitope resembling somehow an anti-idiotypic molecule mimicking BMP-2. It was thus interesting whether the conformations of BMPR-IA$_{ecd}$ bound to either the Fab AbyD1556 and BMP-2 were identical, especially since NMR-studies of isolated BMPR-IA$_{ecd}$ had shown that the majority of the BMP-2 binding epitope of BMPR-IA folds not before binding (Klages et al. 2008). The large conformational change upon binding to BMP-2 was mostly apparent from the formation of a short α-helix segment comprising residues Gly82 to Lys88 in the β4β5-loop. This α-helix, which carried the hot spots of binding for the interaction of BMPR-IA with BMP-2 (Keller et al. 2004b), was absent in the free form of BMPR-IA, but was spontaneously formed in NMR-titrations experiments using the helix-inducing agent trifluoroethanol (Klages et al. 2008). It was thus suggested that the helical element would be in a so-called *status nascendi* thereby forming instantaneously upon changes in the environment without the need of a BMP-2 “casting mold”.
However, a comparison of BMPR-IA bound to AbyD1556 and BMPR-IA bound to BMP-2 (PDB entry 1REW) clearly showed that the helix α1 was also absent in BMPR-IA bound to the AbyD1556 (Fig. 5.16 A). This segment of BMPR-IA adopted a rather irregular conformation with short extended stretches, i.e. Asp84 to Cys87 and Asp89 to Pro91. Interestingly, despite the difference in the conformations of the β4β5-loop in the NMR structure (PDB entry 2K3G) and the complex structure bound AbD1556, all other secondary structure elements, e.g. the three-stranded β-sheet or the N-terminal β-strands 1 and 2 together with the β1β2-loop, overlap almost perfectly (Fig. 5.16 A). Since the conformational rearrangement in BMPR-IA could principally follow either an induced fit or a selection of

conformer mechanism, we compared the structure of BMPR-IA bound to AbyD1556 also with all individual structures of the NMR ensemble (Fig. 5.16 B).

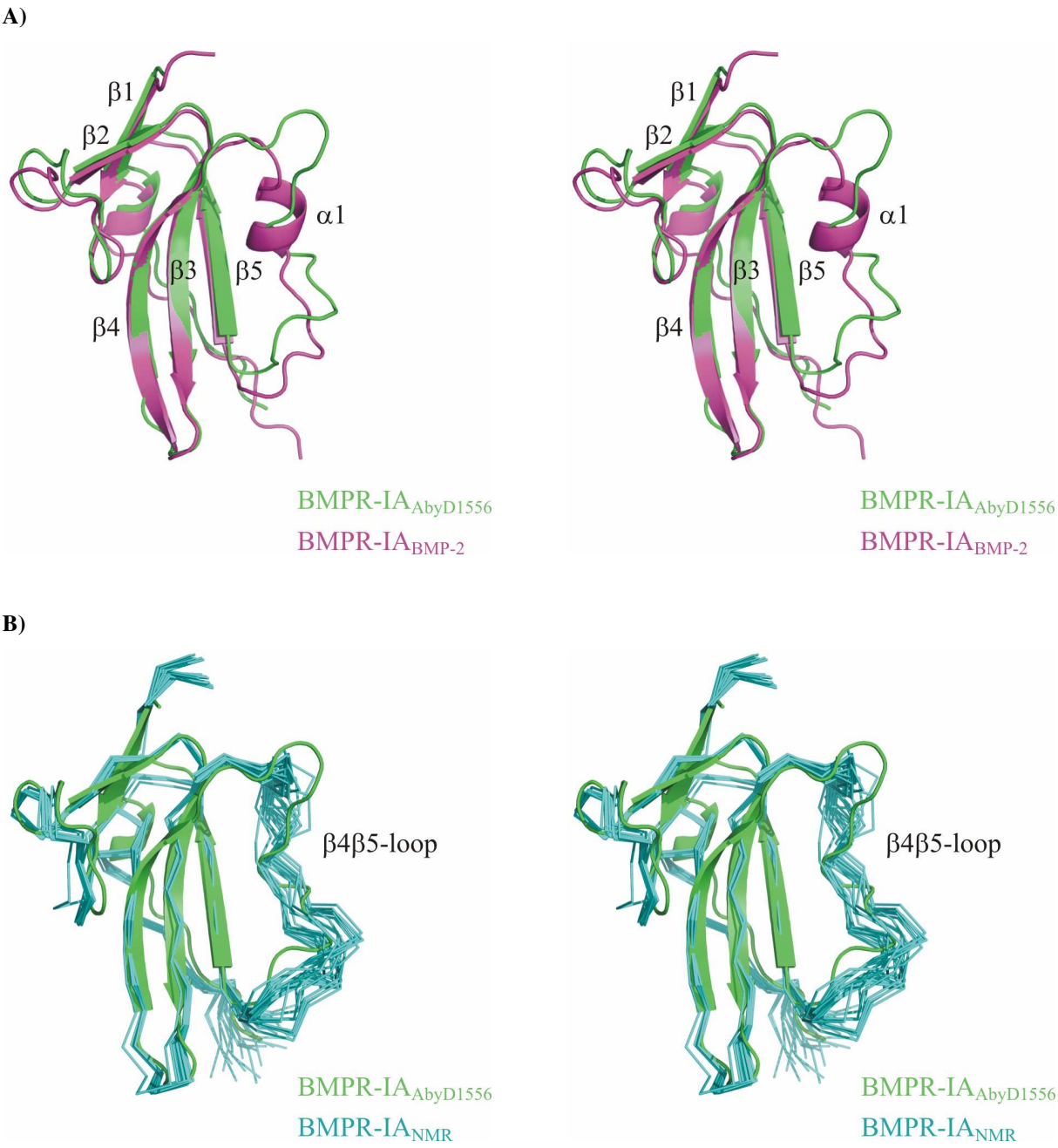

Figure 5.16 – A) Structural superposition (stereo view) of BMPR-IA$_{ecd}$ bound to AbyD1556 (green) and bound to BMP-2 (magenta, PDB entry 1REW). The comparison shows that the short α-helix 1 that is observed in the complex BMP-2/BMPR-IA is absent when BMPR-IA is bound to AbyD1556. The β4β5-loop adopts two different conformations in the two BMPR-IA structures. **B)** Structural alignment (stereo view) of the NMR-ensemble of BMPR-IA$_{ecd}$ (Cα-trace of 21 structures in cyan, PDB entry 2K3G) and BMPR-IA$_{ecd}$ bound to AbyD1556. The β4β5-loop of BMPR-IA in its conformation bound to AbyD1556 has only partial similarity to the structures of the NMR ensemble. Scheme is depicted from (Harth et al. 2010b).

However, this comparison showed that although the loop was also irregular in the NMR structure ensemble, no conformer existed in the ensemble, which was identical to BMPR-IA bound to AbyD1556. Moreover, the conformation of the BMPR-IA β4β5-loop in its AbyD1556 bound form seemed to be a mixture of the conformations seen in the NMR ensemble and the BMP-2 bound form. Residues Ser90 to Ala93 overlapped with the conformer ensemble present in the NMR structures, Asp89 to Gln86 show a helical twist similar to the helical end of the bound form in BMPR-IA bound to BMP-2. Only the N-terminal part of the β4β5-loop, i.e. residues Gly82 to Phe85, exhibited a conformation which is neither present in the NMR ensemble nor the BMP-2 bound form (Fig. 5.17).

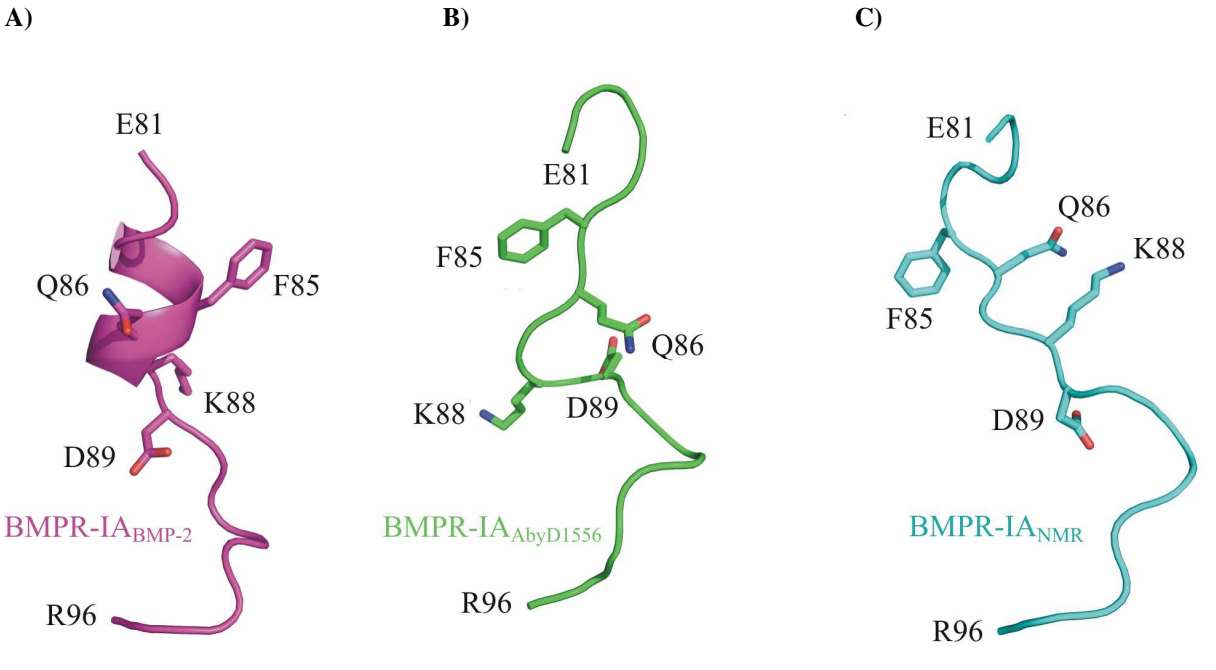

Figure 5.17 – Comparison of the β4β5-loop of BMPR-IA bound to BMP-2 **(A)**, bound to AbD1556 **(B)** and for a representative conformer of the free form **(C)**. The side chains of residues Phe85, Gln86, Lys88 and Asp89 that play an important role in binding to BMP-2 or AbyD1556 show very different orientations in all three structure forms. Figure is taken from (Harth et al. 2010b).

This observation would argue towards an induced fit mechanism, where the flexible, in its free form disordered β4β5-loop BMPR-IA adopts a conformation imposed by the binding partner. In BMP-2 the helix is formed because the highly concave site of the wrist epitope forms a 120° spanning binding site, which is usually seen in structural arrangements of amphipathic helix/helices (e.g. hydrophobic cores in helical bundles). In contrast, the binding site of the Fab is rather flat, thus the interaction to stabilize the helical element is not sufficient and the β4β5-loop adopts a more extended, helical-free structure.

5.3.4. Analysis of structural and functional relationships via mutagenesis studies of BMPR-IA$_{ecd}$

As mentioned above, the structural epitopes of BMPR-IA buried upon binding to the antibody AbyD1556 or to BMP-2 overlapped heavily and an almost identical set of residues of the receptor ectodomain facilitated binding to AbyD1556 as well as to the BMP.
Therefore, a mutational analysis of BMPR-IA was performed in order to see whether the functional epitopes – the main binding determinants for the interaction with both binding partners – are similar. If the AbyD1556 would function as BMP-2 mimic, one would expect that the same residues play similar roles in the recognition and binding of both partners. However, the different number of hydrogen bonds between BMPR-IA and AbD1556 compared with the complex of BMPR-IA and BMP-2 as well as the different residues involved on the BMPR-IA's side suggested that the functional epitopes of BMPR-IA for AbD1556 and BMP-2 differ markedly.

Thus, we mutated 13 receptor residues in the centre of the contact. In most cases, an exchange by alanine was done, at three positions we also substituted these residues for Asp, Arg, or Pro (see table 5.5). The resulting mutant proteins were purified, and their binding affinities were studied by means of surface plasmon resonance. In order to measure comparable binding affinities without avidity effects resulting from different oligomeric states (BMP-2 as homodimer will bind to two receptor molecules simultaneously if used as analyte) we immobilized the monovalent AbyD1556 and AbyD1564 (another neutralizing anti-BMPR-IA antibody) as well as BMP-2 on different flow cells of one biosensor. Each BMPR-IA variant protein was then perfused as analyte over all three ligands in parallel allowing for direct comparison of the binding data (see table 5.5).
It was very surprising to see that the functional epitopes of BMPR-IA for BMP-2 and AbD1556 are highly similar, despite the structural differences in the epitopes of BMPR-IA for binding either to BMP-2 or AbD1556. The affinities of the different receptor mutants for BMP-2 and the AbD1556 antibody investigated here were clearly correlated (see apparent K_D´s in figure 5.18 A).

Table 5.5 – Mutational analysis of the BMPR-IA interface (Biosensor analysis)

Analyte	Proteins (immobilized)		
BMPR-IA$_{ecd}$ mutants	BMP-2	AbyD1556 rel. app. K_D [nM]	AbyD1564
Wildtype	1.0 ± 0.1 (29.7 ± 2.8)	1.0 ± 0.1 (18.6 ± 1.2)	1.0 ± 0.2 (55.7 ± 6.6)
P34R	1.7	1.2	0.9
Y39D	16.4	23.5	n.d.
F60A	n.d. [a]	n.d.	n.d.
I62A	42.4	29.1	1.8
E64A	1.3	2.3	0.5
D67A	1.0	1.7	n.d.
M78A	n.d.	n.d.	3.8
K79A	0.4	0.7	n.d.
E81A	2.3	2.3	0.5
F85A	n.d.	n.d.	0.8
Q86A	17.3	27.1	0.8
K92A	1.8	1.7	n.d.
Q94A	1.2	1.2	19.5
Q94P	3.8	2.9	5.3
R97A	34.2	13.4	n.d.
I99A	25.1	19.8	4.1

[a] Binding could not be determined because it was below detection limit (KD > 1 mM).

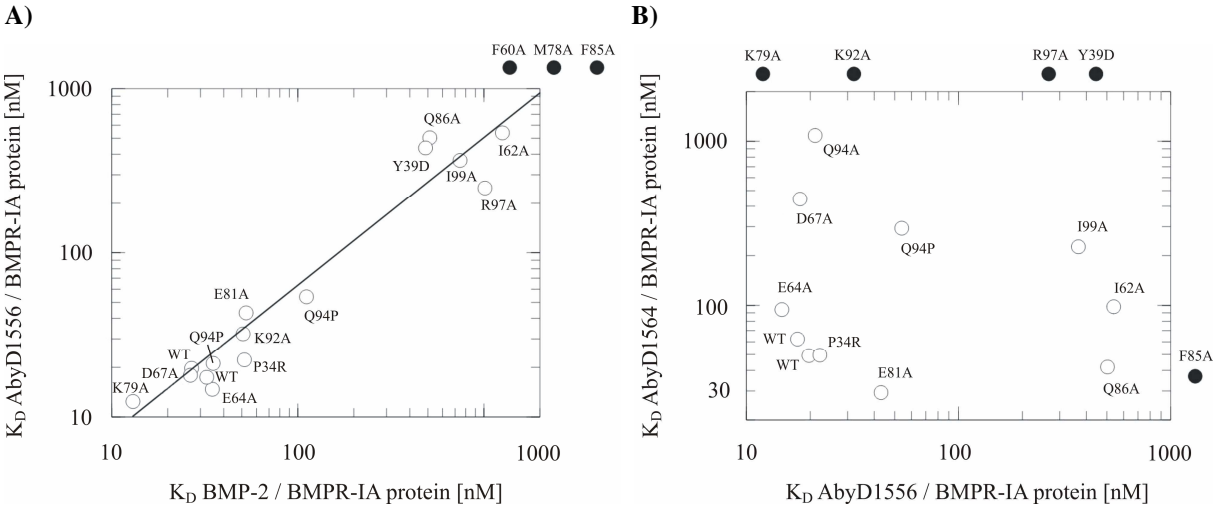

Fig. 5.18 – Analysis of the dissociation constants of BMPR-IA$_{ecd}$ mutants – **A)** The binding of BMPR-IA$_{ecd}$ variants to AbyD1556 correlates clearly with their binding to BMP-2. **B)** The binding constants of AbyD1564 to BMPR-IA$_{ecd}$ in comparison to that of AbyD1556 are randomly distributed and differ notably in their main binding determinants. Figure is taken from (Harth et al. 2010b).

One set of BMPR-IA mutants exhibited affinities for AbyD1556 and BMP-2 similar to the wildtype BMPR-IA. Interestingly, this set comprises almost all polar residues, i.e. Glu64, Asp67, Lys79, Glu81, Lys92, and Gln94, within the Fab-binding epitope of BMPR-IA, which form 11 out of 15 intermolecular hydrogen bonds in the Fab-receptor interface. Thus, polar interactions, despite their large number, seemed not to contribute significantly to the binding energy. This unexpected finding might be explained in two ways:
First, many of these H-bonds evolving from side chains of BMPR-IA residues are located at the periphery of the interface and thus might be solvent-accessible. Without shielding from the solvent, the hydrogen bonds to the protein partner compete with H-bonds from water. Hence, energetic benefit for the protein-protein interaction will be low.
Second, eight of the eleven addressed H-bonds are of the type side chain to side chain, thus the entropy cost from decreasing the conformational flexibility of both side chains involved in the intermolecular H-bond might just be barely paid off by the H-bond formed. A similar observation is reported for the BMP-2/BMPR-IA interaction (Keller et al. 2004b), where only two of the ten intermolecular H-bonds are significant for the ligand-receptor complex formation.

Another set of BMPR-IA mutants (Ile62, Gln86, Arg97, and Ile99) showed affinities for AbyD1556 (or for BMP-2) that are 10- to 30-fold (for the interaction with BMP-2: 20- to 40-fold) lower compared to wild type BMPR-IA. A third group of BMPR-IA mutants exhibited no measurable affinity for AbD1556 or BMP-2. Two of those (F60A and M78A) have likely lost the native fold of BMPR-IA, because these two variant proteins could only be obtained in inhomogeneous form and with very low yield. The BMPR-IA variant F85A, however, seems structurally intact and does neither bind to AbD1556 nor BMP-2.
The same set of BMPR-IA variants was also tested for binding to another Fab antibody AbyD1564, which due to its BMPR-IA neutralizing properties must have a BMPR-IA epitope that (at least partially) overlaps with that of BMP-2. Unfortunately, the lack of structural data for AbyD1564 did not allow directly comparing the structural epitopes. However, the functional epitopes of BMPR-IA for binding AbyD1556 or AbyD1564 are completely different (Table 5.6, Fig. 5.18 B).
With exception of the BMPR-IA variant R97A, all other main binding determinants (K_D(variant)/K_D(BMPR-IA) ≥ 20-fold) differ. This finding also ensured that the BMPR-IA variants included in our epitope analysis were structurally intact and that the residues that

showed strongly reduced binding to either one of the Fabs or BMP-2 were indeed hot spots of binding.

The results were surprising, since the functional epitopes of BMPR-IA for binding to BMP-2 and AbyD1556 seemed identical, despite the fact that the structures of BMPR-IA bound to either BMP-2 or AbD1556 differed significantly. Specifically, the exchange of the BMPR-IA residues Phe85 and Gln86 to alanine affected the binding to AbyD1556 similar as to BMP-2, although both side chains did not directly contact the Fab surface. A closer inspection of the kinetic rate constants of the Fab-BMPR-IA mutant binding showed that in the case of BMPR-IA Q86A only the association rate is affected (data not shown). Analysis of the association and dissociation rates strongly indicated that the binding mechanism of BMPR-IA to AbyD1556 and BMP-2 follows a selection-fit (or selection of conformation) mechanism, thus the strong influence of the mutations F85A and Q86A in BMPR-IA on binding to AbyD1556 is likely due to a shift in the conformer population, eliminating or lowering the conformation required for binding to AbyD1556.

In line with such a selected fit mechanism were the rather slow association rates, e.g. 7 to 9 x 10^4 $M^{-1}s^{-1}$ for the BMPR-IA interaction with AbyD1556 or BMP-2, whereas the association with the second Fab AbyD1564 occurs twice as fast (1.5 x 10^5 $M^{-1}s^{-1}$) (Table 5.6) (Weikl and von Deuster 2009).

Table 5.6 – Mutational analysis of the BMPR-IA interface (Biosensor analysis)

Proteins (immobilized)	$BMPR\text{-}IA_{ecd}$ wildtype (Analyte)		
	Dissociation rate k_{off} [10^{-3} s^{-1}]	Association rate k_{on} [10^4 M^{-1} s^{-1}]	Dissociation binding constant K_D[a] [nM]
BMP-2	1.9	7.2	26.4
AbyD1556	1.7	8.8	19.3
AbyD1564	7.1	15.0	47.3

[a] Dissociation binding constant K_D was derived from calculating $K_D = k_{off} / k_{on}$.

Furthermore, the effect that mutations at the periphery of the interface influence the binding affinity, although the mutated residues are not directly contacting the binding partner, is in line with the theory that those residues affect the population equilibrium of the different conformers and thereby indirectly affect binding (Weikl and von Deuster 2009).

In summary, the comparative structure-/function analysis of the BMPR-IA interaction with the Fab and its ligand BMP-2 suggested that the location of the binding determinant is most important for its contribution to the overall binding energy rather than its chemical nature.

6. Discussion

6.1. Generation and biological analysis of BMP heterodimers 2/6 and 2/7

In this work, the two BMP heterodimers 2/6 and 2/7 were successfully expressed, refolded and purified to homogeneity in mg amounts. They were biologically active as demonstrated in BIAcore measurements and several cell-based activity assays. The expression system was *E.coli*. In previous works, several BMP heterodimers were generated in recombinant form only in eukaryotic cell systems like CHO (Israel et al. 1996), COS (Butler and Dodd 2003) Sf-9 (Aono et al. 1995; Hazama et al. 1995) and Drosophila S2 (Shimmi et al. 2005) or were expressed in gene therapy studies (Zhu et al. 2004; Zhao et al. 2005). Since the expression yield in eukaryotic systems is relatively low, the production of larger protein amounts, e.g. suitable for clinical applications, is therefore expensive both in labor and money. The company R+D offers the proteins BMP-2/7 and BMP-4/7 expressed in *E.coli* for sale (www.rndsystems.com). However, the manufacturing procedure is not published and therefore remains unknown.
Recently, Isaacs and colleagues reported the generation of a BMP-2/6 heterodimer in *E.coli* (Isaacs et al. 2010). They modified an established protocol for their BMP-2/6 production (Groppe et al. 1998) which is very similar to the protocol of Ruppert et al. which was used in this present work (Ruppert et al. 1996). Since the production procedures are alike, both BMP-2/6 proteins were compared extensively as described in the following section.

The monomers BMP-2, -6 and -7 were expressed separately as inclusion bodies in *E.coli*. After isolation, the monomers were purified by means of cation exchange chromatography and then refolded. The renaturation process turned out to be the bottleneck in BMP heterodimer production. Before the refolding step, the protein yields were in line with previous results (e.g. for BMP-2: Ruppert et al. 1996). However, the rate of yield dropped dramatically during renaturation in comparison to that of BMP-2 homodimers (BMP-2: 43% (Vallejo and Rinas 2004); BMP-2/6: 13%; BMP-2/7: 1%). The difficulties during refolding probably arise from limited compatibility between the two different BMP subunits which exhibit distinctive biochemical properties. In the case of BMP-2/7, however, the presence of BMP-2 seems to act as a refolding helper for BMP-7. This is probably due to the incapability

of *E.coli* derived BMP-7 monomers to form a functional dimer during renaturation, since, an active form of BMP-7 could only generated successfully in eukaryotic cell systems so far (Sampath et al. 1992; Jones et al. 1994; Swencki-Underwood et al. 2008). Nevertheless, the refolding yield of 1 % for BMP-2/7 was still low and needs further optimization. Unfortunately, a direct comparison of the refolding efficiency in BMP heterodimers were not possible, since Isaacs and colleagues omitted publishing the rate of yield in their BMP-2/6 heterodimer production (Isaacs et al. 2010).

Surface plasmon resonance (SPR) affinity studies using the BIAcore technique indicated that the BMP heterodimers 2/6 and 2/7 bind to the type I receptor BMPR-IA with almost equal affinity when compared to BMP-2, whereas the affinity for BMP-7 was ~ 25-fold lower in comparison to BMP-2/7 (see table 6.1). In the case of the type II receptors, BMP-2/6 and -2/7 showed also a similar affinity level as compared to both homodimers BMP-2 and BMP-7, respectively.

This result, for the most part, is in line with the work of Isaacs and colleagues (Isaacs et al. 2010). They demonstrated in BIAcore measurements that BMP-2/6 reaches the same affinity for the type I receptor BMPR-IA as BMP-2, whereas the affinity of BMP-6 was approximately 60-fold lower (see table 6.2). The affinity for the type II receptor ActR-IIB was the same compared to BMP-6 and approximately six-fold lower compared to BMP-2.

The discrepancy in the absolute K_D values obtained in this work and the work of Isaac and colleagues can be explained with the different experimental setup. Here, the perfused analyte and the immobilized binding partners were interchanged, i.e., the BMP ligands were immobilized in this work, whereas Isaacs and colleagues immobilized the receptors. Two immobilized receptor molecules may bind to a single ligand resulting in a 1:2 ligand-receptor interaction, thus increasing the apparent affinity through a proximity effect. If the ligand is immobilized, two receptor molecules bind independently, at the lower affinity of a single receptor, therefore resulting in a 1:1 ligand-receptor interaction. Similar observations regarding the K_D differences were made in other published BIAcore studies with TGF-β proteins: Immobilized BMPR-IA displayed a 15- to 40-fold higher affinity for its ligands than did BMPR-IA for the immobilized ligands (Hatta et al. 2000; Kirsch et al. 2000c; Knaus and Sebald 2001; Heinecke et al. 2009). Similarly, immobilized ActR-II(B) even exhibited a 150- to 1500-fold higher affinity for its ligands than did ActR-II(B) for the immobilized ligands (Greenwald et al. 2003; Heinecke et al. 2009).

Taken the BIAcore interaction analyses together, BMP heterodimers seem to adopt the higher affinity receptor sites from its two subunits BMP-2 and BMP-6/-7, providing a mechanistic basis for the higher potency of heterodimers compared to their homodimeric counterparts.

Table 6.1 – Summary of BIAcore interaction analysis of BMP receptor ectodomains bound to immobilized BMP ligands

	Analyte (perfused)					
Proteins (immobilized)	BMPR-IA$_{ecd}$			ActR-I$_{ecd}$	ActR-II$_{ecd}$	ActR-IIB$_{ecd}$
	k_{off} [10^{-3} s^{-1}]	k_{on} [10^{4} M^{-1} s^{-1}]	K_D[a] [nM]	K_D[b] [µM]		
BMP-2	1.99	10.17	20.9 +/- 7.9	n.d.[c]	3.5	3.0
BMP-2/6	1.38	20.78	42.9 +/- 41.3	n.d.	3.8	-
BMP-2/7	0.37	4.98	7.3 +/- 0.7	-	-	2.1
BMP-7	10.67	9.17	202 +/- 151	-	-	1.0

[a] Dissociation binding constant K_D was derived from calculating $K_D = k_{off} / k_{on}$.

[b] Apparent binding constant K_D was obtained from the dose dependence of equilibrium binding.

[c] Binding could not be determined because equilibrium was not reached.

Table 6.2 – Ligand affinity data from SPR experiments

	BMPR-IA			ActR-IIB		
Ligand	k_{off} [10^{-3} s^{-1}]	k_{on} [10^{4} M^{-1} s^{-1}]	K_D [nM]	k_{off} [10^{-3} s^{-1}]	k_{on} [10^{4} M^{-1} s^{-1}]	K_D [nM]
BMP-2	1.11	85.2	1.31	25.7	66.8	38.47
BMP-6	9.37	15.0	62.46	1.82	27.3	6.68
BMP-2/6	1.05	103	1.02	8.61	1.32	6.52

The SPR data are shown as the dissociation rate k_{off}, and the association rate k_{on}, based on a global fit using the kinetic model 1:1 Langmuir binding with mass transfer. The binding constant K_D is calculated $K_D = k_{off} / k_{on}$. The receptors were immobilized to the chip surface, with the ligands flowed over the surface. Data are obtained from the work of Isaacs and colleagues (Isaacs et al. 2010).

To further study the biological potency of BMP-heterodimers, cell-based *in-vitro* activity assays were conducted. First, various BMP-ligands were tested in C2C12 and ATDC5 cell lines regarding their ability to induce the production of alkaline phosphatase (ALP) (Katagiri et al. 1994; Nakamura et al. 1999).
The BMP heterodimers 2/6 and 2/7 exhibited a higher biological activity ranging from two- to ten-fold when compared to their respective homodimeric counterparts. This finding is in agreement with the work of Israel and colleagues, showing that heterodimeric BMP-2/7 produced in eukaryotic CHO cells achieved a specific activity about 20-fold higher than BMP homodimers in ALP assays using the mouse stromal cell line W-20-17 (Israel et al. 1996). The result is also consistent with the finding that a BMP-4/7 heterodimer can induce ALP activity in primary cultures of rat bone marrow stromal cells by the factor of three compared to BMP-7 (Aono et al. 1995).

In addition to ALP activity assays, the ability of BMP heterodimers to phosphorylate Smad proteins was tested in C2C12 and ATDC5 cells. BMP-2 was able to induce Smad phosphorylation in both cell lines in a dose dependent manner with EC_{50} values of approximately 100 pM (ATDC5) and 50 pM (C2C12), which is in the range of the result from previous experiments (Heinecke et al. 2009; ~ 300 pM in C2C12 cells). In the present work, the Smad phosphorylation was tested in smaller BMP-dose intervals when compared to the previous work of Heinecke et al., therefore making the EC_{50} value of 50 pM probably more accurate.
As already seen in ALP assays, the heterodimers BMP-2/6 and -2/7 were considerably more active compared to their respective BMP homodimers with EC_{50} values of 10 – 20 pM in both cell lines. Interestingly, BMP-6 from NSO cells is not as active as BMP-2. BMP-6 exhibits an EC_{50} value which is ten times lower than that of BMP-2. These results correspond to previous observations in a Smad-1 reporter assay (Isaacs et al. 2010). Here, BMP-2/6 showed a ten-fold higher activity compared to BMP-2. Again, the activity of BMP-6 was significant lower compared to BMP-2.

In conclusion, the BMP-2/6 and BMP-2/7 heterodimers produced in *E.coli* exhibited a higher biological activity in the short-term Smad phosphorylation assay and in long-term ALP induction assays than their homodimeric counterparts. This suggests that the heterodimeric BMP proteins are more efficient in the early steps of BMP signalling, i.e., receptor binding and assembly.

6.2. Type I receptor usage in the BMP heterodimer system

A possible explanation for the increased activity of BMP heterodimers are their composed binding epitopes for the type I and type II receptors. Regarding the BIAcore interaction analysis (see chapter 6.1.), BMP heterodimers seem to use the higher affinity receptor sites from its two subunits BMP-2 and BMP-6/-7.

To test which type I receptors were used for heterodimeric BMP signalling in cell activity assays, two antibody Fab fragments were testes in ALP assays. The Fab fragments were directed against the binding epitope of BMPR-IA thus blocking the ligand-receptor interaction.

Both antibodies efficiently prevented the induction of ALP, indicating that BMPR-IA is involved in heterodimeric BMP signalling. That is in line with the work of Little and Mullins (Little and Mullins 2009), who showed that BMP-2/7 recruits one BMPR-IA and one ActR-I receptor, thus patterning the dorsoventral axis in zebrafish. In addition, Isaacs and colleagues reported that a BMP-2/6 mutant carrying one defective type I receptor epitope from BMP-2 (which is the high affinity epitope for BMPR-IA) reduces the activation of a Smad 1 reporter by 80 % in comparison to the BMP-2/6 wildtype (Isaacs et al. 2010).

Since no potent inhibitory antibody for ActR-I was commercially available, the contribution of ActR-I to BMP heterodimers signalling was examined in the cell line INA-6, which expresses only ActR-I as type I receptor (Ro et al. 2004). BMP-6 and BMP-7 from animal cells were able to inhibit cell proliferation as expected. The heterodimers BMP-2/6 and –2/7 exhibited an activity which was more than 100-fold lower than that of BMP-6 and BMP-7. The differences in affinity are probably caused by the glycosylation of BMP-6 and BMP-7 and the non-glycosylation of the heterodimers, respectively. Saremba et al. demonstrated that the ActR-I binding of BMP-6 is dependent on N-glycosylation of the ligand (Saremba et al. 2008). Interestingly, the IC_{50} values of the BMP heterodimers were as low as for glycosylated BMP-2, but were slightly elevated when compared to BMP-2 derived from *E.coli*. However, it is unclear whether differences between the IC_{50} values of the heterodimers and BMP-2 are meaningful, since the applied concentrations are at the limit of solubility for these proteins. Hence, an involvement of ActR-I in BMP heterodimer signalling as seen in previous works (Little and Mullins 2009) could not be confirmed conclusively.

Taken these results together, it seems, however, that BMP-2/6 and -2/7 are able to signal via only one active type I receptor epitope, namely the BMPR-IA epitope. This is also supported

by the work of Heinecke and colleagues (Heinecke et al. 2009), showing that a heterodimeric BMP-2 with one active and one defective binding epitope for BMPR-IA exhibited nearly the same EC_{50} values in ALP assays as the wildtype BMP-2 with two functional binding epitopes. Similar results were obtained from BMP-2/6 mutants carrying one defective type I receptor epitope in the BMP-2 or the BMP-6 subunit, respectively(Isaacs et al. 2010). Both mutants reduce the activation of a Smad 1 reporter in C2C12 cells, but do not abolish the signal completely. The reduction effect, however, was more pronounced in the mutant defective in the type I receptor epitope in BMP-2 (80 % reduction) than in the case of BMP-6 (20 % reduction).

These findings suggest that only one functional type I receptor epitope is necessary for successful signalling in BMP-heterodimers.

6.3. A Fab antibody/BMPR-IA structure shed light on the mechanisms of promiscuity in the BMP system

This study describes the structure of the BMP type I receptor BMPR-IA bound to the antibody fragment AbyD1556, which is an efficient inhibitor for BMP mediated signalling. Up to date, more than 1300 structures for antibodies, fragments thereof (Fv, Fab, sFv, camelid antibodies) or complexes with antigens or small molecule haptens are available in the RCSB structure databank (Berman et al. 2000), demonstrating the enormous interest in this protein class. Their versatile binding properties have been structurally and functionally studied since the early 90's providing a wealth of data on how antibodies in principle recognize and bind their target molecules (Sundberg and Mariuzza 2002; Sundberg 2009). The Fab AbyD1556 binding to the BMP receptor IA is not an exception to the rules that have been derived from other antibody structures. Thus, the binding epitope of Fab AbyD1556 has the expected size for binding to a rather large protein antigen. The binding site is dominated by the variable region of the heavy chain, particularly by the CDR H3 (residues Glu99 to Phe107), which lies in the center of the contact. The loop conformations of the CDRs L1, L2, H1 and H2 follow the classification of Chothia and colleagues, exhibiting the canonical structure classes 4, 1, 1 and 3 (Chothia et al. 1989; Al-Lazikani et al. 1997). The CDR3 loop of the light chain is unusually long and seems not to obey any of the known classes. As observed in other antibody-antigen structures, the number of serine residues is indeed increased in the CDR loops. Due to the rather large size of the antigen BMPR-IA, the binding epitope of the Fab is

quite flat, maximizing the contact between the CDR loops and the antigen. It therefore seems that the antigen binding mechanism of the Fab AbyD1556 does not differ significantly from those observed in other antibody-antigen interactions. Thus, the far more interesting aspect lies in the structure of the antigen: the BMP receptor type IA.

The structure of BMPR-IA bound to the neutralizing Fab AbyD1556 reveals a contact epitope that highly overlaps with the epitope on BMPR-IA, bound to its natural ligand BMP-2. Comparing the binding sites on BMP-2 and AbyD1556 – which might be considered as an anti-idiotypic BMP-2 potentially exhibiting a similar binding surface as BMP-2 – shows that there is very limited similarity in surface shape (see fig. 6.1).

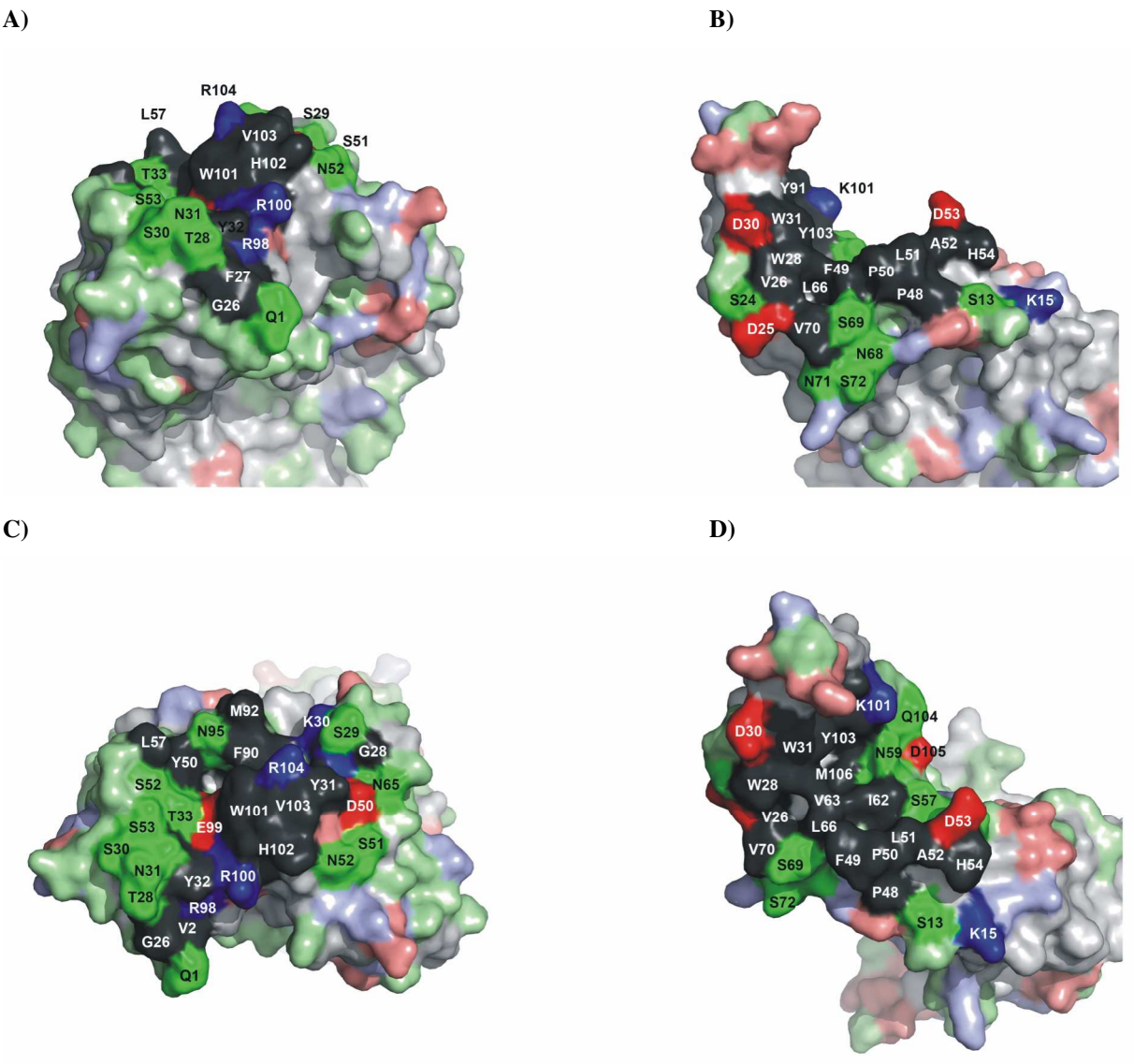

Fig. 6.1 – A) Surface representation of the BMPR-IA binding epitope of AbyD1556. The surface is color-coded with hydrophobic amino acid residues (A, C, F, G, H, I, L, M, P, V, W, and Y) in dark gray, acidic residues in red (D, E), basic residues in blue (K, R) and polar but uncharged residues in green (N, Q, S, T). Residues not

participating in the binding epitope are shown in lighter colors. **B)** As in **A)** but for the BMPR-IA binding epitope of BMP-2 (PDB entry 1REW). BMP-2 oriented such that BMPR-IA in the complexes AbyD1556/BMPR-IA and BMP-2/BMPR-IA (1REW) are structurally aligned. **C)** As in **A)** but rotated by about 70° around the x-axis. **D)** As in **B)** but rotated around the y-axis for about 70°. The top view of the BMPR-IA binding epitopes of AbyD1556 **(A)** and BMP-2 **(B)** show a seemingly similar distribution of the amino acid chemistry at the binding surface, e.g. a large central hydrophobic patch, surrounding polar or charged residues which (in part) occupy similar positions (e.g. AbyD1556 Asp50:BMP-2 Asp53; AbD1556 Trp101:BMP-2 Leu66/Ile62; AbyD1556 Arg104:BMP-2 Lys101, etc.). The side view **(C, D)**, however, shows that surface complementarity is rather limited with the curvature of AbyD1556 being flat and the BMP-2 surface being highly concave. Picture is depicted from (Harth et al. 2010b).

In the BMP-2/BMPR-IA complex, BMPR-IA is buried in a deep, quite concave cleft on BMP-2, whereas in the Fab/BMPR-IA complex the binding site on the Fab is very flat. On the other hand, in both sites the epitope center is dominated almost exclusively by hydrophobic amino acids, which are surrounded by a ring of polar and/or charged residues, suggesting that the surface chemistry involved are similar despite the structural differences.

A previous NMR structure analysis of BMPR-IA illustrated that the ligand-binding epitope of BMPR-IA is largely unordered in its unbound form and subject to a large conformational rearrangement upon BMP-2 binding (Klages et al. 2008). The main changes are located in the long loop between the β-strands 4 and 5 of the BMPR-IA ectodomain.

In its BMP-2 bound form this loop adopts a rigid extended conformation with a short 1.5 turn helix consisting of residues Ser83 to Lys88 (Kirsch et al. 2000b; Keller et al. 2004b). NMR titration studies using the helix-inducing agent trifluoroethanol point towards an induced fit mechanism, which seems to lead to a spontaneous helix induction upon changes in the environment (Klages et al. 2008). However, in the structure of BMPR-IA bound to the Fab AbyD1556 the β4β5-loop adopts a rather different conformation, which resembles a mixture of the conformation(s) found in the NMR structure ensemble and the BMP-2 bound form. Thus, the helix formation does not precede complex formation. Whether a helix is formed in the BMPR-IA β4β5-loop depends on the nature of the binding partner. This structural plasticity of the BMP type I receptor epitope, which allows BMPR-IA to adapt to different binding partners without deteriorating binding affinities to either one of the partners, is possibly a key mechanism by which proteins can achieve binding to more than one interaction partner utilizing the same binding site.

The so-called binding promiscuity has become an increasingly observed phenomenon in numerous protein superfamilies rather than an exotic exception. For a limited number of

examples, see (Hodivala-Dilke et al. 2003; Muller-Newen 2003; Barker 2004; Mohammadi et al. 2005; Eagle and Trowsdale 2007; Nickel et al. 2009).

For some protein families, e.g. antibodies, T-cell receptors and other "receptors" of the immune system, binding to numerous (or even an unlimited number of) other proteins is a generally accepted phenomenon. But it has still been assumed that a particular antibody would recognize only a single antigen. An antibody binding to different antigens, i.e. showing cross-reactivity, was considered rare and its promiscuous binding due to structural similarities between the cognate antigens. A promiscuous protein is determined as a protein with a defined sequence that can bind various partners (but still exhibits high specificity for this particular group of partners) without utilizing different epitopes, making promiscuity an incomprehensible process in protein-protein recognition. In its most extreme form, so-called hub proteins at central positions of interaction networks were postulated, which supposedly bind to tens or even hundreds of partners (Gavin et al. 2002; Ho et al. 2002).

Although this postulate possibly might explain the numerical discrepancy between the rather small number of genes and the complexity of the signaling network in complex organisms such as humans (Gavin and Superti-Furga 2003), it raises questions about how a single hub protein can interact with so many different partners (Tsai et al. 2009).

Several solutions to this logical obstacle have been proposed. Many hub proteins exhibit a modular architecture in which several different protein interaction domains, that typically bind linear epitopes, are shuffled together (Pawson and Nash 2003). Depending on post-translational modifications or splicing, these hub proteins can form different interaction complexes thereby enhancing the complexity in binding promiscuity. The discovery of intrinsically disordered proteins has added another powerful example of how protein-protein interactions can be extended (Dyson and Wright 2002).

The often under-appreciated fact that proteins are inherently flexible, from side chain to backbone level, allows proteins to adapt to different binding sites (Dunker et al. 2005; Boehr et al. 2009). Although neither BMPR-IA nor its BMP ligands are classical hub proteins, the manifold interactions of BMPR-IA and other BMP type I receptors with various BMPs as well as the interaction of these BMPs with other receptors, co-receptors or modulator proteins show similarities to hub proteins in these interaction networks. Neither the ligand nor the receptor are modular proteins, but modularity of binding epitopes has been described to allow for promiscuity (Kraich et al. 2006). Cooperativity from using two (or several) discontinuous binding elements – as observed in the interaction of the von Willebrand domain VWC1 of

Crossveinless 2 with BMP-2 – allows to combine the weak affinities of two small epitopes and broader binding specificity (Zhang et al. 2008).

The local intrinsic disorder in the binding epitope of BMPR-IA allows for adaptation of its interface to very different binding partners. Even though the Fab is not a physiological BMP interaction partner, the very same mechanism, by selecting the matching conformation from a pre-existing population, might also explain the promiscuous binding of BMPR-IA to other BMPs, like BMP-6, -7 or GDF-5 (Heinecke et al. 2009) or to structurally unrelated molecules like RGMA/DRAGON (Babitt et al. 2005). As flexible loop elements in BMP type I receptors have indeed been shown to modulate promiscuity and specificity (Kotzsch et al. 2008; Kotzsch et al. 2009), further structural studies of protein-protein complexes involving BMPR-IA are necessary to reveal to its full extent whether and how other binding partners utilize the conformational flexibility of BMPR-IA for recognition and binding.

6.4. Outlook

This work described the generation and production of the biologically active BMP heterodimers 2/6 and 2/7. First insights in the type I receptor usage of these BMP heterodimers were obtained but not revealed in its full extent. To unravel which additional receptors are recruited by BMP heterodimers, several possibilities exist.

The generation of new inhibiting antibodies for other type I receptors than BMPR-IA and type II receptors are possible, but time-consuming and laborious. During a diploma thesis (Harth 2006), several antibodies raised against ActR-I, BMPR-IB as well as ActR-II, ActR-IIB and BMPR-II were already tested regarding their signalling inhibiting properties. The antibodies exhibited either a very low affinity to their receptors or did not inhibit their receptor signalling. Therefore, other experiments should be more promising. Crosslinking experiments as shown for example for BMP-4 and BMP-7 (ten Dijke et al. 1994) could identify both the type I and type II receptors which are recruited by BMP heterodimers in cell-based assays. In addition, a transient gene knockdown using siRNA, which down-regulates the expression of receptors are also powerful tools to identify the receptors which were bound by BMP heterodimers as shown previously (Lavery et al. 2008). A structural and functional analysis of BMP heterodimers in combination with one or more receptors of both types of receptors, however, might be the best way to explain the mode of receptor recruitment in

BMP heterodimers. The methods and results presented in this work provide a sufficient amount of proteins to perform successfully crystallization studies to answer this question.

In the second part, this work described the crystal structure of a complex consisting of the extracellular domain of BMPR-IA bound to the antibody Fab fragment AbyD1556.
A comparison of the structures of BMPR-IA bound to AbyD1556 and to BMP-2 with the structure of unbound BMPR-IA revealed that binding of BMPR-IA to its interaction partners follows a selection fit mechanism, possibly indicating that the ligand promiscuity of BMPR-IA is inherently encoded by structural adaptability. Therefore, further structural studies of ligand-BMPR-IA complexes are necessary to reveal in detail how other BMP-ligands use the structural adaptability of BMPR-IA for recognition and binding. In addition, the results of the AbyD1556-BMPR-IA studies may pave the way for the design of low-molecular weight synthetic BMPR-IA binders or inhibitors suitable for clinical applications.

7. References

Adams, F. (1891). The Genuine Works of Hippocrates - http://ebooks.adelaide.edu.au/h/hippocrates/. New York, William Wood and Company.

Adams, P. D., P. V. Afonine, G. Bunkoczi, V. B. Chen, I. W. Davis, N. Echols, J. J. Headd, L. W. Hung, G. J. Kapral, R. W. Grosse-Kunstleve, A. J. McCoy, N. W. Moriarty, R. Oeffner, R. J. Read, D. C. Richardson, J. S. Richardson, T. C. Terwilliger and P. H. Zwart (2010). "PHENIX: a comprehensive Python-based system for macromolecular structure solution." Acta Crystallogr D Biol Crystallogr **66**(Pt 2): 213-21.

Akiyama, H., C. Shukunami, T. Nakamura and Y. Hiraki (2000). "Differential expressions of BMP family genes during chondrogenic differentiation of mouse ATDC5 cells." Cell Struct Funct **25**(3): 195-204.

Akiyama, S., T. Katagiri, M. Namiki, N. Yamaji, N. Yamamoto, K. Miyama, H. Shibuya, N. Ueno, J. M. Wozney and T. Suda (1997). "Constitutively active BMP type I receptors transduce BMP-2 signals without the ligand in C2C12 myoblasts." Exp Cell Res **235**(2): 362-9.

Al-Lazikani, B., A. M. Lesk and C. Chothia (1997). "Standard conformations for the canonical structures of immunoglobulins." J Mol Biol **273**(4): 927-48.

Allendorph, G. P., M. J. Isaacs, Y. Kawakami, J. C. Izpisua Belmonte and S. Choe (2007). "BMP-3 and BMP-6 structures illuminate the nature of binding specificity with receptors." Biochemistry **46**(43): 12238-47.

Allendorph, G. P., W. W. Vale and S. Choe (2006). "Structure of the ternary signaling complex of a TGF-beta superfamily member." Proc Natl Acad Sci U S A **103**(20): 7643-8.

Aono, A., M. Hazama, K. Notoya, S. Taketomi, H. Yamasaki, R. Tsukuda, S. Sasaki and Y. Fujisawa (1995). "Potent ectopic bone-inducing activity of bone morphogenetic protein-4/7 heterodimer." Biochem Biophys Res Commun **210**(3): 670-7.

Attisano, L., J. Carcamo, F. Ventura, F. M. Weis, J. Massague and J. L. Wrana (1993). "Identification of human activin and TGF beta type I receptors that form heteromeric kinase complexes with type II receptors." Cell **75**(4): 671-80.

Attisano, L., J. L. Wrana, S. Cheifetz and J. Massague (1992). "Novel activin receptors: distinct genes and alternative mRNA splicing generate a repertoire of serine/threonine kinase receptors." Cell **68**(1): 97-108.

Attisano, L., J. L. Wrana, E. Montalvo and J. Massague (1996). "Activation of signalling by the activin receptor complex." Mol Cell Biol **16**(3): 1066-73.

Avsian-Kretchmer, O. and A. J. Hsueh (2004). "Comparative genomic analysis of the eight-membered ring cystine knot-containing bone morphogenetic protein antagonists." Mol Endocrinol **18**(1): 1-12.

Babitt, J. L., Y. Zhang, T. A. Samad, Y. Xia, J. Tang, J. A. Campagna, A. L. Schneyer, C. J. Woolf and H. Y. Lin (2005). "Repulsive guidance molecule (RGMa), a DRAGON homologue, is a bone morphogenetic protein co-receptor." J Biol Chem **280**(33): 29820-7.

Balemans, W. and W. Van Hul (2002). "Extracellular regulation of BMP signaling in vertebrates: a cocktail of modulators." Dev Biol **250**(2): 231-50.

Baneyx, F. and M. Mujacic (2004). "Recombinant protein folding and misfolding in Escherichia coli." Nat Biotechnol **22**(11): 1399-408.

Barker, P. A. (2004). "p75NTR is positively promiscuous: novel partners and new insights." Neuron **42**(4): 529-33.

Bassing, C. H., J. M. Yingling, D. J. Howe, T. Wang, W. W. He, M. L. Gustafson, P. Shah, P. K. Donahoe and X. F. Wang (1994). "A transforming growth factor beta type I receptor that signals to activate gene expression." Science **263**(5143): 87-9.

Berman, H. M., J. Westbrook, Z. Feng, G. Gilliland, T. N. Bhat, H. Weissig, I. N. Shindyalov and P. E. Bourne (2000). "The Protein Data Bank." Nucleic Acids Res **28**(1): 235-42.

Bernard, D. J., S. C. Chapman and T. K. Woodruff (2001). "An emerging role for co-receptors in inhibin signal transduction." Mol Cell Endocrinol **180**(1-2): 55-62.

Bessa, P. C., M. Casal and R. L. Reis (2008a). "Bone morphogenetic proteins in tissue engineering: the road from the laboratory to the clinic, part I (basic concepts)." J Tissue Eng Regen Med **2**(1): 1-13.

Bessa, P. C., M. Casal and R. L. Reis (2008b). "Bone morphogenetic proteins in tissue engineering: the road from laboratory to clinic, part II (BMP delivery)." J Tissue Eng Regen Med **2**(2-3): 81-96.

BIPM (2006). The International System of Units (SI) - http://www.bipm.org/utils/common/pdf/si_brochure_8_en.pdf.

Blanco Calvo, M., V. Bolos Fernandez, V. Medina Villaamil, G. Aparicio Gallego, S. Diaz Prado and E. Grande Pulido (2009). "Biology of BMP signalling and cancer." Clin Transl Oncol **11**(3): 126-37.

Boehr, D. D., R. Nussinov and P. E. Wright (2009). "The role of dynamic conformational ensembles in biomolecular recognition." Nat Chem Biol **5**(11): 789-96.

Boesen, C. C., S. Radaev, S. A. Motyka, A. Patamawenu and P. D. Sun (2002). "The 1.1 A crystal structure of human TGF-beta type II receptor ligand binding domain." Structure **10**(7): 913-9.

Brown, M. A., Q. Zhao, K. A. Baker, C. Naik, C. Chen, L. Pukac, M. Singh, T. Tsareva, Y. Parice, A. Mahoney, V. Roschke, I. Sanyal and S. Choe (2005). "Crystal structure of BMP-9 and functional interactions with pro-region and receptors." J Biol Chem **280**(26): 25111-8.

Brunger, A. T. (2007). "Version 1.2 of the Crystallography and NMR system." Nat Protoc **2**(11): 2728-33.

Butler, S. J. and J. Dodd (2003). "A role for BMP heterodimers in roof plate-mediated repulsion of commissural axons." Neuron **38**(3): 389-401.

Chang, H., C. W. Brown and M. M. Matzuk (2002). "Genetic analysis of the mammalian transforming growth factor-beta superfamily." Endocr Rev **23**(6): 787-823.

Cheifetz, S., J. A. Weatherbee, M. L. Tsang, J. K. Anderson, J. E. Mole, R. Lucas and J. Massague (1987). "The transforming growth factor-beta system, a complex pattern of cross-reactive ligands and receptors." Cell **48**(3): 409-15.

Chen, H. B., J. Shen, Y. T. Ip and L. Xu (2006). "Identification of phosphatases for Smad in the BMP/DPP pathway." Genes Dev **20**(6): 648-53.

Chothia, C., A. M. Lesk, A. Tramontano, M. Levitt, S. J. Smith-Gill, G. Air, S. Sheriff, E. A. Padlan, D. Davies, W. R. Tulip and et al. (1989). "Conformations of immunoglobulin hypervariable regions." Nature **342**(6252): 877-83.

Chung, C. T., S. L. Niemela and R. H. Miller (1989). "One-step preparation of competent Escherichia coli: transformation and storage of bacterial cells in the same solution." Proc Natl Acad Sci U S A **86**(7): 2172-5.

Constam, D. B. and E. J. Robertson (1999). "Regulation of bone morphogenetic protein activity by pro domains and proprotein convertases." J Cell Biol **144**(1): 139-49.

Corradini, E., J. L. Babitt and H. Y. Lin (2009). "The RGM/DRAGON family of BMP co-receptors." Cytokine Growth Factor Rev **20**(5-6): 389-98.

Daopin, S., K. A. Piez, Y. Ogawa and D. R. Davies (1992). "Crystal structure of transforming growth factor-beta 2: an unusual fold for the superfamily." Science **257**(5068): 369-73.

de Caestecker, M. (2004). "The transforming growth factor-beta superfamily of receptors." Cytokine Growth Factor Rev **15**(1): 1-11.

Derynck, R., W. M. Gelbart, R. M. Harland, C. H. Heldin, S. E. Kern, J. Massague, D. A. Melton, M. Mlodzik, R. W. Padgett, A. B. Roberts, J. Smith, G. H. Thomsen, B. Vogelstein and X. F. Wang (1996). "Nomenclature: vertebrate mediators of TGFbeta family signals." Cell **87**(2): 173.

Dunker, A. K., M. S. Cortese, P. Romero, L. M. Iakoucheva and V. N. Uversky (2005). "Flexible nets. The roles of intrinsic disorder in protein interaction networks." Febs J **272**(20): 5129-48.

Dyson, H. J. and P. E. Wright (2002). "Coupling of folding and binding for unstructured proteins." Curr Opin Struct Biol **12**(1): 54-60.

Eagle, R. A. and J. Trowsdale (2007). "Promiscuity and the single receptor: NKG2D." Nat Rev Immunol **7**(9): 737-44.

Ebisawa, T., K. Tada, I. Kitajima, K. Tojo, T. K. Sampath, M. Kawabata, K. Miyazono and T. Imamura (1999). "Characterization of bone morphogenetic protein-6 signaling pathways in osteoblast differentiation." J Cell Sci **112 (Pt 20)**: 3519-27.

Ebner, R., R. H. Chen, S. Lawler, T. Zioncheck and R. Derynck (1993). "Determination of type I receptor specificity by the type II receptors for TGF-beta or activin." Science **262**(5135): 900-2.

Eigenbrot, C. and N. Gerber (1997). "X-ray structure of glial cell-derived neurotrophic factor at 1.9 A resolution and implications for receptor binding." Nat Struct Biol **4**(6): 435-8.

Faber, C., L. Shan, Z. Fan, L. W. Guddat, C. Furebring, M. Ohlin, C. A. Borrebaeck and A. B. Edmundson (1998). "Three-dimensional structure of a human Fab with high affinity for tetanus toxoid." Immunotechnology **3**(4): 253-70.

Franzen, P., P. ten Dijke, H. Ichijo, H. Yamashita, P. Schulz, C. H. Heldin and K. Miyazono (1993). "Cloning of a TGF beta type I receptor that forms a heteromeric complex with the TGF beta type II receptor." Cell **75**(4): 681-92.

Gasteiger E., H. C., Gattiker A., Duvaud S., Wilkins M.R., Appel R.D., Bairoch A. (2005). Protein Identification and Analysis Tools on the ExPASy Server. The Proteomics Protocols Handbook. J. M. Walker, Humana Press**:** pp. 571-607.

Gavin, A. C., M. Bosche, R. Krause, P. Grandi, M. Marzioch, A. Bauer, J. Schultz, J. M. Rick, A. M. Michon, C. M. Cruciat, M. Remor, C. Hofert, M. Schelder, M. Brajenovic, H. Ruffner, A. Merino, K. Klein, M. Hudak, D. Dickson, T. Rudi, V. Gnau, A. Bauch, S. Bastuck, B. Huhse, C. Leutwein, M. A. Heurtier, R. R. Copley, A. Edelmann, E. Querfurth, V. Rybin, G. Drewes, M. Raida, T. Bouwmeester, P. Bork, B. Seraphin, B. Kuster, G. Neubauer and G. Superti-Furga (2002). "Functional organization of the yeast proteome by systematic analysis of protein complexes." Nature **415**(6868): 141-7.

Gavin, A. C. and G. Superti-Furga (2003). "Protein complexes and proteome organization from yeast to man." Curr Opin Chem Biol **7**(1): 21-7.

Greenwald, J., W. H. Fischer, W. W. Vale and S. Choe (1999). "Three-finger toxin fold for the extracellular ligand-binding domain of the type II activin receptor serine kinase." Nat Struct Biol **6**(1): 18-22.

Greenwald, J., J. Groppe, P. Gray, E. Wiater, W. Kwiatkowski, W. Vale and S. Choe (2003). "The BMP7/ActRII extracellular domain complex provides new insights into the cooperative nature of receptor assembly." Mol Cell **11**(3): 605-17.

Greenwald, J., M. E. Vega, G. P. Allendorph, W. H. Fischer, W. Vale and S. Choe (2004). "A flexible activin explains the membrane-dependent cooperative assembly of TGF-beta family receptors." Mol Cell **15**(3): 485-9.

Griffith, D. L., P. C. Keck, T. K. Sampath, D. C. Rueger and W. D. Carlson (1996). "Three-dimensional structure of recombinant human osteogenic protein 1: structural paradigm for the transforming growth factor beta superfamily." Proc Natl Acad Sci U S A **93**(2): 878-83.

Groppe, J., J. Greenwald, E. Wiater, J. Rodriguez-Leon, A. N. Economides, W. Kwiatkowski, M. Affolter, W. W. Vale, J. C. Belmonte and S. Choe (2002). "Structural basis of BMP signalling inhibition by the cystine knot protein Noggin." Nature **420**(6916): 636-42.

Groppe, J., C. S. Hinck, P. Samavarchi-Tehrani, C. Zubieta, J. P. Schuermann, A. B. Taylor, P. M. Schwarz, J. L. Wrana and A. P. Hinck (2008). "Cooperative assembly of TGF-beta superfamily signaling complexes is mediated by two disparate mechanisms and distinct modes of receptor binding." Mol Cell **29**(2): 157-68.

Groppe, J., K. Rumpel, A. N. Economides, N. Stahl, W. Sebald and M. Affolter (1998). "Biochemical and biophysical characterization of refolded Drosophila DPP, a homolog of bone morphogenetic proteins 2 and 4." J Biol Chem **273**(44): 29052-65.

Guo, X. and X. F. Wang (2009). "Signaling cross-talk between TGF-beta/BMP and other pathways." Cell Res **19**(1): 71-88.

Han, S., P. Loulakis, M. Griffor and Z. Xie (2007). "Crystal structure of activin receptor type IIB kinase domain from human at 2.0 Angstrom resolution." Protein Sci **16**(10): 2272-7.

Hanahan, D. (1983). "Studies on transformation of Escherichia coli with plasmids." J Mol Biol **166**(4): 557-80.

Harrington, A. E., S. A. Morris-Triggs, B. T. Ruotolo, C. V. Robinson, S. Ohnuma and M. Hyvonen (2006). "Structural basis for the inhibition of activin signalling by follistatin." Embo J **25**(5): 1035-45.

Hart, P. J., S. Deep, A. B. Taylor, Z. Shu, C. S. Hinck and A. P. Hinck (2002). "Crystal structure of the human TbetaR2 ectodomain--TGF-beta3 complex." Nat Struct Biol **9**(3): 203-8.

Harth, S. (2006). Diplomarbeit: "Rekombinante Antikörper als Werkzeuge zur Analyse von BMP-Rezeptoren". Physiologische Chemie II. Würzburg, Julius Maximilians Universität**:** 89 S.

Harth, S., A. Kotzsch, J. Hu, W. Sebald and T. D. Mueller (2010b). "A selection fit mechanism in BMP receptor IA as a possible source for BMP ligand-receptor promiscuity." PLoS One **5** (9): e13049. doi:10.1371/journal.pone.0013049.

Harth, S., A. Kotzsch, W. Sebald and T. D. Mueller (2010a). "Crystallization of BMP receptor type IA bound to the antibody Fab fragment AbD1556." Acta Crystallogr Sect F Struct Biol Cryst Commun **66**(Pt 8): 964-8.

Hatta, T., H. Konishi, E. Katoh, T. Natsume, N. Ueno, Y. Kobayashi and T. Yamazaki (2000). "Identification of the ligand-binding site of the BMP type IA receptor for BMP-4." Biopolymers **55**(5): 399-406.

Hazama, M., A. Aono, N. Ueno and Y. Fujisawa (1995). "Efficient expression of a heterodimer of bone morphogenetic protein subunits using a baculovirus expression system." Biochem Biophys Res Commun **209**(3): 859-66.

Heinecke, K., A. Seher, W. Schmitz, T. D. Mueller, W. Sebald and J. Nickel (2009). "Receptor oligomerization and beyond: a case study in bone morphogenetic proteins." BMC Biol **7**: 59.

Hill, C. S. (2001). "TGF-beta signalling pathways in early Xenopus development." Curr Opin Genet Dev **11**(5): 533-40.

Hinck, A. P., S. J. Archer, S. W. Qian, A. B. Roberts, M. B. Sporn, J. A. Weatherbee, M. L. Tsang, R. Lucas, B. L. Zhang, J. Wenker and D. A. Torchia (1996). "Transforming growth factor beta 1: three-dimensional structure in solution and comparison with the X-ray structure of transforming growth factor beta 2." Biochemistry **35**(26): 8517-34.

Hjertner, O., H. Hjorth-Hansen, M. Borset, C. Seidel, A. Waage and A. Sundan (2001). "Bone morphogenetic protein-4 inhibits proliferation and induces apoptosis of multiple myeloma cells." Blood **97**(2): 516-22.

Ho, Y., A. Gruhler, A. Heilbut, G. D. Bader, L. Moore, S. L. Adams, A. Millar, P. Taylor, K. Bennett, K. Boutilier, L. Yang, C. Wolting, I. Donaldson, S. Schandorff, J. Shewnarane, M. Vo, J. Taggart, M. Goudreault, B. Muskat, C. Alfarano, D. Dewar, Z. Lin, K. Michalickova, A. R. Willems, H. Sassi, P. A. Nielsen, K. J. Rasmussen, J. R. Andersen, L. E. Johansen, L. H. Hansen, H. Jespersen, A. Podtelejnikov, E. Nielsen, J. Crawford, V. Poulsen, B. D. Sorensen, J. Matthiesen, R. C. Hendrickson, F. Gleeson, T. Pawson, M. F. Moran, D. Durocher, M. Mann, C. W. Hogue, D. Figeys and M. Tyers (2002). "Systematic identification of protein complexes in Saccharomyces cerevisiae by mass spectrometry." Nature **415**(6868): 180-3.

Hodivala-Dilke, K. M., A. R. Reynolds and L. E. Reynolds (2003). "Integrins in angiogenesis: multitalented molecules in a balancing act." Cell Tissue Res **314**(1): 131-44.

Hogan, B. L. (1996a). "Bone morphogenetic proteins: multifunctional regulators of vertebrate development." Genes Dev **10**(13): 1580-94.

Hogan, B. L. (1996b). "Bone morphogenetic proteins in development." Curr Opin Genet Dev **6**(4): 432-8.

Hoodless, P. A., T. Haerry, S. Abdollah, M. Stapleton, M. B. O'Connor, L. Attisano and J. L. Wrana (1996). "MADR1, a MAD-related protein that functions in BMP2 signaling pathways." Cell **85**(4): 489-500.

Huse, M., Y. G. Chen, J. Massague and J. Kuriyan (1999). "Crystal structure of the cytoplasmic domain of the type I TGF beta receptor in complex with FKBP12." Cell **96**(3): 425-36.

Imamura, T., M. Takase, A. Nishihara, E. Oeda, J. Hanai, M. Kawabata and K. Miyazono (1997). "Smad6 inhibits signalling by the TGF-beta superfamily." Nature **389**(6651): 622-6.

Isaacs, M. J., Y. Kawakami, G. P. Allendorph, B. H. Yoon, J. C. Belmonte and S. Choe (2010). "Bone morphogenetic protein-2 and -6 heterodimer illustrates the nature of ligand-receptor assembly." Mol Endocrinol **24**(7): 1469-77.

Israel, D. I., J. Nove, K. M. Kerns, R. J. Kaufman, V. Rosen, K. A. Cox and J. M. Wozney (1996). "Heterodimeric bone morphogenetic proteins show enhanced activity in vitro and in vivo." Growth Factors **13**(3-4): 291-300.

JCBN (1984). "IUPAC-IUB Joint Commission on Biochemical Nomenclature (JCBN). Nomenclature and symbolism for amino acids and peptides. Recommendations 1983." Eur J Biochem **138**(1): 9-37.

Jones, W. K., E. A. Richmond, K. White, H. Sasak, W. Kusmik, J. Smart, H. Oppermann, D. C. Rueger and R. F. Tucker (1994). "Osteogenic protein-1 (OP-1) expression and processing in Chinese hamster ovary cells: isolation of a soluble complex containing the mature and pro-domains of OP-1." Growth Factors **11**(3): 215-25.

Katagiri, T., S. Boorla, J. L. Frendo, B. L. Hogan and G. Karsenty (1998). "Skeletal abnormalities in doubly heterozygous Bmp4 and Bmp7 mice." Dev Genet **22**(4): 340-8.

Katagiri, T., A. Yamaguchi, M. Komaki, E. Abe, N. Takahashi, T. Ikeda, V. Rosen, J. M. Wozney, A. Fujisawa-Sehara and T. Suda (1994). "Bone morphogenetic protein-2 converts the differentiation pathway of C2C12 myoblasts into the osteoblast lineage." J Cell Biol **127**(6 Pt 1): 1755-66.

Katz, R. W. and A. H. Reddi (1988). "Dissociative extraction and partial purification of osteogenin, a bone inductive protein, from rat tooth matrix by heparin affinity chromatography." Biochem Biophys Res Commun **157**(3): 1253-7.

Keller, S., J. Nickel, J. L. Zhang, W. Sebald and T. D. Mueller (2004b). "Molecular recognition of BMP-2 and BMP receptor IA." Nat Struct Mol Biol **11**(5): 481-8.

Kirsch, T., J. Nickel and W. Sebald (2000a). "Isolation of recombinant BMP receptor IA ectodomain and its 2:1 complex with BMP-2." FEBS Lett **468**(2-3): 215-9.

Kirsch, T., J. Nickel and W. Sebald (2000c). "BMP-2 antagonists emerge from alterations in the low-affinity binding epitope for receptor BMPR-II." Embo J **19**(13): 3314-24.

Kirsch, T., W. Sebald and M. K. Dreyer (2000b). "Crystal structure of the BMP-2-BRIA ectodomain complex." Nat Struct Biol **7**(6): 492-6.

Klages, J., A. Kotzsch, M. Coles, W. Sebald, J. Nickel, T. Muller and H. Kessler (2008). "The solution structure of BMPR-IA reveals a local disorder-to-order transition upon BMP-2 binding." Biochemistry **47**(46): 11930-9.

Knaus, P. and W. Sebald (2001). "Cooperativity of binding epitopes and receptor chains in the BMP/TGFbeta superfamily." Biol Chem **382**(8): 1189-95.

Koenig, B. B., J. S. Cook, D. H. Wolsing, J. Ting, J. P. Tiesman, P. E. Correa, C. A. Olson, A. L. Pecquet, F. Ventura, R. A. Grant and et al. (1994). "Characterization and cloning of a receptor for BMP-2 and BMP-4 from NIH 3T3 cells." Mol Cell Biol **14**(9): 5961-74.

Koli, K., J. Saharinen, M. Hyytiainen, C. Penttinen and J. Keski-Oja (2001). "Latency, activation, and binding proteins of TGF-beta." Microsc Res Tech **52**(4): 354-62.

Kotzsch, A., J. Nickel, A. Seher, K. Heinecke, L. van Geersdaele, T. Herrmann, W. Sebald and T. D. Mueller (2008). "Structure analysis of bone morphogenetic protein-2 type I receptor complexes reveals a mechanism of receptor inactivation in juvenile polyposis syndrome." J Biol Chem **283**(9): 5876-87.

Kotzsch, A., J. Nickel, A. Seher, W. Sebald and T. D. Muller (2009). "Crystal structure analysis reveals a spring-loaded latch as molecular mechanism for GDF-5-type I receptor specificity." Embo J **28**(7): 937-47.

Kraich, M., M. Klein, E. Patino, H. Harrer, J. Nickel, W. Sebald and T. D. Mueller (2006). "A modular interface of IL-4 allows for scalable affinity without affecting specificity for the IL-4 receptor." BMC Biol **4**: 13.

Lacroix, P. (1945). "Recent investigastions on the growth of bone." Nature **156**(3967): 576.

Laemmli, U. K. (1970). "Cleavage of structural proteins during the assembly of the head of bacteriophage T4." Nature **227**(5259): 680-5.

LaVallie, E. R., E. A. DiBlasio, S. Kovacic, K. L. Grant, P. F. Schendel and J. M. McCoy (1993). "A thioredoxin gene fusion expression system that circumvents inclusion body formation in the E. coli cytoplasm." Biotechnology (N Y) **11**(2): 187-93.

Lavery, K., P. Swain, D. Falb and M. H. Alaoui-Ismaili (2008). "BMP-2/4 and BMP-6/7 differentially utilize cell surface receptors to induce osteoblastic differentiation of human bone marrow-derived mesenchymal stem cells." J Biol Chem **283**(30): 20948-58.

Ling, N., S. Y. Ying, N. Ueno, S. Shimasaki, F. Esch, M. Hotta and R. Guillemin (1986). "Pituitary FSH is released by a heterodimer of the beta-subunits from the two forms of inhibin." Nature **321**(6072): 779-82.

Little, S. C. and M. C. Mullins (2009). "Bone morphogenetic protein heterodimers assemble heteromeric type I receptor complexes to pattern the dorsoventral axis." Nat Cell Biol **11**(5): 637-43.

Liu, F., F. Ventura, J. Doody and J. Massague (1995). "Human type II receptor for bone morphogenic proteins (BMPs): extension of the two-kinase receptor model to the BMPs." Mol Cell Biol **15**(7): 3479-86.

Lopez-Casillas, F., J. L. Wrana and J. Massague (1993). "Betaglycan presents ligand to the TGF beta signaling receptor." Cell **73**(7): 1435-44.

Lyons, K. M., B. L. Hogan and E. J. Robertson (1995). "Colocalization of BMP 7 and BMP 2 RNAs suggests that these factors cooperatively mediate tissue interactions during murine development." Mech Dev **50**(1): 71-83.

Mace, P. D., J. F. Cutfield and S. M. Cutfield (2006). "High resolution structures of the bone morphogenetic protein type II receptor in two crystal forms: implications for ligand binding." Biochem Biophys Res Commun **351**(4): 831-8.

Massague, J. (1998). "TGF-beta signal transduction." Annu Rev Biochem **67**: 753-91.

Massague, J. and Y. G. Chen (2000). "Controlling TGF-beta signaling." Genes Dev **14**(6): 627-44.

Massague, J., J. Seoane and D. Wotton (2005). "Smad transcription factors." Genes Dev **19**(23): 2783-810.

Matthews, B. W. (1968). "Solvent content of protein crystals." J Mol Biol **33**(2): 491-7.

McCoy, A. J., R. W. Grosse-Kunstleve, P. D. Adams, M. D. Winn, L. C. Storoni and R. J. Read (2007). "Phaser crystallographic software." J Appl Crystallogr **40**(Pt 4): 658-674.

McDonald, N. Q. and W. A. Hendrickson (1993). "A structural superfamily of growth factors containing a cystine knot motif." Cell **73**(3): 421-4.

Mittl, P. R., J. P. Priestle, D. A. Cox, G. McMaster, N. Cerletti and M. G. Grutter (1996). "The crystal structure of TGF-beta 3 and comparison to TGF-beta 2: implications for receptor binding." Protein Sci **5**(7): 1261-71.

Miyazawa, K., M. Shinozaki, T. Hara, T. Furuya and K. Miyazono (2002). "Two major Smad pathways in TGF-beta superfamily signalling." Genes Cells **7**(12): 1191-204.

Mohammadi, M., S. K. Olsen and O. A. Ibrahimi (2005). "Structural basis for fibroblast growth factor receptor activation." Cytokine Growth Factor Rev **16**(2): 107-37.

Moustakas, A., S. Souchelnytskyi and C. H. Heldin (2001). "Smad regulation in TGF-beta signal transduction." J Cell Sci **114**(Pt 24): 4359-69.

Muller-Newen, G. (2003). "The cytokine receptor gp130: faithfully promiscuous." Sci STKE **2003**(201): PE40.

Murshudov, G. N., A. A. Vagin and E. J. Dodson (1997). "Refinement of macromolecular structures by the maximum-likelihood method." Acta Crystallogr D Biol Crystallogr **53**(Pt 3): 240-55.

Nagaso, H., A. Suzuki, M. Tada and N. Ueno (1999). "Dual specificity of activin type II receptor ActRIIb in dorso-ventral patterning during zebrafish embryogenesis." Dev Growth Differ **41**(2): 119-33.

Nakamura, K., T. Shirai, S. Morishita, S. Uchida, K. Saeki-Miura and F. Makishima (1999). "p38 mitogen-activated protein kinase functionally contributes to chondrogenesis induced by growth/differentiation factor-5 in ATDC5 cells." Exp Cell Res **250**(2): 351-63.

Nakao, A., M. Afrakhte, A. Moren, T. Nakayama, J. L. Christian, R. Heuchel, S. Itoh, M. Kawabata, N. E. Heldin, C. H. Heldin and P. ten Dijke (1997). "Identification of Smad7, a TGFbeta-inducible antagonist of TGF-beta signalling." Nature **389**(6651): 631-5.

Nickel, J., A. Kotzsch, W. Sebald and T. D. Mueller (2005). "A single residue of GDF-5 defines binding specificity to BMP receptor IB." J Mol Biol **349**(5): 933-47.

Nickel, J., W. Sebald, J. C. Groppe and T. D. Mueller (2009). "Intricacies of BMP receptor assembly." Cytokine Growth Factor Rev **20**(5-6): 367-77.

Nishitoh, H., H. Ichijo, M. Kimura, T. Matsumoto, F. Makishima, A. Yamaguchi, H. Yamashita, S. Enomoto and K. Miyazono (1996). "Identification of type I and type II serine/threonine kinase receptors for growth/differentiation factor-5." J Biol Chem **271**(35): 21345-52.

Onichtchouk, D., Y. G. Chen, R. Dosch, V. Gawantka, H. Delius, J. Massague and C. Niehrs (1999). "Silencing of TGF-beta signalling by the pseudoreceptor BAMBI." Nature **401**(6752): 480-5.

Parker, L., D. G. Stathakis and K. Arora (2004). "Regulation of BMP and activin signaling in Drosophila." Prog Mol Subcell Biol **34**: 73-101.

Pawson, T. and P. Nash (2003). "Assembly of cell regulatory systems through protein interaction domains." Science **300**(5618): 445-52.

Piek, E., M. Afrakhte, K. Sampath, E. J. van Zoelen, C. H. Heldin and P. ten Dijke (1999). "Functional antagonism between activin and osteogenic protein-1 in human embryonal carcinoma cells." J Cell Physiol **180**(2): 141-9.

Radaev, S., Z. Zou, T. Huang, E. M. Lafer, A. P. Hinck and P. D. Sun (2010). "Ternary complex of transforming growth factor-beta1 reveals isoform-specific ligand recognition and receptor recruitment in the superfamily." J Biol Chem **285**(19): 14806-14.

Rebbapragada, A., H. Benchabane, J. L. Wrana, A. J. Celeste and L. Attisano (2003). "Myostatin signals through a transforming growth factor beta-like signaling pathway to block adipogenesis." Mol Cell Biol **23**(20): 7230-42.

Reddi, A. H. (2005). "BMPs: from bone morphogenetic proteins to body morphogenetic proteins." Cytokine Growth Factor Rev **16**(3): 249-50.

Ro, T. B., R. U. Holt, A. T. Brenne, H. Hjorth-Hansen, A. Waage, O. Hjertner, A. Sundan and M. Borset (2004). "Bone morphogenetic protein-5, -6 and -7 inhibit growth and induce apoptosis in human myeloma cells." Oncogene **23**(17): 3024-32.

Rosenzweig, B. L., T. Imamura, T. Okadome, G. N. Cox, H. Yamashita, P. ten Dijke, C. H. Heldin and K. Miyazono (1995). "Cloning and characterization of a human type II receptor for bone morphogenetic proteins." Proc Natl Acad Sci U S A **92**(17): 7632-6.

Ruppert, R., E. Hoffmann and W. Sebald (1996). "Human bone morphogenetic protein 2 contains a heparin-binding site which modifies its biological activity." Eur J Biochem **237**(1): 295-302.

Samad, T. A., A. Rebbapragada, E. Bell, Y. Zhang, Y. Sidis, S. J. Jeong, J. A. Campagna, S. Perusini, D. A. Fabrizio, A. L. Schneyer, H. Y. Lin, A. H. Brivanlou, L. Attisano and C. J. Woolf (2005). "DRAGON, a bone morphogenetic protein co-receptor." J Biol Chem **280**(14): 14122-9.

Sampath, T. K., J. C. Maliakal, P. V. Hauschka, W. K. Jones, H. Sasak, R. F. Tucker, K. H. White, J. E. Coughlin, M. M. Tucker, R. H. Pang and et al. (1992). "Recombinant human osteogenic protein-1 (hOP-1) induces new bone formation in vivo with a specific activity

comparable with natural bovine osteogenic protein and stimulates osteoblast proliferation and differentiation in vitro." J Biol Chem **267**(28): 20352-62.

Sampath, T. K., N. Muthukumaran and A. H. Reddi (1987). "Isolation of osteogenin, an extracellular matrix-associated, bone-inductive protein, by heparin affinity chromatography." Proc Natl Acad Sci U S A **84**(20): 7109-13.

Saremba, S., J. Nickel, A. Seher, A. Kotzsch, W. Sebald and T. D. Mueller (2008). "Type I receptor binding of bone morphogenetic protein 6 is dependent on N-glycosylation of the ligand." Febs J **275**(1): 172-83.

Savage-Dunn, C. (2005). "TGF-beta signaling." WormBook: 1-12.

Scheufler, C., W. Sebald and M. Hulsmeyer (1999). "Crystal structure of human bone morphogenetic protein-2 at 2.7 A resolution." J Mol Biol **287**(1): 103-15.

Schreuder, H., A. Liesum, J. Pohl, M. Kruse and M. Koyama (2005). "Crystal structure of recombinant human growth and differentiation factor 5: evidence for interaction of the type I and type II receptor-binding sites." Biochem Biophys Res Commun **329**(3): 1076-86.

Sebald, W., J. Nickel, J. L. Zhang and T. D. Mueller (2004). "Molecular recognition in bone morphogenetic protein (BMP)/receptor interaction." Biol Chem **385**(8): 697-710.

Seemann, P., R. Schwappacher, K. W. Kjaer, D. Krakow, K. Lehmann, K. Dawson, S. Stricker, J. Pohl, F. Ploger, E. Staub, J. Nickel, W. Sebald, P. Knaus and S. Mundlos (2005). "Activating and deactivating mutations in the receptor interaction site of GDF5 cause symphalangism or brachydactyly type A2." J Clin Invest **115**(9): 2373-81.

Sengle, G., N. L. Charbonneau, R. N. Ono, T. Sasaki, J. Alvarez, D. R. Keene, H. P. Bachinger and L. Y. Sakai (2008). "Targeting of bone morphogenetic protein growth factor complexes to fibrillin." J Biol Chem **283**(20): 13874-88.

Senn, N. (1889). "Senn on the Healing of Aseptic Bone Cavities by Implantation of Antiseptic Decalcified Bone." Ann Surg **10**(5): 352-68.

Shi, Y. and J. Massague (2003). "Mechanisms of TGF-beta signaling from cell membrane to the nucleus." Cell **113**(6): 685-700.

Shimmi, O., D. Umulis, H. Othmer and M. B. O'Connor (2005). "Facilitated transport of a Dpp/Scw heterodimer by Sog/Tsg leads to robust patterning of the Drosophila blastoderm embryo." Cell **120**(6): 873-86.

Smith, P. K., R. I. Krohn, G. T. Hermanson, A. K. Mallia, F. H. Gartner, M. D. Provenzano, E. K. Fujimoto, N. M. Goeke, B. J. Olson and D. C. Klenk (1985). "Measurement of protein using bicinchoninic acid." Anal Biochem **150**(1): 76-85.

Solloway, M. J. and E. J. Robertson (1999). "Early embryonic lethality in Bmp5;Bmp7 double mutant mice suggests functional redundancy within the 60A subgroup." Development **126**(8): 1753-68.

Sundberg, E. J. (2009). "Structural basis of antibody-antigen interactions." Methods Mol Biol **524**: 23-36.

Sundberg, E. J. and R. A. Mariuzza (2002). "Molecular recognition in antibody-antigen complexes." Adv Protein Chem **61**: 119-60.

Suzuki, A., E. Kaneko, J. Maeda and N. Ueno (1997). "Mesoderm induction by BMP-4 and -7 heterodimers." Biochem Biophys Res Commun **232**(1): 153-6.

Swencki-Underwood, B., J. K. Mills, J. Vennarini, K. Boakye, J. Luo, S. Pomerantz, M. R. Cunningham, F. X. Farrell, M. F. Naso and B. Amegadzie (2008). "Expression and characterization of a human BMP-7 variant with improved biochemical properties." Protein Expr Purif **57**(2): 312-9.

ten Dijke, P., K. Miyazono and C. H. Heldin (1996). "Signaling via hetero-oligomeric complexes of type I and type II serine/threonine kinase receptors." Curr Opin Cell Biol **8**(2): 139-45.

ten Dijke, P., H. Yamashita, T. K. Sampath, A. H. Reddi, M. Estevez, D. L. Riddle, H. Ichijo, C. H. Heldin and K. Miyazono (1994). "Identification of type I receptors for osteogenic protein-1 and bone morphogenetic protein-4." J Biol Chem **269**(25): 16985-8.

Thompson, T. B., T. K. Woodruff and T. S. Jardetzky (2003). "Structures of an ActRIIB:activin A complex reveal a novel binding mode for TGF-beta ligand:receptor interactions." Embo J **22**(7): 1555-66.

Tong, L. and M. G. Rossmann (1997). "Rotation function calculations with GLRF program." Methods Enzymol **276**: 594-611.

Tsai, C. J., B. Ma and R. Nussinov (2009). "Protein-protein interaction networks: how can a hub protein bind so many different partners?" Trends Biochem Sci **34**(12): 594-600.

Urist, M. R. (1965). "Bone: formation by autoinduction." Science **150**(698): 893-9.

Urist, M. R. and B. S. Strates (1971). "Bone morphogenetic protein." J Dent Res **50**(6): 1392-406.

Urist, M. R. and B. S. Strates (2009). "The classic: Bone morphogenetic protein." Clin Orthop Relat Res **467**(12): 3051-62.

Valera, E., M. J. Isaacs, Y. Kawakami, J. C. Izpisua Belmonte and S. Choe (2010). "BMP-2/6 heterodimer is more effective than BMP-2 or BMP-6 homodimers as inductor of differentiation of human embryonic stem cells
" PLoS One **5**(6): e11167.

Vallejo, L. F. and U. Rinas (2004). "Optimized procedure for renaturation of recombinant human bone morphogenetic protein-2 at high protein concentration." Biotechnol Bioeng **85**(6): 601-9.

Wagner, D. O., C. Sieber, R. Bhushan, J. H. Borgermann, D. Graf and P. Knaus (2010). "BMPs: from bone to body morphogenetic proteins." Sci Signal **3**(107): mr1.

Weber, D., A. Kotzsch, J. Nickel, S. Harth, A. Seher, U. Mueller, W. Sebald and T. D. Mueller (2007). "A silent H-bond can be mutationally activated for high-affinity interaction of BMP-2 and activin type IIB receptor." BMC Struct Biol **7**: 6.

Weikl, T. R. and C. von Deuster (2009). "Selected-fit versus induced-fit protein binding: kinetic differences and mutational analysis." Proteins **75**(1): 104-10.

Wieser, R., J. L. Wrana and J. Massague (1995). "GS domain mutations that constitutively activate T beta R-I, the downstream signaling component in the TGF-beta receptor complex." Embo J **14**(10): 2199-208.

Wiesmann, C. and A. M. de Vos (2000). "Variations on ligand-receptor complexes." Nat Struct Biol **7**(6): 440-2.

Wotton, D. and J. Massague (2001). "Smad transcriptional corepressors in TGF beta family signaling." Curr Top Microbiol Immunol **254**: 145-64.

Wozney, J. M., V. Rosen, A. J. Celeste, L. M. Mitsock, M. J. Whitters, R. W. Kriz, R. M. Hewick and E. A. Wang (1988). "Novel regulators of bone formation: molecular clones and activities." Science **242**(4885): 1528-34.

Wrana, J. L., L. Attisano, J. Carcamo, A. Zentella, J. Doody, M. Laiho, X. F. Wang and J. Massague (1992). "TGF beta signals through a heteromeric protein kinase receptor complex." Cell **71**(6): 1003-14.

Wrana, J. L., L. Attisano, R. Wieser, F. Ventura and J. Massague (1994). "Mechanism of activation of the TGF-beta receptor." Nature **370**(6488): 341-7.

Xu, D., C. J. Tsai and R. Nussinov (1997). "Hydrogen bonds and salt bridges across protein-protein interfaces." Protein Eng **10**(9): 999-1012.

Zeng, S., J. Chen and H. Shen (2010). "Controlling of bone morphogenetic protein signaling." Cell Signal **22**(6): 888-93.

Zhang, J. L., L. Y. Qiu, A. Kotzsch, S. Weidauer, L. Patterson, M. Hammerschmidt, W. Sebald and T. D. Mueller (2008). "Crystal structure analysis reveals how the Chordin family member crossveinless 2 blocks BMP-2 receptor binding." Dev Cell **14**(5): 739-50.

Zhang, Y. E. (2009). "Non-Smad pathways in TGF-beta signaling." Cell Res **19**(1): 128-39.

Zhao, M., Z. Zhao, J. T. Koh, T. Jin and R. T. Franceschi (2005). "Combinatorial gene therapy for bone regeneration: cooperative interactions between adenovirus vectors expressing bone morphogenetic proteins 2, 4, and 7." J Cell Biochem **95**(1): 1-16.

Zhu, H., P. Kavsak, S. Abdollah, J. L. Wrana and G. H. Thomsen (1999). "A SMAD ubiquitin ligase targets the BMP pathway and affects embryonic pattern formation." Nature **400**(6745): 687-93.

Zhu, W., J. Kim, C. Cheng, B. A. Rawlins, O. Boachie-Adjei, R. G. Crystal and C. Hidaka (2006). "Noggin regulation of bone morphogenetic protein (BMP) 2/7 heterodimer activity in vitro." Bone **39**(1): 61-71.

Zhu, W., B. A. Rawlins, O. Boachie-Adjei, E. R. Myers, J. Arimizu, E. Choi, J. R. Lieberman, R. G. Crystal and C. Hidaka (2004). "Combined bone morphogenetic protein-2 and -7 gene transfer enhances osteoblastic differentiation and spine fusion in a rodent model." J Bone Miner Res **19**(12): 2021-32.

8. Publication list

Publications

1. **Harth, S.**, A. Kotzsch, J. Hu, W. Sebald and T. D. Mueller (2010b). "A selection fit mechanism in BMP receptor IA as a possible source for BMP ligand-receptor promiscuity." PLoS One **5** (9): e13049. doi:10.1371/journal.pone.0013049.

2. **Harth, S.**, A. Kotzsch, W. Sebald and T. D. Mueller (2010). "Crystallization of BMP receptor type IA bound to the antibody Fab fragment AbD1556." Acta Crystallogr Sect F Struct Biol Cryst Commun **66**(Pt 8): 964-8.

Completed during my diploma thesis:

3. Weber, D., A. Kotzsch, J. Nickel, **S. Harth**, A. Seher, U. Mueller, W. Sebald and T. D. Mueller (2007). "A silent H-bond can be mutationally activated for high-affinity interaction of BMP-2 and activin type IIB receptor." BMC Struct Biol **7**: 6.

Congress participations – Posters

1. 2nd International Conference on Molecular Perspectives on Protein-Protein Interactions, Dubrovnik, Croatia, 2008
   Harth, S., S. Saremba, D. Weber, J. Nickel, A. Seher, A. Kotzsch, T. D. Mueller and W. Sebald,

   Title: “Protein-Protein interactions during BMP-Receptor activation”

2. 6th International Conference on Bone Morphogenetic Proteins, Dubrovnik, Croatia, 2006
   Nickel, J., D. Weber, A. Kotzsch, S. Gebhardt, **S. Harth**, K. Heinecke, J. Ulbrich, M. Rattel, T. Müller and W. Sebald

   Title: “Structure and assembly of a ternary complex of BMP-2 and the ectodomains of its BMPR-IA and ActR-IIB receptor chains”

Atomic coordinates

The atomic coordinates and structure factors for the structures of the complex of AbyD1556/BMPR-IA_{ecd} have been deposited with the Protein Data Bank (http://www.pdb.org/), (Berman et al. 2000). The accession code is 3NH7.

9. Danksagung

Mein besonderer Dank gilt Herrn Prof. Walter Sebald für die Möglichkeit, diese Arbeit an seinem Lehrstuhl anzufertigen. Seine Diskussionsbereitschaft und die zu jeder Zeit gewährte großzügige Unterstützung waren für mich Motivation und Hilfe gleichermaßen. Herr Sebald, ich habe sehr viel von Ihnen gelernt, vielen herzlichen Dank dafür!

Ein großes Dankeschön möchte ich Herrn Prof. Thomas Müller aussprechen. Zum einen dafür, dass er die Arbeit auf sich nimmt, als Gutachter der Fakultät für Biologie bei dieser Dissertation zu fungieren. Zum anderen dafür, dass er immer ein offenes Ohr für meine Anliegen hatte, vor allem bei röntgenkristallographischen Fragestellungen sowie beim Verfassen der Publikationen. Thomas, vielen Dank!

Herrn Prof. Martin Eilers danke ich recht herzlich für die freundliche Bereitstellung von Räumen und Geräten in der letzten Phase dieser Arbeit.

I would also like to say thank you to Prof Anders Sundan for my research stay in Trondheim. It was a short, but fascinating time. Thank you Anders!

Besonders möchte ich mich bei Herrn Christian Söder und Herrn (hoffentlich bald Dr.) Jannes Ulbrich bedanken. Eure zahlreichen großen wie kleinen Hilfestellungen im täglichen Laborbetrieb haben sehr zum Gelingen dieser Arbeit beigetragen. Herr Söder, Jannes, Ihr habt meinen Laboralltag ungemein bereichert. Ich wünsche Euch weiterhin alles Gute an Euren „neuen“ Lehrstühlen!

Herrn Alexander Kotzsch möchte ich ganz herzlich für die jederzeit großzügig gewährte Hilfe in allen röntgenkristallographischen Fragen danken. Alexander, dankeschön!

Besonders bedanken möchte ich mich außerdem bei meinen Kollegen, bestehend aus Frau Dr. Junli Hu, Herrn Dr. Takuo Fujisawa, Herrn Dr. Joachim Nickel, Herrn Dr. Axel Seher, Herrn Dr. Werner Schmitz, Herrn Dr. Jinli Zhang, sowie meinen Mitdoktoranden Frau Dr. Gebhardt und Herrn Dr. Heinecke für das alltägliche gute Arbeitsklima. Euch allen vielen Dank!

Des Weiteren möchte ich Frau Lakeit und allen anderen Damen im Sekretariat von ganzem Herzen danken, vor allem für Euren unermüdlichen Einsatz, organisatorische Probleme so unbürokratisch wie möglich und mit vollem persönlichem Einsatz zu lösen.

Ein großer Dank gilt auch den Frauen in der Spülküche, Frau Ak, Frau Schneider und Frau Schwind. Ohne Euch würde der tägliche Laborbetrieb einfach nur zusammenbrechen!

Schließlich möchte ich mich bei allen weiteren Kollegen des Lehrstuhls für Physiologische Chemie II für die gute Zusammenarbeit und das angenehme Arbeitsklima bedanken.

遥、どもうありがとうございました。大好き！

Das größte Dankeschön gilt natürlich meinen Eltern und meinem Bruder. Eure Unterstützung und Zuversicht nicht nur während der Doktorarbeit, sondern während meines gesamten Studiums waren und sind eine große Stütze für mich. Herzlichen Dank!

10. Lebenslauf

Persönliche Angaben

Name	Stefan Wolfgang Harth
Geboren	5. April 1980 in Bad Neustadt an der Saale
Nationalität	Deutsch

Bildungsweg

04/2010 – heute	Aufbaustudium „Interkulturelle Japan-Kompetenz“ an der Eberhard-Karls-Universität Tübingen und der Dōshisha-Universität, Kyoto, Japan
04/2006 – heute	Promotion bei Prof. Dr. Walter Sebald am Lehrstuhl für Physiologische Chemie II an der Bayerischen Julius-Maximilians Universität Würzburg Titel der Promotion: “Molecular Recognition in BMP Ligand-Receptor Interactions“
06/2005 – 03/2006	Diplomarbeit bei Prof. Dr. Walter Sebald am Lehrstuhl für Physiologische Chemie II an der Bayerischen Julius-Maximilians-Universität Würzburg Titel der Diplomarbeit: „Rekombinante Antikörper als Werkzeuge zur Analyse von BMP-Rezeptoren“
04/2005	Diplomprüfungen: Hauptfach: Neurobiologie, Nebenfächer: Physiologische Chemie, Verhaltensphysiologie und Soziobiologie
10/2000 – 03/2006	Studium der Biologie an der Bayerischen Julius-Maximilians-Universität Würzburg, Abschluss: Diplom
09/1999 – 09/2000	Zivildienst, Rotes Kreuz Krankenhaus Frankfurt am Main
09/1990 – 08/1999	Abitur Gymnasium Bad Königshofen, Abschluss: Allgemeine Hochschulreife
09/1986 – 08/1990	Grundschule Großbardorf

11. Erklärungen

Erklärungen gemäß § 4 Absatz 3 der Promotionsordnung der Fakultät für Biologie der Bayerischen Julius-Maximilians-Universität Würzburg vom 15. März 1999:

Hiermit erkläre ich ehrenwörtlich, dass ich die vorliegende Dissertation in allen Teilen selbständig angefertigt und keine anderen als die von mir angegebenen Quellen und Hilfsmittel verwendet habe.

Ich erkläre weiterhin, dass ich diese Dissertation weder in gleicher noch in ähnlicher Form in anderen Prüfungsverfahren vorgelegt habe.

Ich habe außer den mit dem Zulassungsgesuch urkundlich vorgelegten Graden keine weiteren akademischen Grade erworben oder zu erwerben versucht.

Großbardorf, September 2010 Stefan Harth